

**FEDERAL UNIVERSITY OF ESPIRITO SANTO
TECHNOLOGICAL CENTER
GRADUATE PROGRAM IN ELECTRICAL ENGINEERING**

Anibal Cotrina Atencio

**A Novel Stimulation Paradigm for a
Brain-Computer Interface Based on SSVEP**

Vitoria-ES, Brazil

2015

Anibal Cotrina Atencio

A Novel Stimulation Paradigm for a Brain-Computer Interface Based on SSVEP

Thesis presented to the Graduate Program
in Electrical Engineering at the Federal Uni-
versity of Espirito Santo, as a partial requi-
rement for the degree of Doctor in Electrical
Engineering.

Federal University of Espirito Santo
Technological Center
Graduate Program in Electrical Engineering

Supervisor: Prof. Dr. Teodiano Freire Bastos-Filho
Co-supervisor: Prof. Dr. Andre Ferreira

Vitoria-ES, Brazil

2015

Dados Internacionais de Catalogação-na-publicação (CIP)
(Biblioteca Setorial Tecnológica,
Universidade Federal do Espírito Santo, ES, Brasil)

A864n Atencio, Anibal Cotrina, 1978-
*A novel stimulation paradigm for a brain-computer interfaces
based on SSVEP* / Anibal Cotrina Atencio. – 2015.
143 f. : il.

Orientador: Teodiano Freire Bastos Filho.

Coorientador: Andre Ferreira.

Tese (Doutorado em Engenharia Elétrica) – Universidade
Federal do Espírito Santo, Centro Tecnológico.

1. Interação homem-máquina. 2. Interface cérebro-computador. 3. Potencial evocado. 4. Profundidade – Percepção. 5. Comunicação não-verbal. 6. Sinais cerebrais. 7. Potenciais evocados visuais de regime permanente (Steady state visual evoked potential - SSVEP). I. Bastos Filho, Teodiano Freire. II. Ferreira, Andre. III. Universidade Federal do Espírito Santo. Centro Tecnológico. IV. Título.

CDU: 621.3

Anibal Cotrina Atencio

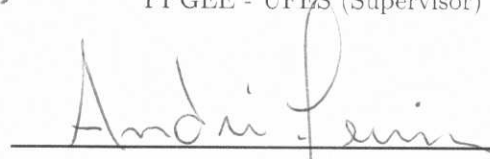
A Novel Stimulation Paradigm for a Brain-Computer Interface Based on SSVEP

Thesis presented to the Postgraduate Program in Electrical Engineering at the Federal University of Espirito Santo, as a partial requirement for the degree of Doctor in Electrical Engineering.

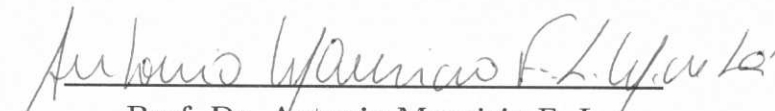
Approved on November 30, 2015.



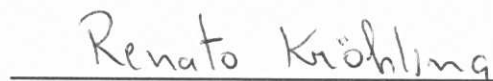
Prof. Dr. Teodiano Freire Bastos-Filho
PPGEE - UFES (Supervisor)




Prof. Dr. Andre Ferreira
DEE - UFES (Co-supervisor)



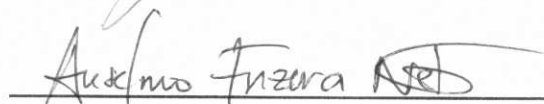
Prof. Dr. Antonio Mauricio F. L. Miranda de Sa
PEB - COPPE/UFRJ



Prof. Dr. Renato Krohling
PPI - UFES



Prof. Dr. Mario Sarcinelli-Filho
PPGEE - UFES



Prof. Dr. Anselmo Frizera Neto
PPGEE - UFES

To you, dear reader.

Acknowledgements

I am grateful to all the people who supported, collaborated with, and contributed directly and indirectly to the present work, especially to my supervisor Prof. Dr. Teodiano Bastos for his support and encouragement and for his scientific discussions. Also, I would like to express my thanks to Dr. Alessandro Benevides, Dr Javier Castillo, and Dr Andre Ferreira for their companionship.

I am grateful to CAPES/Brazil agency which provided the scholarship and funds for this work and the FAPES/Brazil Foundation for additional financial support. Also, I am grateful to the International Center of Theoretical Physics for the Full Grant to attend the International School on Complex Networks and Applications to Neuroscience.

I want to thank the team of the Automation Intelligent Lab. of the Federal University of Espirito Santo, which contributed to this project that obtained the first place in the Brain-computer interface Brazilian Competition organized by the Brazilian Society of Biomedical Engineering.

My heartfelt thanks goes to my parents Priscila and Saul; to my brothers Saul, David and Roy; and to my girlfriend Jane.

*“Scientific revolution
is the phase in which the underlying assumptions of the field
are reexamined and a new paradigm is established.”
(Thomas Kuhn, 1962)*

Abstract

Brain-computer interfaces (BCIs) are systems that provide a direct connection between users' brain signals and a computer, generating an alternative channel of communication that does not involve the traditional way as muscles and nerves. They help to restore or replace useful functions of people with paralysis. For instance, BCI systems based on SSVEP (SSVEP-BCI) present a set of stimuli flickering at different frequencies to the users, detect which stimulus is being gazed and associate this information to commands that can be used to control a robotic wheelchair, an exoskeleton, or a speller. Nowadays, SSVEP-BCIs are being widely used due to the high SNR of their response that is achieved when the target stimulus is brought to the center of the user's field of view. Paradoxically, it is their main disadvantage because bringing a stimulus to the center of the field of view demands muscular activity making them not suitably for paralyzed people who cannot control their head, neck and/or eyeball movements for redirecting their gaze.

In optical systems, the range of distance near the point of focus where objects are perceived sharp is referred as Depth-of-field; objects outside this region are defocused and blurred. The mechanism of the visual system that adjusts the eye focal length for focusing does not demand neck, head and/or eyeball movements. Furthermore, ophthalmology studies state that the amplitude and the latency of visual evoked potentials are affected by defocusing. In this context, this Thesis proposes a novel SSVEP-BCI paradigm, in which two stimuli are presented together in the center of the user's field of view but at different distances from him, ensuring that if one stimulus is focused on, the other one is non-focused, and vice versa; with the aim of providing an alternative way of sending commands through a stimuli selection by a focusing mechanism. In this sense, first, a model of VEP generation for two stimuli is introduced and the hypothesis that distinguishable SSVEP can be elicited by the focused stimulus, regardless of the non-focused stimulus is also present, is tested by employing the SFT-based ORD. Next, a demodulation method based in LPF and HPF is proposed for the case in that two stimuli are present in the field of view; and spatial-temporal retinal response for flickering stimuli is described by using PSF and NPSF functions. Finally, CCA, PSDA, LASSO with EEG signals re-referenced at Pz and CAR are employed to detect the SSVEP pattern. Accuracy rate, Kappa coefficient, AUC, and ITR are used to evaluate the detection performance. As a result of the hypothesis test, the absence of evoked potentials due to a focused stimulus, when a non-focused stimulus is also present was rejected in most of the cases. In SSVEP detection experiments, an average accuracy rate of 0.93 was achieved for a time window of 7s and for eight healthy subjects who were asked to focus on just one stimulus at a time.

Keywords: Human-machine interaction, Brain-computer interface, Steady-state visual evoked potential, Depth-of-field, Electroencephalography.

List of Figures

Figure 1 – Setup for conventional BCI-SSVEP system.	21
Figure 2 – Setup for the novel BCI-SSVEP paradigm.	22
Figure 3 – Representation of the visual system	25
Figure 4 – The electromagnetic spectrum	26
Figure 5 – Schematic diagram of the human eye	27
Figure 6 – Focusing light from distant and near sources.	28
Figure 7 – Relative distribution of the cones and rods on the retina	29
Figure 8 – Topographic maps of cones e rods.	30
Figure 9 – Functional representation of visual pathways	31
Figure 10 – Representation of the visual field on the retina and the visual cortex.	32
Figure 11 – Perimeter chart of the field of view.	33
Figure 12 – Simplified flowchart of parallel visual pathways	33
Figure 13 – Example of EEG signals	34
Figure 14 – Location and nomenclature of EEG electrodes.	35
Figure 15 – Typical Visual evoked potentials (VEP) waveform	36
Figure 16 – Comparison between VEP waveforms	37
Figure 17 – VEP waveform as a function of stimulation frequency	38
Figure 18 – Waveforms responses to flickering stimulus and frequency spectra.	39
Figure 19 – Design and operation of a BCI system.	40
Figure 20 – Design and operation of a SSVEP-BCI	41
Figure 21 – Covert versus overt attention	42
Figure 22 – Timeline of BCI research	43
Figure 23 – Timeline of gaze-independent SSVEP-BCI research.	44
Figure 24 – The novel stimulation setup based on Depth-of-Field	47
Figure 25 – Distances of placement of stimuli in the novel setup	48
Figure 26 – Projections of focused and non-focused stimulus in the field of vision	49
Figure 27 – Blurriness of non-focused objects.	50
Figure 28 – Schematic diagram of Depth-of-field and depth-of-focus.	51
Figure 29 – Point spread function caused by diffraction	52
Figure 30 – Some point spread functions and their corresponding simulated images	53
Figure 31 – Images of focused and non-focused objects	53
Figure 32 – Example of Depth-of-field with three cards.	54
Figure 33 – Retinal blur and distance.	55
Figure 34 – Depth-of-field and defocusing.	56
Figure 35 – Accommodation of the lens.	57
Figure 36 – Illustration of spectral EEG responses for three cases	60

Figure 37 – Conventional linear model of the Electroencephalographic (EEG) signal during visual stimulation	61
Figure 38 – Linear model of VEP generation for two stimuli.	63
Figure 39 – Protocol of an experiment that includes ten trials of three tasks of 7s.	66
Figure 40 – Bartlett periodogram of signals recorded at electrode Oz.	67
Figure 41 – SFT results and Hypothesis test evaluation	68
Figure 42 – Bartlett periodogram of spontaneous signals	70
Figure 43 – Bartlett periodogram of signals due to isolated stimulus flickering at 5.6 Hz	71
Figure 44 – Bartlett periodogram of EEG signals caused by focused and non-focused stimuli flickering at 5.6 Hz and 6.4 Hz, respectively.	72
Figure 45 – H_0^{yb} evaluated with EEG signals due to isolated stimulus flickering at 5.6 Hz.	74
Figure 46 – H_0^{xb} evaluated with EEG signals recorded when focused (5.6 Hz) and non focused (6.4 Hz) stimuli were present in the subjects’ field of view	75
Figure 47 – H_0^{yb} evaluated with EEG signals recorded when focused (5.6 Hz) and non focused (6.4 Hz) stimuli were present in the subjects’ field of view	76
Figure 48 – Bartlett periodogram of spontaneous signals	79
Figure 49 – Bartlett periodogram of EEG signals due to isolated stimulus flickering at 6.4 Hz	80
Figure 50 – Bartlett periodogram of signals caused by focused and non-focused stimuli flickering at 6.4 Hz and 5.6 Hz, respectively.	81
Figure 51 – H_0^{yb} evaluated with signals due to isolated stimulus flickering at 6.4 Hz	82
Figure 52 – H_0^{xb} evaluated with EEG signals recorded when focused (6.4 Hz) and non focused (5.6 Hz) stimuli were present in the subjects’ field of view.	83
Figure 53 – H_0^{yb} evaluated with EEG signals recorded when focused (6.4 Hz) and non focused (5.6 Hz) stimuli were present in the subjects’ field of view.	84
Figure 54 – Traditional Brain-computer interface based on Steady-state visual evoked potentials (SSVEP-BCI) modulation/demodulation	86
Figure 55 – Modulation/demodulation for the Novel Setup	88
Figure 56 – Image projection due to an isolated stimulus	94
Figure 57 – Image projection of two stimuli placed in the traditional setup way when stimulus flickering at f_1 was gazed.	95
Figure 58 – Image projection of two stimuli placed in the traditional setup way when stimulus flickering at f_2 was gazed.	95
Figure 59 – Image projection of two stimuli placed in the novel setup way when stimulus flickering at f_1 was focused on.	97
Figure 60 – Image projection of two stimuli placed in the novel setup way when stimulus flickering at f_2 was focused on.	97

Figure 61 – Experimental procedure to evaluate the inequality of visual evoked response due to defocusing	99
Figure 62 – Spectral response of occipital-parietal electrodes for NxF5 and N6F5 tasks.	101
Figure 63 – Spectral response of occipital-parietal electrodes for NxF5 and N6F5 tasks	102
Figure 64 – Normalized spectral power of the amplitude of focused and non-focused stimuli.	103
Figure 65 – Experimental procedure to evaluate the demodulation based on power spectrum peak detection.	108
Figure 66 – Detection accuracy for N6F5/N6F5 tasks	110
Figure 67 – Detection accuracy for N5F6/N5F6 tasks	111
Figure 68 – Experimental procedure to evaluate the eyeball movements by using EOG device.	112
Figure 69 – Search criteria of scientific production in SSVEP-BCI	130
Figure 70 – Documents published in SSVEP-based BCI between 2005 and 2015 . . .	131
Figure 71 – Countries with highest number of SSVEP-BCI documents.	132
Figure 72 – Important research groups in SSVEP-BCI.	134
Figure 73 – Electrode placement	139
Figure 74 – Simulation of retinal blurry.	140
Figure 75 – Object $O(x, y)$ and its image projection $I(x, y)$	141

List of Tables

Table 1 – Comparison of the accuracy and ITR of BCI reviewed paper	46
Table 2 – Detection accuracy for all subjects, average of the accuracy and its standard deviation for CCA-12, CCA-8, LASO, and PSDA detection methods, N6F5 and N5F6 settings and TW = 7s.	109
Table 3 – Average of the accuracy (Acc.), Cohen’s Kappa Coefficient, Area under curve (AUC) and Information transfer rate (ITR) for CCA-12, CCA-8, Least absolute shrinkage and selection operator (LASSO), and Power spectral density analysis (PSDA) detection methods, N6F5 and N5F6 settings and for Time window (TW) of 4 and 7 s.	109
Table 4 – Comparison of the accuracy and ITR of this Thesis with the reviewed papers. H : Healthy, End : End user, on : online, and off : offline.	117

Acronyms

ALS Amyotrophic lateral sclerosis.

AUC Area under curve.

BCI Brain-computer interface.

BPF Band-pass filter.

CAR Common average reference.

CCA Canonical correlation analysis.

CNS Central nervous system.

CRT cathode ray tube.

DFT Discret Fourier transform.

DMD Duchenne muscular dystrophy.

ECoG electrocorticographic.

EEG Electroencephalographic.

EMG Electromyographic.

EOG Electrooculographic.

ERD event related to desynchronization.

ERP event related potentials.

ERS event related to synchronization.

F Fisher.

FFT Fast Fourier transform.

FIR Finite impulse response.

fMRI functional magnetic resonance imaging.

GBS Guillain-Barre syndrome.

HMI Human-machine interaction.

HPF High-pass filter.

ITR Information transfer rate.

LASSO Least absolute shrinkage and selection operator.

LCD liquid crystal display.

LED Light-emitting diode.

LGN Lateral geniculate nucleus.

LIS Locked-in state.

LPF Low-pass filter.

MEG magnetoencephalographic.

NPSF Neural point spread function.

ORD Objective response detection.

PSD Power spectral density.

PSDA Power spectral density analysis.

PSF Point spread function.

ROC Receiver operating characteristic.

SCP slow cortical potentials.

SFT Spectral F-test.

SMR sensorimotor rhythms.

SNR Signal noise rate.

SSVEP Steady-state visual evoked potentials.

SSVEP-BCI Brain-computer interface based on Steady-state visual evoked potentials.

TW Time window.

VEP Visual evoked potentials.

List of symbols

λ	Wavelength
φ_h	Horizontal angle
φ_v	Vertical angle
f_i	Frequency of the i -th stimulus
d_i	Distance of the i -th stimulus
z_f	Distance of the farthest stimulus
z_n	Distance of the nearest stimulus
z_0	Distance of the focused stimulus
ΔD	Defocusing degree
\mathbf{x}	Bi-dimensional coordinates
D	Pupil size
P	Pupil factor
b_0	Distance from the lens to the retina
f_a	Focal length
d	Diameter of blurriness
$u(n)$	Input caused by an isolated stimulus
$v(n)$	Visual evoked potential of an isolated stimulus
$y(n)$	Output signal for an isolated stimulus
$H(f)$	Transfer function of the visual pathway for an isolated stimulus
$u_i(n)$	Input caused by the i -th stimulus
$v_i(n)$	Visual evoked potential of the i -th stimulus
$x(n)$	Output signal for two stimuli
$b(n)$	Background EEG

$H_i(f)$	Transfer function for the i -th stimulus
$Y(f)$	DFT of $y(n)$
$P_{bb}(f)$	PSD of signal $b(n)$
$P_{yy}(f)$	PSD of signal $y(n)$
$P_{xx}(f)$	PSD of signal $x(n)$
$\hat{P}_{bb}(f)$	Bartlett periodogram of of signal $b(n)$
$\hat{P}_{yy}(f)$	Bartlett periodogram of of signal $y(n)$
$\hat{P}_{xx}(f)$	Bartlett periodogram of of signal $x(n)$
M_b	Number of segments of $b(n)$
M_y	Number of segments of $y(n)$
M_x	Number of segments of $x(n)$
ϕ_{yb}	SFT between $y(n)$ and $b(n)$
ϕ_{xb}	SFT between $x(n)$ and $b(n)$
ϕ_{xy}	SFT between $x(n)$ and $y(n)$
α	Significance level
$F_{2M_y, 2M_b, \alpha}$	Critical value of SFT between $y(n)$ and $b(n)$ for α
$F_{2M_x, 2M_b, \alpha}$	Critical value of SFT between $x(n)$ and $b(n)$ for α
$F_{2M_x, 2M_y, \alpha}$	Critical value of SFT between $x(n)$ and $y(n)$ for α
H_0^{yb}	Null hypothesis of absence of effects of $y(n)$ in $b(n)$
H_0^{xb}	Null hypothesis of absence of effects of $x(n)$ in $b(n)$
H_0^{xy}	Null hypothesis of absence of effects of $x(n)$ in $y(n)$
$s(t)$	EEG signal
$g(t)$	Analytical signal
$A(t)$	Envelope of the EEG signal
$\phi(t)$	Phase of the EEG signal
$\omega(t)$	Instantaneous angular frequency ($2\pi f$)

$P_{ss}(\omega)$	Power spectrum of $s(t)$
$s_i(t)$	Filtered EEG signal for i -th stimulus
$g_i(t)$	Amplitude of $s_i(t)$
$A_i(t)$	Phase of $s_i(t)$
ω_i	instantaneous frequency for s_i
a_i	Scalar values for analytical demodulation for i -th stimulus.
M	Magnification coefficient
$O(\mathbf{x})$	Bi-dimensional coordinates of object points
$I(\mathbf{x}, \lambda)$	Bi-dimensional coordinates of image points
ϵ	Eccentricity
ω_0	Frequency of an isolated stimulus
ξ	Spontaneous EEG
θ	Angle of an isolated stimulus
$\Delta\theta$	Angle required to gaze an stimulus
θ_i	Angle of the i -th stimulus
w_i	Temporal window
ρ	Correlation coefficient
β	Regression coefficient
$\hat{\beta}$	Sparsity solution for LASSO
ε	Noise vector for LASSO
λ_L	Penalty parameter for LASSO
κ	Cohen's Kappa coefficient
S_{snr}	SNR for PSDA

Contents

1	INTRODUCTION	19
2	FUNDAMENTALS AND LITERATURE REVIEW	25
2.1	Background: From Light to Command	25
2.1.1	Image Formation	27
2.1.2	Visual Pathway	30
2.1.3	Topographic Representation	32
2.1.4	EEG and VEP	34
2.1.4.1	VEP	35
2.1.4.2	Influence of Refractive Error in VEP	36
2.1.4.3	SSVEP	37
2.1.4.4	SSVEP stimulation	38
2.1.5	BCI based on SSVEP	39
2.1.5.1	SSVEP-BCI	40
2.1.5.2	SSVEP-BCI and the Selective Attention	41
2.2	Current State of Gaze-independent SSVEP-BCI Research	42
3	THE NOVEL STIMULATION SETUP	47
3.1	Non-focused Objects and Depth-of-field	50
3.2	Optical Point spread function	52
3.3	Retinal Blurry Model	54
3.4	Accommodation of the Eye	57
3.5	Summary	58
4	STATISTICAL EVALUATION	59
4.1	Model of VEP generation and the Objective response detection (ORD) based on Spectral F-test (SFT)	61
4.2	Model of VEP generation for two stimuli and the ORD based on SFT	63
4.3	Materials	65
4.4	Results	67
4.5	Discussion	77
5	EQUATION FOR SSVEP DEMODULATION	85
5.1	Traditional Modulation/Demodulation	86
5.2	Proposed Modulation/Demodulation	88
5.3	Spatio-temporal Retinal Response for a Flickering Stimulus	90

5.4	Power Spectrum of the Retinal Response	93
5.5	Experimental Evaluation	98
5.5.1	Materials	99
5.5.2	Results	100
5.6	Discussion	103
6	SSVEP PEAK DETECTION	105
6.1	Analysis Methods	105
6.1.1	Experimental Procedure	107
6.2	Results	108
6.3	EOG measurements	112
6.4	Summary	113
7	GENERAL DISCUSSION AND CONCLUSION	114
7.1	General Discussion	114
7.2	Conclusion	119
	Bibliography	120
	APPENDIX	129
	APPENDIX A – SSVEP-BCI IN THE LAST TEN YEARS	130
	APPENDIX B – PUBLICATIONS, AWARDS AND SCHOOLS	135
	APPENDIX C – EEG POSITIONS	139
	APPENDIX D – SIMULATION OF RETINAL BLURRY MODEL	140
	APPENDIX E – PSF AND NPSF	141
	Index	143

1 Introduction

Nowadays, the interaction between humans beings and machines, or [Human-machine interaction \(HMI\)](#), has reached a high level of developing, as can be observed in devices with touchscreen interfaces or wireless keyboards. However, many times this kind of technology is not suitable for people with physical handicaps, such as quadriplegic individuals. In this cases, alternative interfaces could be proposed by employing biological signals in order provide an alternative way to externalize the user intentions. Biological signals can be recorded by employing [Electromyographic \(EMG\)](#) or [Electrooculographic \(EOG\)](#) devices, accelerometers, gyroscopes, or eye-tracking devices. For instance, a system with eye-tracking can be used to control devices, such as robotic wheelchair. But, what about people with severe paralysis who cannot control voluntarily their muscles? In recent years, neuro-degenerative diseases such as [Amyotrophic lateral sclerosis \(ALS\)](#) ([HUGGINS, 2010](#)), [Duchenne muscular dystrophy \(DMD\)](#) ([BUSHBY et al., 2010](#)) or [Guillain-Barre syndrome \(GBS\)](#) ([BIRBAUMER, 2005](#); [NIJBOER; BROERMANN, 2010](#)) have become relevant. Patients with these diseases lose progressively the control of their muscles ending in a situation called [Locked-in state \(LIS\)](#), in which people are almost paralyzed and only conserve a residual control of few muscles. It is a condition in which patients are aware but cannot move or communicate verbally due to the paralysis of nearly all voluntary muscles of the body. The [ALS](#) is the most known of these diseases because in 2014, the Ice Bucket Challenge¹ that promote the awareness of the this disease, received media attention around the world. It is a progressive neurodegenerative disease that affects nerve cells in the brain and the spinal cord. Another disease that has captured the attention of the media is the [GBS](#) because in late 2015 by its possible relation with the Zika virus². Notwithstanding, [LIS](#) also might be a result from traumatic brain-injury, hypoxia, stroke, encephalitis, or a brain tumor ([NIJBOER; BROERMANN, 2010](#)).

A [Brain-computer interface \(BCI\)](#) is a system that provides an alternative channel of communication between brain signals and a computer that does not involve traditional ways as muscle and nerves. It can be used by healthy people or patients who retain some voluntary muscle control in rehabilitation to command a robotic wheelchair or a prosthesis. In people with reduced mobility in [LIS](#), [BCIs](#) became a good alternative for communication with their environment or with other people, such as a nurse or a therapist. Patients could use these systems to express their basic needs such as thirst, hunger or pain, even for expressing their preferences in terms of treatment planning, like

¹ For details, please refer to www.alsa.org.

² In 2015, several cases of patients presenting Zika virus was detected in Brazil ([ZANLUCA et al., 2015](#)) and an unusual increase of [GBS](#) also was reported in the Northeast of the country; possible associations began to be investigated (www.who.int).

pain management or end-of-life decision-making (LAUREYS, 2005; GANTNER et al., 2013) The most common non-invasive method employed in BCI is based on EEG signals. In 2002, a first patient in LIS regains some measure of communication through EEG-based BCI, developed by neurological researcher Niels Birbaumer (BENEVIDES, 2013). Riccio et al. (2012) conducted an analysis of EEG-based BCI for people with reduced mobility. Also, Marchetti & Priftis (2014) performed a meta-analysis about BCI in ALS. EEG based BCIs have attracted the interest of Brazilian researchers. For instance, Ferreira (2008) proposes a BCI to command a robotic wheelchair, Muller (2010) developed a BCI based on Steady-state visual evoked potentials (SSVEP) with high performance that also was tested with a robotic wheelchair, and Benevides (2013) proposed a BCI architecture based on motor mental tasks. These studies were developed at the Intelligent Automation Lab of the Federal University of Espirito Santo led by the supervisor of this Thesis. Relevant research groups around the world are described briefly in Appendix A.

Problem statement

Currently, SSVEP-BCI systems are presenting good performance, because they achieve high accuracy rates in the detection of brain activity associated to a BCI command. In traditional SSVEP-BCI systems, a set of stimuli are presented to users and they are asked to gaze on one stimulus (Figure 1a). Then, analyzing their EEG signals, systems detect which stimulus the subjects is gazing on. Finally, a command that is associated with a target stimulus is sent to computers. However, as shown in Figure 1b, in SSVEP-BCI systems, users must perform movements redirecting their neck, head or eyeball to chose another stimulus. When users redirect their gazing, a target stimulus is placed in the center of the field of view and the non-target stimulus is placed outside the field of view. The main advantage of SSVEP-BCI systems is given by their high Signal noise rate (SNR) that is attained when the target stimulus is in the center of this view. Paradoxically, it main disadvantage is given by the dependence of muscular movements. It makes that traditional SSVEP-BCI systems are not suitable for patients with paralysis.

To overcome this muscle dependence, independent SSVEP-BCI have been proposed, in which the user selects one out of several superimposed stimuli or stimuli close to each other by selective attention without redirecting their gaze. This kind of system represents a good option for paralyzed people who cannot control with precision their gaze in order to select a target by performing an exhaustive attention activity instead of voluntary muscular activity. But this time, the disadvantage is given by the low accuracy rates achieved by attention-based SSVEP-BCI systems. Also, previous training stages are necessary because subjects must learn to maintain their covert attention on the target stimulus that is placed next to the non-attended one, and at the same distance.

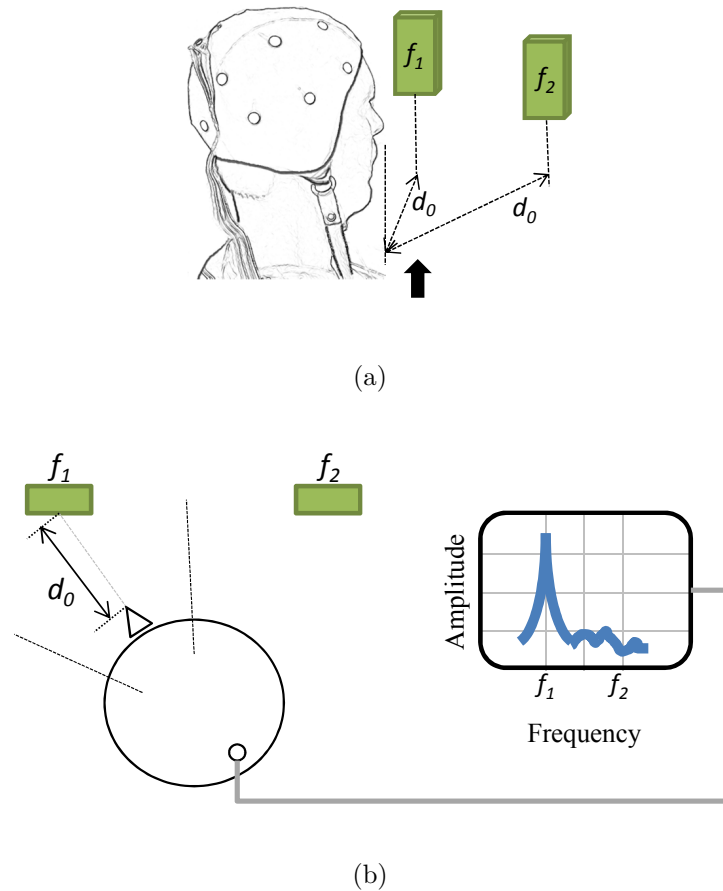


Figure 1 – Setup for conventional **SSVEP-BCI** system. (a) A subject with two **SSVEP** stimuli placed at the same distance d_0 and flickering at frequencies f_1 and f_2 . (b) Representation of subject and stimuli, in which dotted lines are the user’s field of view. Frequency vs amplitude display represents the frequency of the attended stimulus that can be extracted from **EEG** signals.

Purpose of this Thesis

In this Thesis a novel paradigm for **SSVEP-BCI** is proposed in which two stimuli also are presented together in the center of the user’s field of view but at different distances from him/her, as shown in Figure 2a. It makes for that if one stimulus is focused on, the other one is non-focused on, and viceversa.

Considering that a) when an object is being focused on by the eye, objects behind and in front of the point of focus are blurred, and the zone where objects are judged to be in focus is referred to as the Depth-of-Field ([HOWARD, 2012](#); [PENTLAND, 1987](#)); b) the human’s eye is able to refocus and sharpen the image in a certain range when the distance from the object changes, and the “accommodation” is the mechanism of the eye to adjust its focal length to focus on objects at different distances ([EBENHOLTZ, 2001](#); [GREGORY, 1997](#)); and c) the amplitude of the response in a pattern of **VEP** is dependent on the degree of retinal image focus ([SONGNIAN et al., 2014](#); [SOKOL](#); [MOSKOWITZ,](#)

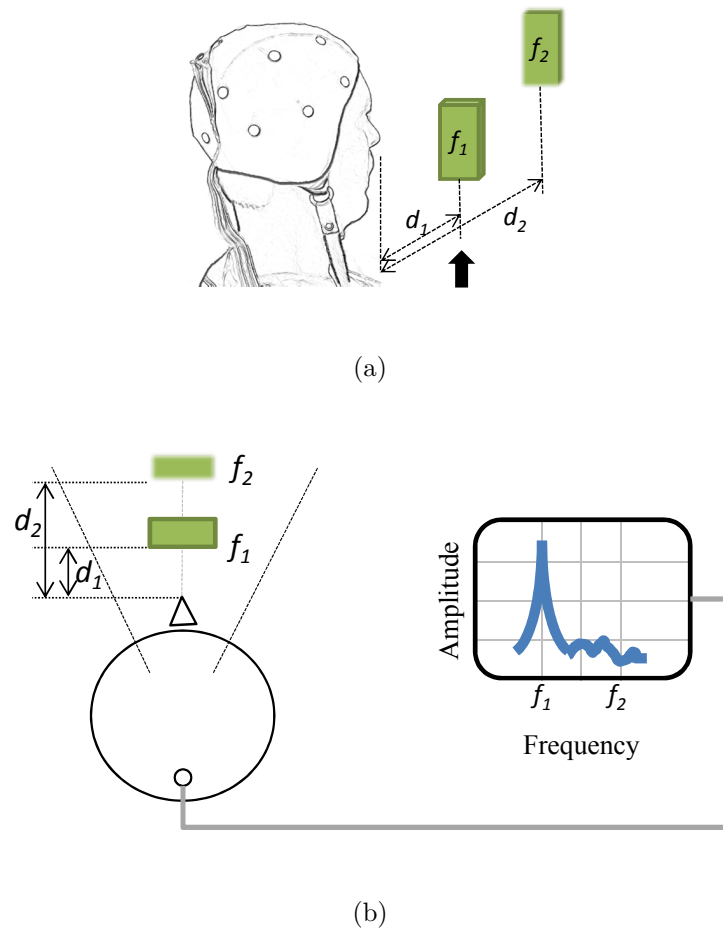


Figure 2 – Setup for the novel BCI-SSVEP paradigm. (a) A subject with two SSVEP stimuli placed at the same direction but at different distances (d_1 and d_2) and flickering at frequencies f_1 and f_2 . (b) Representation of subject and stimuli, in which dotted lines are the user's field of view. Frequency vs. amplitude display represents the frequency of the attended stimulus that can be extracted from EEG signals.

1981); then, the novel setup here proposed allows users to make a selection by a refocusing mechanism that in turn does not demand neck, head and/or eyeball movements. A high accuracy rate will be achieved if the amplitude of the response of focused stimulus due to it is higher than the amplitude of the response of the non-focused one.

Hypothesis

If two stimuli are presented simultaneously in the center of the field of view of the BCI user, flickering at different frequencies and located at different distances from the user, then, the focused stimulus will be able to elicit a distinguishable SSVEP pattern regardless of the presence of the non-focused stimulus.

Objective

The main objective of this Thesis is to propose a novel SSVEP-BCI paradigm based on Depth-of-field optical phenomenon, in which two stimuli are presented together in the center of the user's field of view but at different distances from him, ensuring that if one stimulus is focused on, the other one is non-focused on, and vice versa; with the aim of providing an alternative way of sending commands through a stimuli selection by focusing mechanism. In this sense, first, a model of VEP generation for two stimuli is introduced and the hypothesis that distinguishable SSVEP can be elicited by the focused stimulus, regardless of the non-focused stimulus is also present, is tested by employing the ORD based on SFT. Next, a demodulation method based in Low-pass filter (LPF) and High-pass filter (HPF) is proposed for the case in which two stimuli are present in the field of view; and spatial-temporal retinal response for flickering stimuli is described by using Point spread function (PSF) and Neural point spread function (NPSF) functions. Finally, Canonical correlation analysis (CCA), PSDA, LASSO with EEG signals re-referenced at Pz and Common average reference (CAR) are employed to detect the SSVEP pattern. Accuracy rate, Kappa coefficient, AUC, and ITR are used to evaluate the detection performance.

Contribution

As a result of the hypothesis test, the absence of evoked potentials due to a focused stimulus, when a non-focused stimulus is also present was rejected in most of cases. In SSVEP detection experiments, an average accuracy rate of 0.93 was achieved for a time window of 7s for eight healthy subjects who were asked to focus on just one stimulus at a time. Therefore, the novel paradigm proposed in this Thesis that is based on Depth-of-field phenomenon represents a promissory alternative for communication in patients with reduced mobility, because focusing mechanism does not demands head, neck and/or eyeball movement, even they occur.

Production

It was produced three publications in journals, an original article is under review, and another one is being prepared; two book chapters; and twelve conference papers, nine and three in international and national events, respectively. For details please refer Appendix B.

Thesis Outline

In Chapter 2 a brief review of theoretical background is performed with the intention to show a concepts sequence starting to light external stimulus and ending into the BCI command obtained after demodulating the visual information within EEG signal recorded

at occipital brain region. Furthermore, a revision of the current situation of [SSVEP-BCI](#) and gaze independence was conducted. It has been convenient to talk about covert and overt attention and the gaze-independence before to talk about relevant works. In [Chapter 3](#) the stimulation setup is described. Also, Depth-of-Field, [PSF](#), retinal blurry models and accommodation mechanism of the human eye are shown briefly. The PSF key concept that associates the blurriness degree of the non-focused stimulus and the distance is explained together with the retinal blur model. Then, a stimulation unit is built considering these optical and physiological concepts. Next, in [Chapter 4](#), the hypothesis of the absence of responses due to focused and non-focused stimuli are tested. Also, a linear model of [VEP](#) generation presented in ([MELGES; SA; INFANTOSI, 2012](#)) is described and a model for two stimuli are proposed. Then, in order to evaluate the amplitude of the response of focused and non-focused stimuli, in [Chapter 5](#) an expression to denotes the spatio-temporal retinal response is elaborated based on visual perception parameters as wavelength, distance of the stimulus or density of photoreceptors. Furthermore, a equation to express the demodulation process for two stimuli is proposed. After performing the hypothesis test and proposing the equation for demodulation, in [Chapter 6](#) the proposal of this Thesis is evaluated by employing well know [SSVEP-BCI](#) detection methods. Accuracy of the detection, the Kappa coefficient, the [AUC](#) and the [ITR](#) are used int he evaluation. The eyeball movement also is evaluated. Finally, a general discussion and the conclusion of the Thesis are conducted.

2 Fundamentals and Literature Review

In this chapter, a theoretical background is provided. It starts by defining the light and ends by presenting a BCI command due to the light stimulus. Figure 3 illustrates the “way of the light” that is emitted by a visual stimulus and sensed by the human visual system. The, visual information is carried to the brain visual cortex in which the signal evoked by the object can be measured. A BCI takes the measured signal and translate it into a command. In this sense, basic concepts about light, eye and brain are briefly presented. Next, the image formation, the visual pathway, the topographic representation of the image and the response of visual cortex are described. Then, EEG and VEP are presented. Transient VEP, steady-state VEP and how the refraction errors affect the VEP are discussed. Also, SSVEP-BCI and how the light is translated into commands, are addressed. This theoretical background is principally based on well-know medical physiology, optics, neural science and human eye books (GUYTON; HALL, 2006; KANDEL; SCHWARTZ; JESSELL, 1991; GREGORY, 1997; EBENHOLTZ, 2001; ATCHINSON; SMITH, 2000; HOWARD, 2012).

Finally, a literature review of the more relevant works in the gaze-independent SSVEP-BCI research is performed.

2.1 Background: From Light to Command

Light is a form of electromagnetic radiation emitted by the oscillation of materials electrically charged. Light travels in straight lines unless it encounters an object that causes it to be reflected or refracted when it turns back in the opposite direction or it

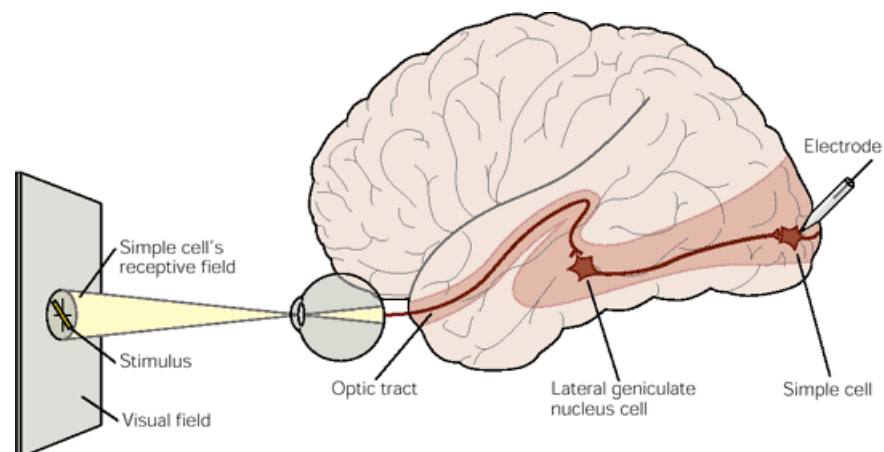


Figure 3 – Representation of the visual system, together with a stimulus, visual field and single cell electrode. Modified from Kandel, Schwartz & Jessell (1991).

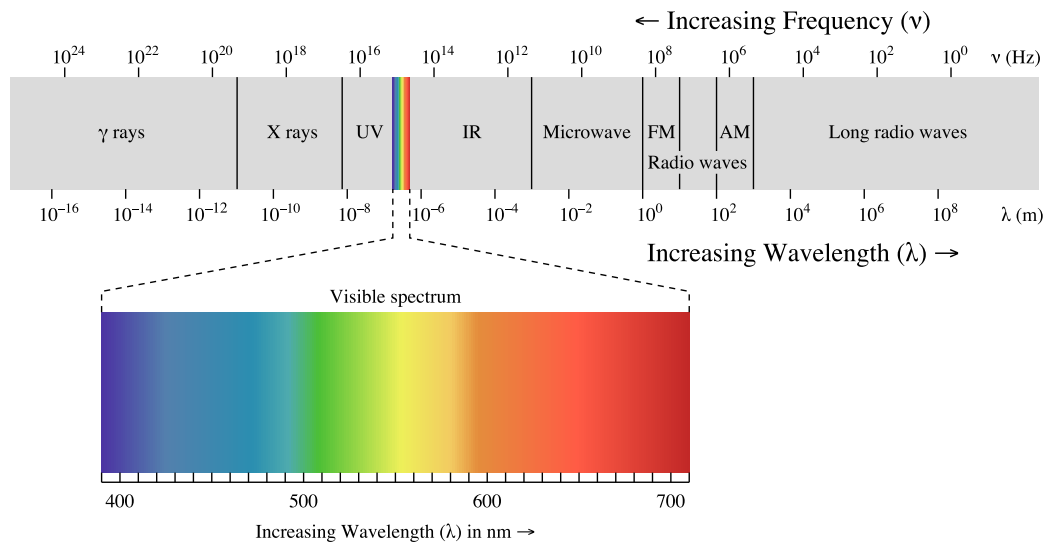


Figure 4 – The electromagnetic spectrum. The numbers indicate wavelength in nanometers ($1 \text{ nm} = 1 \times 10^{-9} \text{ m}$). The band of visible light is highlighted. Adapted from Gregory (1997).

bends traveling at an angle relative to the original path, respectively. Also, the light can be absorbed by the object. Electromagnetic oscillations have a regular sinusoidal pattern that can be characterized in terms of its wavelength that is perceived as a color. Visible light includes electromagnetic waves that have wavelengths between about 350nm and 750nm; in which different colors correspond to different wavelengths within this range (GREGORY, 1997). All objects reflect light to different degrees and the luminance determine they relative contrasts. Vision is based primarily on the perception of bright-dark contrasts and color contrast enables complex organisms to distinguish surfaces if they reflect different portions of the visual spectrum.

The eye is a complex optic system in the human body that contains about 125 million neurons specialized to turn light into electrical signals called photoreceptors (GUYTON; HALL, 2006). A schematic diagram of a horizontal, sectional view through a human eye is shown in Figure 5. The cornea and the sclera are the transparent membrane over the front of the eye and the white membrane around the sides and back of the eyeball, respectively. The iris, which is the colored part of the eye, controls the aperture of the pupil regulating the amount of light entering the eye. The pupil is the aperture at the center of the iris, through which light enters the eye. The crystalline lens of the eye or lens is a transparent and flexible structure; by changing its curvature through the contraction or relaxation of the intrinsic muscles of the eye, light coming from different sources is projected on the back of the eye.

Vision is the faculty or state of being able to see. In human eye, the light enters through the cornea and then passes through the pupil. Gazed objects are projected onto

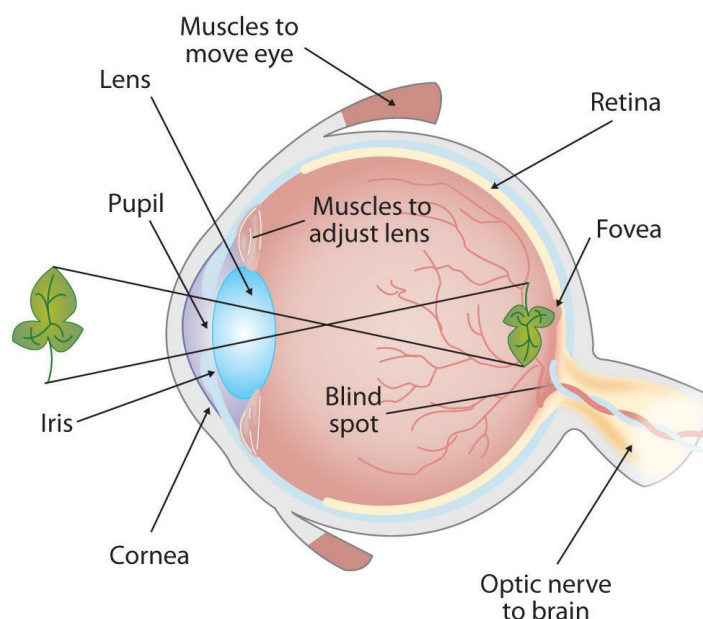


Figure 5 – Schematic diagram of the human eye. The image of the external object passes through the focusing system to be projected on the fovea of the retina; note that it becomes inverted in doing so. The blind spot is the region of the retina without photoreceptors. Adapted from [Stangor \(2012\)](#).

the retinal surface that acts like a movie screen of the eye. Images are projected sharp when lens focuses on the object. Any image formed on the retina should cause nerves to fire sending a signal along the optic nerve to be “seen” by the brain. The retina is the innermost layer of the eye whose functions is the phototransduction, converting the light energy into the electrical energy. The retinal surface consists of neural tissue that contains the photoreceptors, which are the cells that detect the light waves. Photoreceptors that detect dim light and bright light are named as rods and cones, respectively. The optic nerve consists of the axons of neurons in the retina; it transmits information from the retina to the brain. The fovea is the central region on the retina, in which light from the center of the visual field strikes. It is the area of the retina with the greatest visual acuity. The optic disk is the portion of the retina where the optic nerve passes through the retina.

2.1.1 Image Formation

Light is composed by divergent waves that propagate in all directions from every point of a visible object. Before a sharp image of the object is projected into the retina, light is focused on by the human optical system; then, the light of the projected image attains light-sensitive receptor cells of the retina; next, signals of receptors arrive to the brain through the visual pathway. Responses measured at the visual cortex are related to the topographic association between retinal and cortex fields ([KANDEL; SCHWARTZ; JESSELL, 1991](#)).

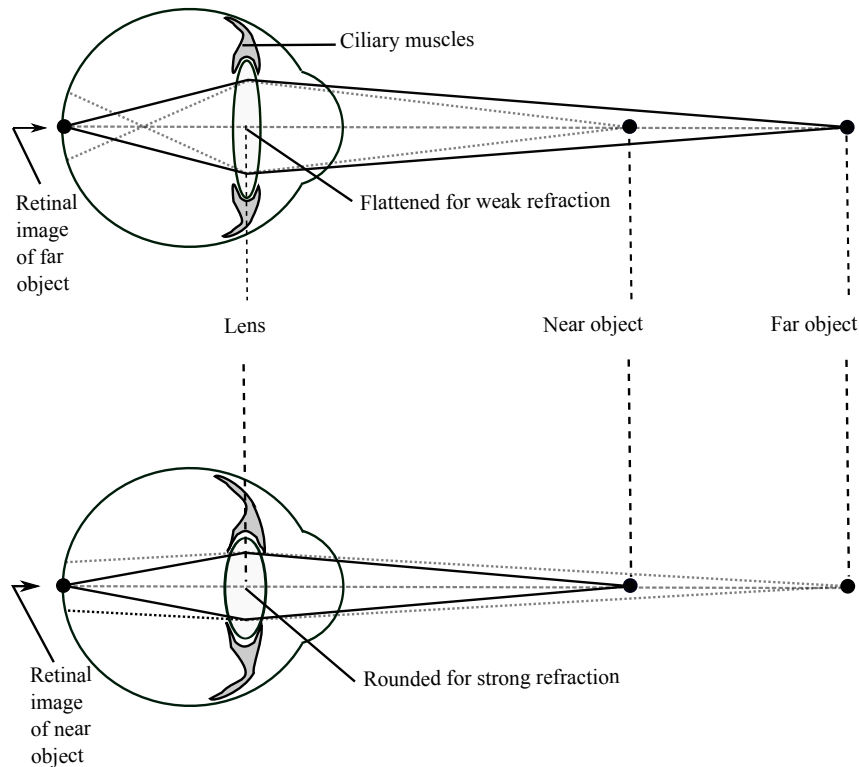


Figure 6 – Focusing light from distant and near sources. a) A relatively flat (weak) lens is sufficient to converge the light waves reflected from a distant object on the retina. b) A rounder (strong) lens is needed to converge the light waves reflected from a near object on the retina.

Focusing the light

Lens is the primary structure responsible for making adjustments for viewing objects at various distances. The mechanism to adjust the focus of the eye so that we can concentrate the attention on an object of interest altering the shape of the lens is called accommodation. Depending on the distance of the object, small muscles attached to the lens, contract or relax, changing its curvature (Figure 6). These muscles are named as ciliary muscles. The amount of light entering the eye is controlled by the iris and the pupil. Stimulation of sympathetic nerves to the iris causes these muscles to contract, which then enlarges the pupil, whereas stimulation of the parasympathetic nerves causes the diameter of the iris to get smaller (EBENHOLTZ, 2001).

Imaging the object

The photoreceptors cones are the cells in which transduction takes place, converting light energy to electrochemical energy that results in patterns of action potentials in the optic nerve. In human eyes two different types of photoreceptors, commonly called rods and cones can be found (Figure 7). Cones are concentrated in the fovea, dispersed retinal pathways and have high acuity in bright light. It makes the fovea essential for daytime

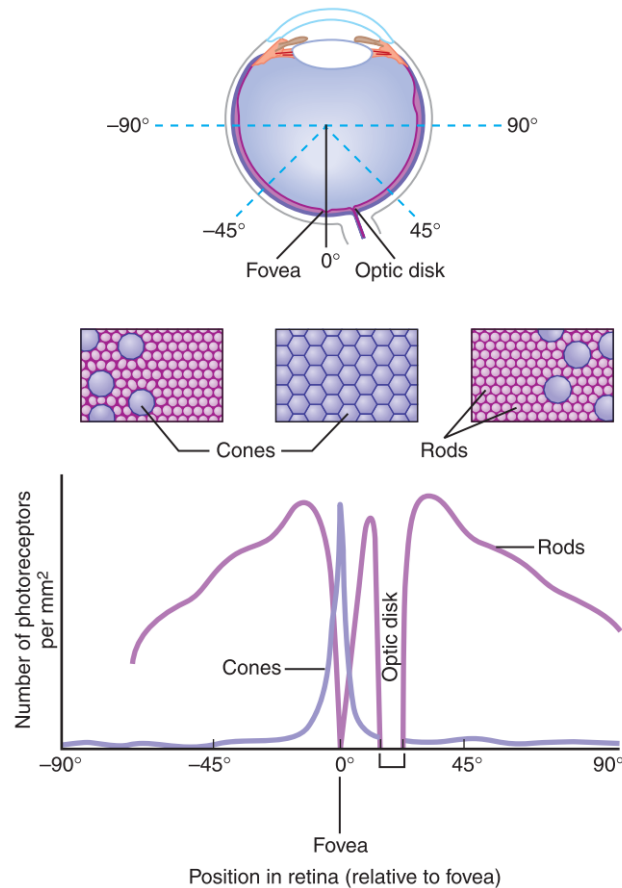


Figure 7 – Relative distribution of the cones and rods on the retina. The y-axis is the receptor density and the x-axis is the relative distance from the fovea. Note that the highest density of cone receptors is located in the fovea and there are no receptors where the optic nerve leaves the eyeball, thus creating a blind spot. The peripheral vision is primarily due to rods, hence we have minimal abilities to detect colors in those areas Adapted from [Kandel, Schwartz & Jessell \(1991\)](#).

vision. This is also the region of the retina where the image of an object of primary interest is being projected (hence, one controls the gaze towards it). Light-sensitive molecules are activated by specific ranges of wavelengths in the cones. Rods are not present in the fovea and are designed to provide some vision in dim light. Light molecules are activated by a broad range of wavelengths in the rods.

The fovea is the region of the retina with high density of photoreceptors that measures about 1.2mm in diameter. In this region, cone density increases almost 200-fold, reaching, at its center, the highest receptor packing density found anywhere else in the retina. This high density is achieved by decreasing the diameter of the cone outer segments such that foveal cones resemble rods in their appearance. The increased density of cones in the fovea is accompanied by a sharp decline in the density of rods as shown in Figure 8 ([KANDEL; SCHWARTZ; JESSELL, 1991](#); [PACKER; R.WILLIAMS, 2003](#)). In this Thesis, from here cones are referred as photoreceptors.

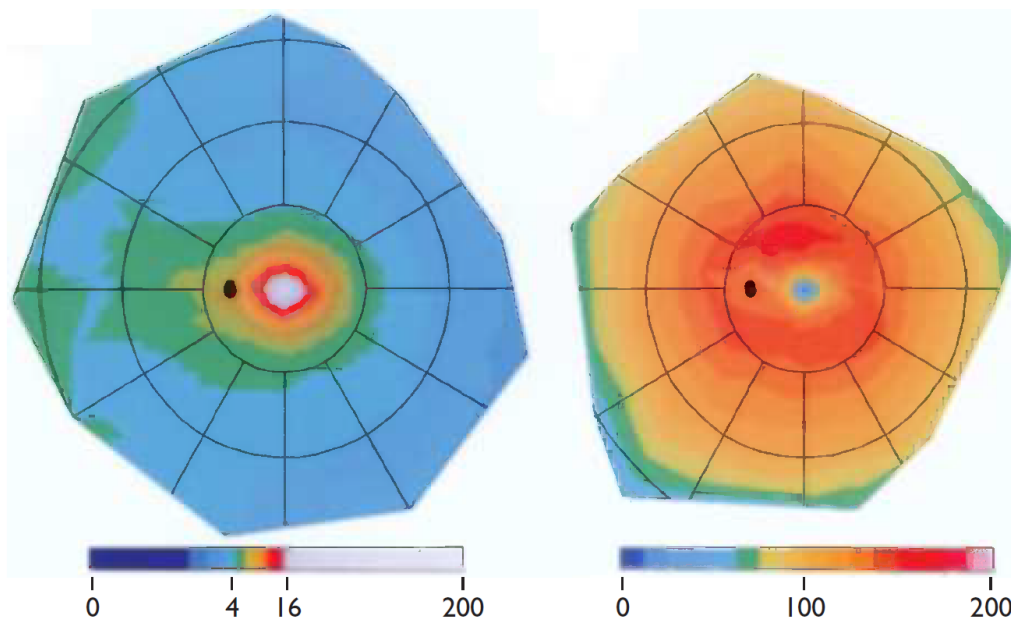


Figure 8 – Color topographic maps of cone (Left) and rod (Right) numerical density. The density scale, shown under each map, is photoreceptors/ $\text{mm}^2 \times 1000$. Blue and white colors represent regions with low and high densities, respectively. Areas in white exceed 16000 photoreceptors/ mm^2 . The rings are spaced at intervals of about 20° . The fovea is at the center of the inner ring. Nasal and temporal retina are to the left and right of the fovea, respectively. Adapted from [Packer & R.Williams \(2003\)](#).

2.1.2 Visual Pathway

The visual pathway is a pathway over which a visual sensation is transmitted from the eyes to the brain ([KANDEL; SCHWARTZ; JESSELL, 1991](#)). As illustrated in Figure 3, the pathway starts in a receptive field of a cells and can be recorded in a single cell of cortex. The visual pathway includes the retina, optic nerve, the [Lateral geniculate nucleus \(LGN\)](#) and visual cortex, in which a) optic nerve is formed by the axons of ganglion cells that are the output neurons from the retina, which generate action potentials that are transmitted to the [Central nervous system \(CNS\)](#); b) [LGN](#) that is a sensory relay that is located in the thalamus that transmits information captured by the retina to the visual cortex is composed of six layers; layers 1 and 2 are called the magnocellular layers, while Layers 3, 4, 5 and 6 are called parvocellular layers; and c) the primary visual area of the cerebral cortex, that is known as striated cortex or cortex V1, is the first stage of cortical processing of visual information.

Cortex V1 contains a complete map of the visual field covered by the eyes. It receives its main visual input from the [LGN](#) of the thalamus, and sends its main output to subsequent cortical visual areas. Cortex V1 is traditionally divided in 6 horizontal layers, with a characteristic distribution of inputs and outputs across layers. Inputs from [LGN](#) arrive in layer 4. For instance, this layer is divided into sublayers 4A, 4B, 4C α , and 4C β .

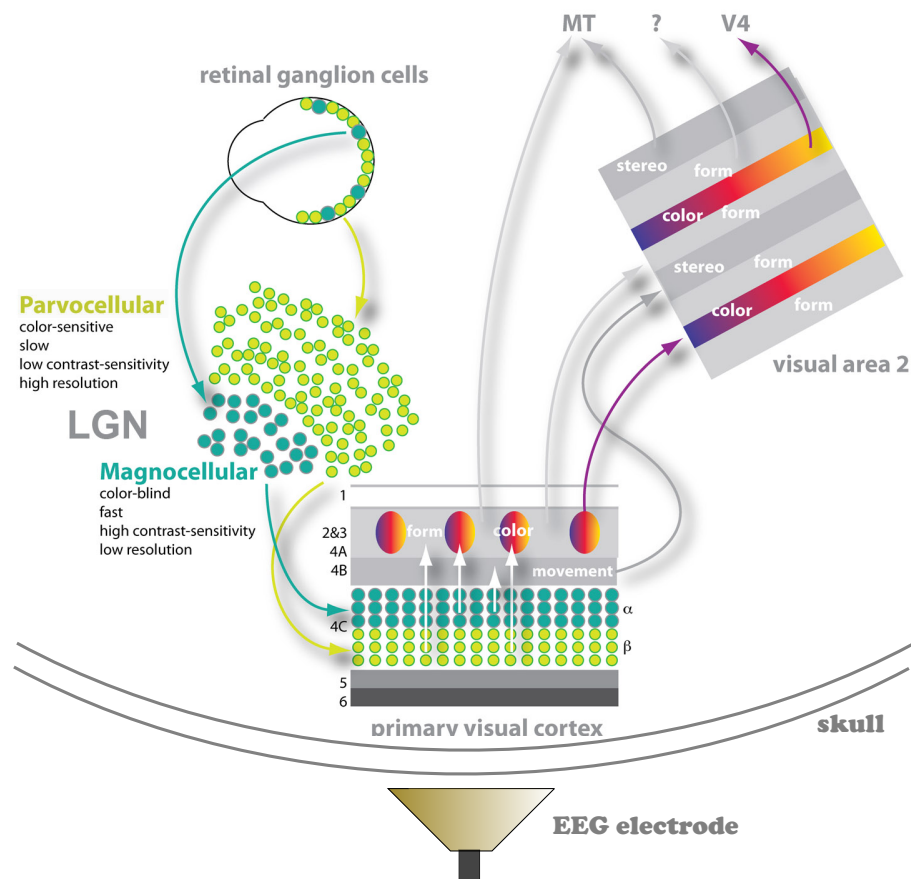


Figure 9 – Functional representation of visual pathways. Magnocellular (dark green) pathway starts at ganglion cells, and arrives to layer 4C α of cortex V1 after passing the layers 1 and 2 of LGN. Parvocellular (light green) pathway starts at ganglion cells, passes the layers 3-6 of LGN and arrives to layer 4C β of cortex V1. Then visual information flows to superior brain regions such as V2, V4 or V5 (also called MT). Modified from [Livingsstone & Hubel \(1988\)](#).

The main LGN inputs arrive in 4C, and segregate depending on the source: magnocellular LGN cells to 4C α and parvocellular cells to 4C β .

In summary, the visual system possesses parallel processing, in which segregated pathways transmit different attributes of a stimulus, for example to color and luminance contrast sensations they have different pathways. Figure 9 shows the Parvocellular (or P-pathway) and Magnocellular (or M-pathway) pathways. M-pathway has high contrast sensitivity and does not perceive color. P-pathway is color-sensitive and has low contrast sensitivity. M-pathway (dark green) starts at large ganglion cells, projects first into magnocellular layers of LGN and then into layer 4C α primary visual cortex. P-pathway (light green) starts at small ganglion cells, projects first into parvocellular layers of LGN and then into layer 4C β primary visual cortex ([LIVINGSSTONE; HUBEL, 1988](#); [KANDEL; SCHWARTZ; JESSELL, 1991](#); [GUYTON; HALL, 2006](#)).

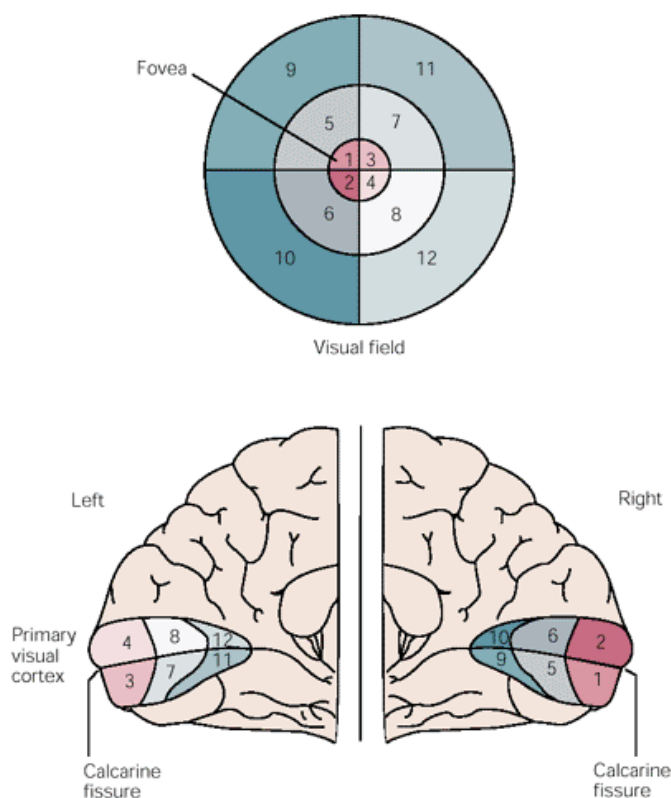


Figure 10 – Representation of the visual field in the fovea and in the primary visual cortex. This representation is not proportional, for the neural information obtained by the receptors within the fovea projects onto a large portion of the visual cortex. Adapted from [Kandel, Schwartz & Jessell \(1991\)](#).

2.1.3 Topographic Representation

The representation of different points in the visual field across a population of cortex neurons is called a topographic representation or topographic map. As shown in Figure 10, areas in the primary visual cortex are destined to specific parts of the visual field, as indicated by the corresponding numbers. Beginning with the ganglion cells, each level of the visual system projects to the next level in an organized way so that the map of visual space on the retina is preserved. The area at the center of the visual field (areas 1-4) that corresponds to the fovea is expanded in the cortex so that it occupies about half of the entire cortical representation ([KANDEL; SCHWARTZ; JESSELL, 1991](#)).

Field of Vision

Figure 11 shows the field of vision and its perimeter of the left eye. Field of vision corresponds to the visual area seen by the eye at a given instant. It is plotted when the eye is looking toward a central spot directly in front of the eye. Numbers are degrees, and the eccentricity angle in degrees is the distance by which a target is displaced from the fovea. A blind spot caused by lack of rods and cones in the retina over the optic disc is found about 15 degrees lateral to the central point of vision.

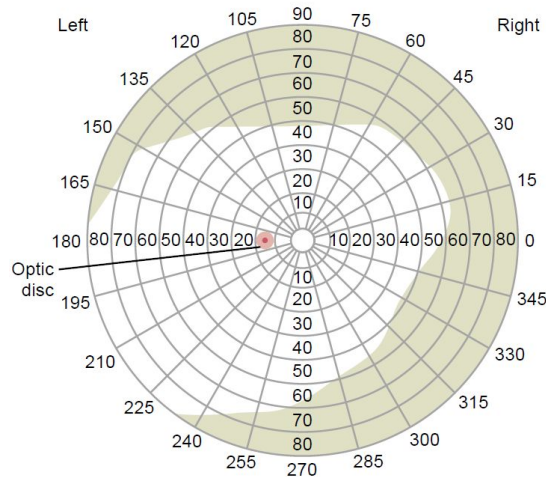


Figure 11 – Perimeter chart showing the field of vision for the left eye. White and gray regions indicate where the light or object can be seen or it cannot, respectively. Adapted from [Guyton & Hall \(2006\)](#).

Response at the Visual Cortex

In general, the visual system processes visual features such as motion, color, form, and depth separately and carries this information in parallel neural pathways ([KANDEL; SCHWARTZ; JESSELL, 1991](#)). Although information is projected to superior visual, temporal and parietal areas, activity of Cortex V1 can be measure with non-invasive [EEG](#) electrode. Figure 12 shows a simplified flowchart of parallel processing for contrast and luminance information, in which the skull effect is represented by a low-pass filter ([HUGGINS, 2010](#)) that acts over responses of both layers ($4C\alpha$ and $4C\beta$). [EEG](#) signal in visual cortex denoted by $s(t)$ can be intended as the sum of the response due to parallel pathways with spontaneous [EEG](#) denoted as ξ .

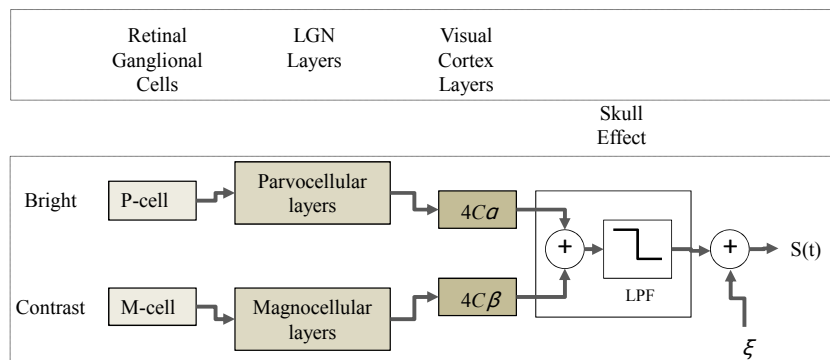


Figure 12 – Simplified flowchart of parallel visual pathways. [LGN](#), lateral geniculate nucleus; M, magnocellular; P, parvocellular. Parvo pathway is composed by P-cell, Parvocellular layers of [LGN](#), and $4C\alpha$ layer of visual cortex. Magno pathway is composed by M-cell, PMagnocellular layers of [LGN](#), and $4C\beta$ layer of visual cortex. [LPF](#) and ξ represent the effect of the skull and the spontaneous [EEG](#), respectively.

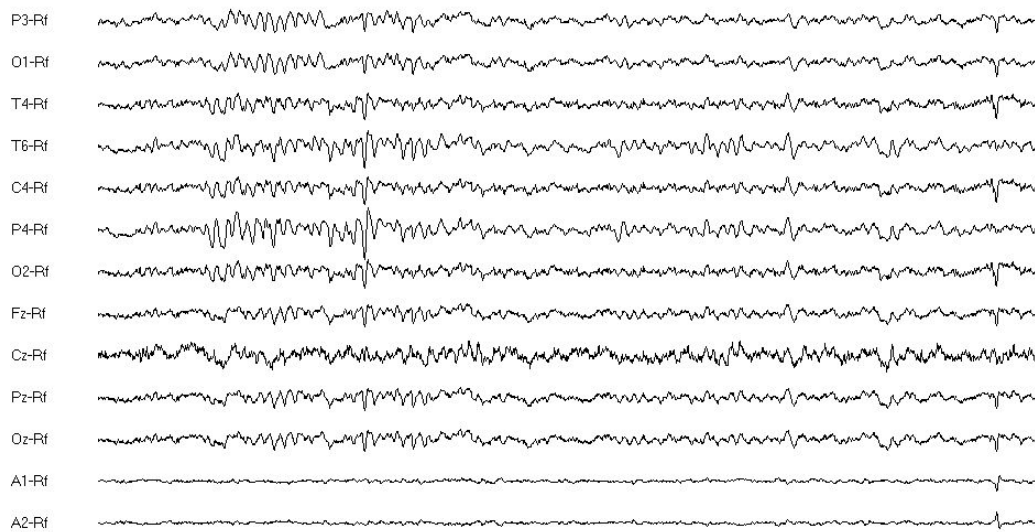


Figure 13 – Example of EEG signals of a set of channels with bi-auricular reference and grounded at forehead. Signals of high amplitude and low frequency are signals recorded when user was asked to close his eyes.

2.1.4 EEG and VEP

EEG signals are the neuro-physiologic measurements of the electrical activity of the brain using electrodes placed on the scalp. The resulting traces are known as EEG waves and they represent the electrical activity of a large number of neurons. The capture of EEG is a non-invasive procedure that reads scalp electrical activity generated by brain structures and frequently used for diagnostic purpose. The electroencephalographic traces (Figure 13) are defined as electrical activity recorded from the scalp surface after being picked up by metal electrodes and conductive medium. Only large populations of active neurons can generate electrical activity recordable on the head surface. Between electrode and neuronal layers current penetrates through skin, skull and several other layers. Weak electrical signals detected by the scalp electrodes are massively amplified, and then displayed on paper or stored in computer memory. Due to capability to reflect both the normal and abnormal electrical activity of the brain, EEG has been found to be a very powerful tool in the field of neurology and clinical neurophysiology. Unfortunately, in addition, the EEG also reflects activation of the head musculature, eye movements, interference from nearby electric devices, and changing conductivity in the electrodes due to the movements of the subject or physicochemical reactions at the electrode sites. EEG corrupted by other signals are called artifacts (NUNEZ; SRINIVASAN, 2006).

The internationally standardized 10-20 system is usually employed to record the spontaneous EEG, in which the electrode locations are determined by dividing the perimeter into 10% and 20% intervals. An extension to the 10/20 system is the 10/10 system characterized by intervals of 10% that provides a higher channel density. Jurcak, Tsuzuki &

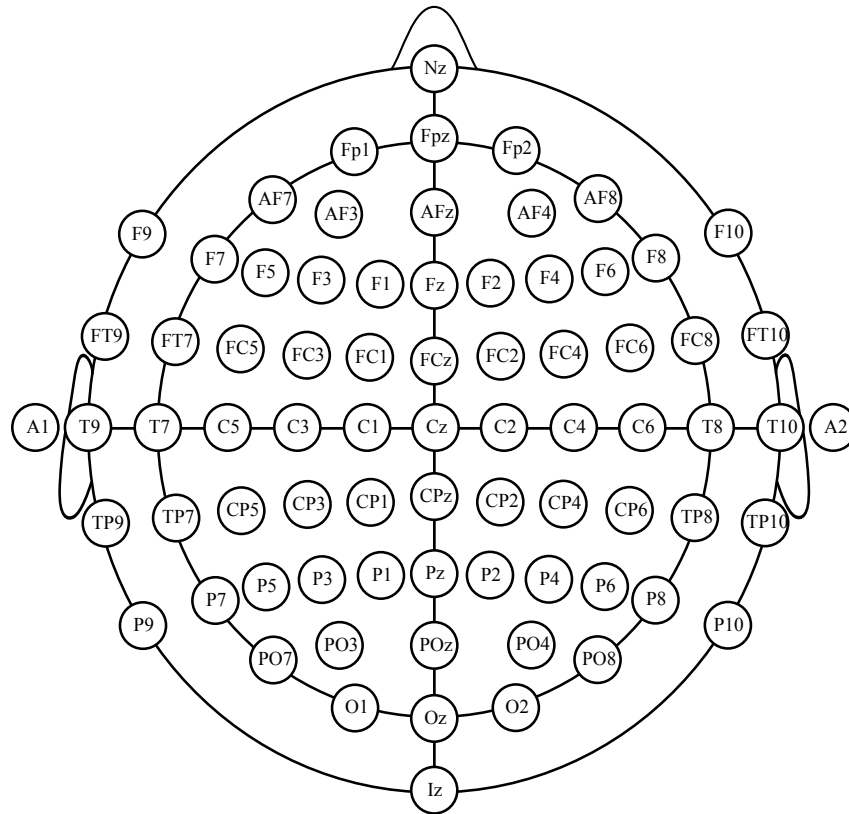


Figure 14 – Location and nomenclature of the intermediate 10% electrodes, as standardized by the American Electroencephalographic Society. The electrodes are named by a capital letter corresponding to the initial of the brain lobe where they are placed (“F”, “C”, “P”, “O” and “T” for Frontal, Central, Parietal, Occipital and Temporal, respectively), followed by an even number for the right hemisphere and an odd number for the left hemisphere. The letter “A” is used for electrodes placed in the ear. For the electrodes placed in the frontal lobe, near the nasion, the letter “p” is added (Fp = Frontal pole). For the electrodes in the line connecting the nasion to the inion, the letter “z” is added.

Dan (2007) describe standardization of electrode locations and nomenclature, and evaluate both position systems. Figure 14 shows electrode positions according to the American Electroencephalographic Society.

2.1.4.1 VEP

An evoked potential is the electrical response recorded from the human nervous system following presentation of a stimulus that can be detected by EEG and EMG devices. VEP refer to electrical potentials, initiated by brief visual stimuli, which are recorded from the scalp overlying visual cortex. VEP occurs when a subject observes a visual stimulus, such as a flash of light or a pattern on a monitor. VEP are used primarily to measure the functional integrity of the visual pathways from retina via the optic nerves to the visual cortex of the brain. Their waveforms are usually extracted from the EEG signals by averaging. As shown in Figure 15, VEP waveforms are represented on curve

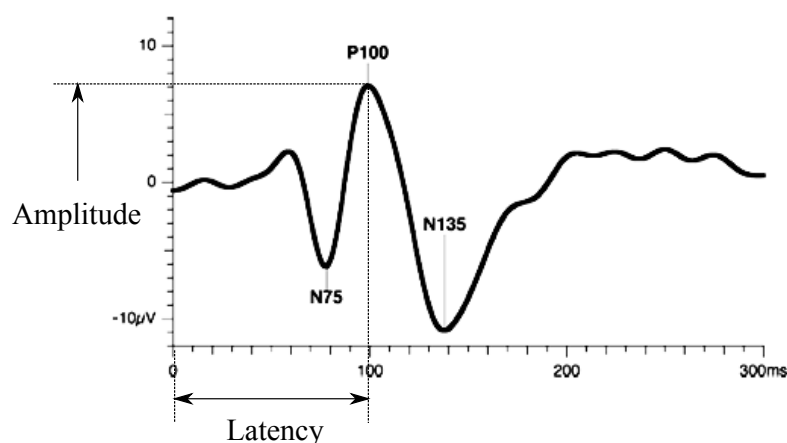


Figure 15 – Typical **VEP** waveform. Abnormal waveform may indicate a problem with the visual information reaching the cortex. In general terms, the amplitude indicates the integrity of the neural structures including axons conducting information along the visual pathway. Latency indicates the time the electrical signal takes to travel from the retina to the visual cortex. The combination of amplitude and latency is helpful in determining the health of the visual pathway (ODOM et al., 2010; SOKOL, 1976).

using amplitude and time (latency) measurements (ODOM et al., 2010; SOKOL, 1976). A transient **VEP** is obtained when the stimulus rate is low and the response is recorded over one single stimulus cycle. A typical waveform of transient **VEP** is composed of two positive peaks, P50 and P100, and a negative peak referred to as N75, which are shown at about 50, 100, and 75 ms after visual stimulation, respectively. Any abnormality that affects the visual pathways or visual cortex in the brain can affect the **VEP** waveform. **VEP** elicited by flash stimuli can be recorded from many scalp locations in humans; visual stimuli stimulate both primary visual cortices and secondary areas.

2.1.4.2 Influence of Refractive Error in VEP

It was found that technical and physiological factors such as pupil diameter or refractive errors affect the **VEP** (HARTER; WHITE, 1970 apud KOTHARI et al., 2014), because the amplitude of the pattern of an evoked potential is extremely sensitive to optical blurring. In ophthalmology this effect can be used as a means of determining refractive error by measuring the amplitude of the **VEP** with changes in power of trial lenses (SOKOL; MOSKOWITZ, 1981). Refractive errors will affect the interpretation of the **VEP** results, therefore it is important to take the subject visual acuity into consideration. In the 70s, it was shown that the amplitude of the pattern is sensitive to the optical blurring (MILLODOT; RIGGS; HARTER; WHITE, 1970, 1970 apud SOKOL, 1976). Defocusing causes a degradation of the sharpness of the contours of the checkerboard. Figure 16 shows an example in which VEPs are elicited in one subject with and without lenses. It was used lenses of various dioptric powers to adjust the defocus degree. It can

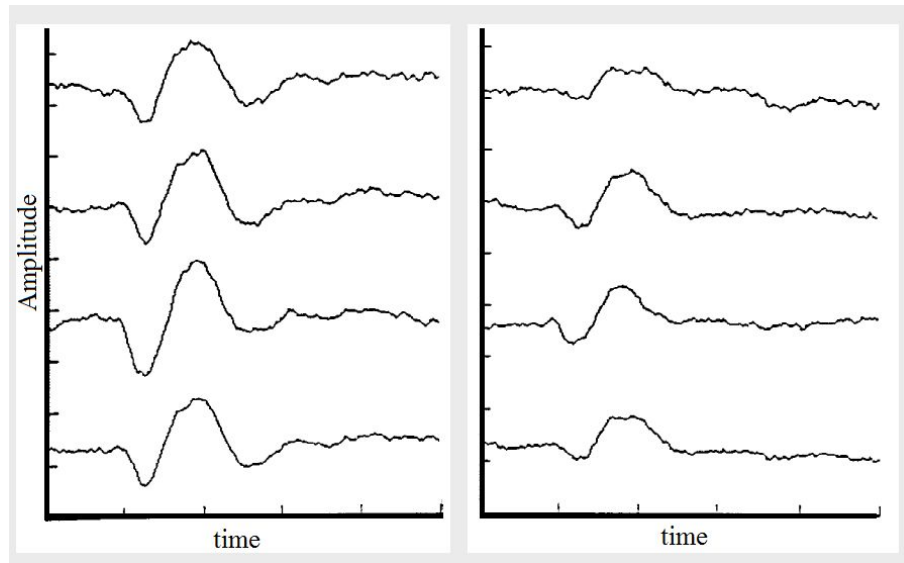


Figure 16 – Comparison between **VEP** waveforms with (left traces) and without correction lenses (right traces) of a subject with refraction deficit. From top to bottom, first and second are traces of right and left eye, respectively; the third trace corresponds to both eyes; and the lowest trace is the grand average of the potentials. Adapted from [Summa et al. \(1999\)](#).

be seen that the **VEP** amplitude is hardly influenced by refraction errors or by the degree of visual acuity of both eyes or in one of them.

2.1.4.3 SSVEP

VEP elicited by brief stimuli are usually transient responses of the visual system. These potentials are called “transient” because the slow rate of stimulation allows the sensory pathways to recover or “reset” before the next stimulus appears. When visual stimuli are presented at a constant rate that is rapid enough to prevent the evoked neural activity from returning to baseline state, the elicited response becomes continuous and is called as **SSVEP**. With steady-state stimulation the typical **VEP** wave form is markedly changed. At more rapid stimulation rates, the brain response to the same stimulus becomes sinusoidal and is typically modulated at the fundamental stimulus frequency in the case of an unstructured stimulus (e.g. flash) or at the second harmonic (double the stimulation frequency) if the stimulus is a pattern-reversal [17](#). Like any sinusoidal wave form, the **SSVEP** can be measured in terms of its amplitude and phase that vary as function of the temporal frequency, spatial frequency, contrast, luminance, and hue of the driving stimulus ([REGAN, 1989](#) apud [RUSSO; TEDER-SALEJARVI; HILLYARD, 2003](#)). Consequently, the amplitude distribution of the spectral content of SSVEP with characteristic SSVEP peaks remains stable over time. Because these characteristics are constant, many applications can be derived from SSVEP propagation properties ([VIALATTE et al., 2010](#)).

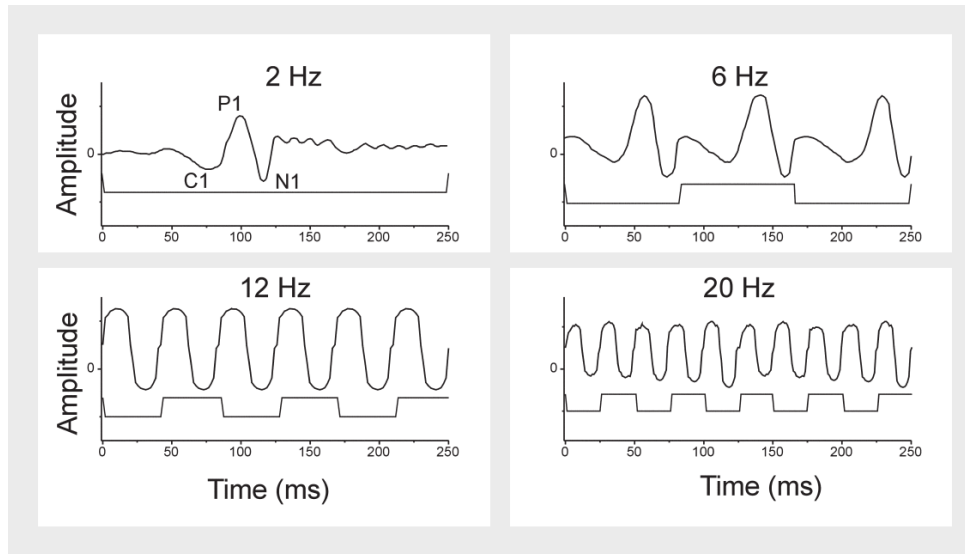


Figure 17 – VEP waveform as a function of stimulation frequency. Note that the waveform is basically modulated at the second harmonic of the stimulus frequency. At the slowest rate (2 Hz) the components of the transient VEP can be seen. C1, P1 and N1 represents N75, P100 and N135, respectively. Adapted from Russo, Teder-salejarvi & Hillyard (2003).

2.1.4.4 SSVEP stimulation

In SSVEP research, three main categories of repetitive visual stimuli exist a) Pattern reversal stimuli are rendered on a computer screen by oscillatory alternation of graphical patterns, for example, checkerboards. They consist of at least two patterns that are alternated at a specified number of alternations per second. b) Light stimuli are rendered using light sources such as Light-emitting diode (LED), fluorescent lights, and Xe-lights, which are modulated at a specified frequency. These devices are generally driven by dedicated electronic circuitry which enables them to accurately render any illumination sequence or waveform; c) And, single graphics stimuli (e.g., rectangle, square, or arrow) are rendered on a computer screen and appear from and disappear into the background at a specified rate. The stimulation rate is reported as the number of full cycles per second, normally simply referred to as the frequency of the stimulus.

As shown by Wu et al. (2008), the frequency spectrum of the SSVEP due to LED, cathode ray tube (CRT) or liquid crystal display (LCD) are very different from each other. It can be seen in Figure 18 that the frequency spectrum was the simplest for the LED which only contained the fundamental frequency and harmonics. The response of CRT contains additionally the monitor refreshing frequency (HERRMANN, 2001; PASTOR et al., 2003). For the LCD flicker, the frequency spectrum contains no refreshing frequency but many low-frequency components in addition to the fundamental frequency and harmonics. Due to the easy way of stimulation, SSVEP techniques are gaining increasing application in BCI research (WANG et al., 2010; KELLY et al., 2005a).

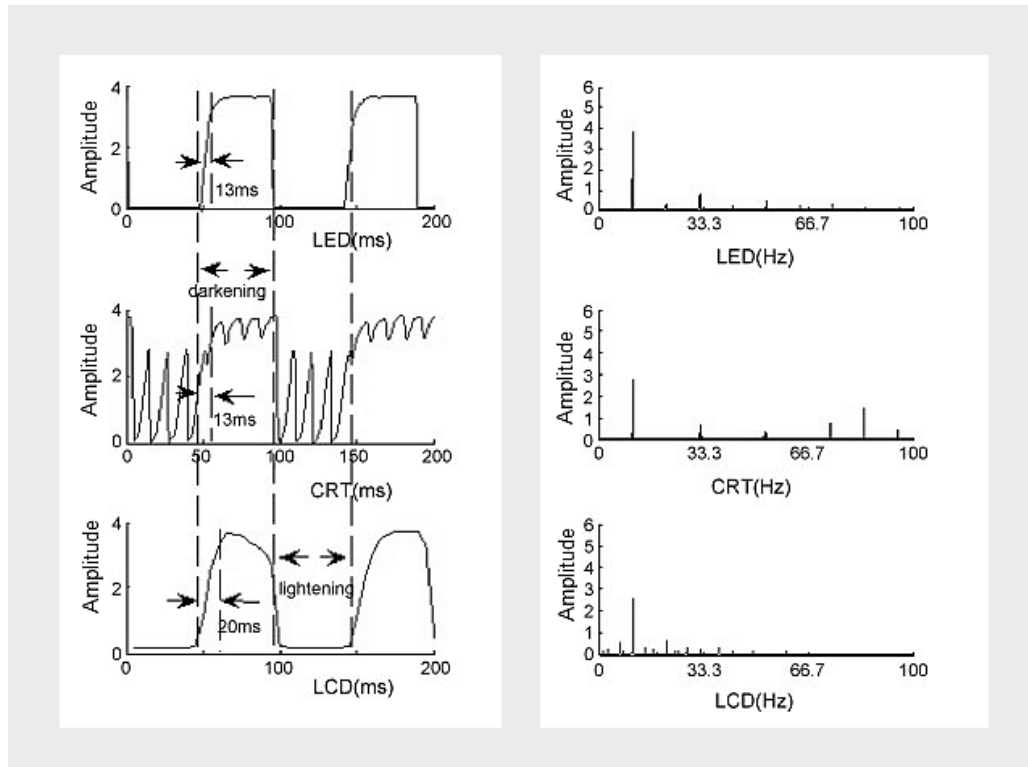


Figure 18 – Waveforms responses to flickering stimulus and frequency spectra. The stimulus frequency is 10.8 Hz. The left column shows the waveform in two cycles of the three flickers, and the right column is the frequency spectrum. Adapted from [Wu et al. \(2008\)](#).

2.1.5 BCI based on SSVEP

BCIs are systems that could help to restore useful functions to people severely disabled by a wide variety of devastating CNS and neuromuscular disorders and to enhance functions in healthy individuals ([WOLPAW et al., 2002](#)). These systems that measures EEG activity and converts it into artificial output that also can replace, restore, enhance, supplement, or improve natural CNS output and thereby changes the ongoing interactions between users and they external environment (Figure 19). A BCI is a computer-based system that acquires brain signals, analyzes, and translates them into commands that are relayed to an output device to carry out a desired action. Thus, BCIs do not use the brain's normal output pathways of peripheral nerves and muscles. This definition strictly limits the term BCI to systems that measure and use signals produced by the CNS.

A BCI records brain signals, extracts particular features from them, and translates the features into new artificial outputs that act on the environment or on the body itself. The output could replace natural output that has been lost for injury or disease, and help to restore lost natural output of someone with a spinal cord injury whose limbs are paralyzed. Also, it could enhance natural CNS output of someone who is engaged in a task that needs continuous attention, and supplement natural neuromuscular output of a

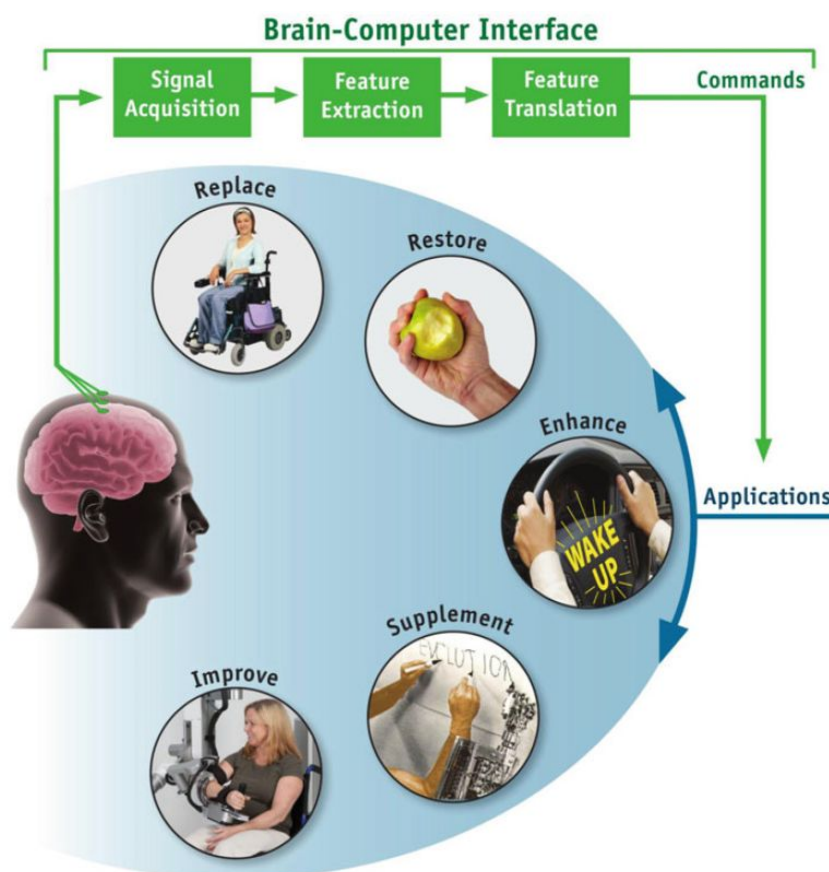


Figure 19 – Design and operation of a BCI system. It records brain signals, extracts specific features and translates them into commands. BCIs applications improve, supplement, enhance, restore or replace natural neuromuscular outputs. Adapted from He et al. (2013)

subject who is able to control, e.g. a robotic arm. In this sense, recent years have seen BCI applications as a novel and promising new channel of communication, control and entertainment not only for people with disabilities but also for healthy people.

2.1.5.1 SSVEP-BCI

As shown in Figure 17, the waveform of SSVEP is a function of the stimulation frequency. Two light sources flickering at different frequencies will evoked a brain response of different characteristics (amplitude, frequency or phase). In BCIs, evoked responses are associated to commands. Two or more stimuli oscillating at different constant frequencies are presented to users, who are instructed to attend an specific stimulus to send a command to the computer. When SSVEP is elicited, oscillatory components can be observed in the EEG signals that match the stimulation frequency over visual cortex (MIDDENDORF et al., 2000). The SSVEP-BCI has some advantages over other EEG-based BCI systems, including 1) high SNR (VIALATTE et al., 2010); 2) high ITR (VIALATTE et al., 2010); 3) less susceptibility to eye movements and blink artifacts as well as to EMG artifacts

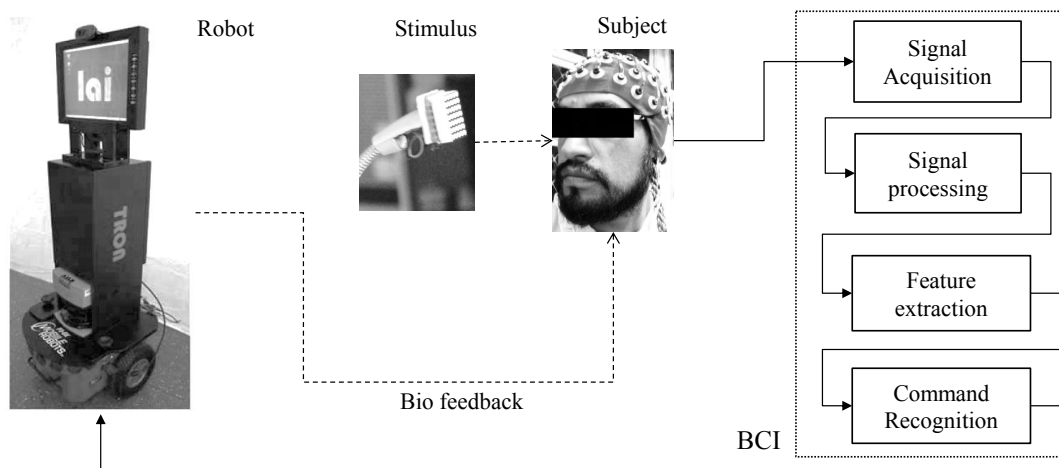


Figure 20 – Design and operation of a [SSVEP-BCI](#). Subject are asked to attend a flickering stimulus. Brain signals recorded during the stimulation are processed in order to extract representative features that are translated into commands. Robot are controlled with [BCI](#) commands. Adapted from [Ferreira et al. \(2008\)](#).

([LALOR et al., 2005](#)); and 4) the very little (or no) requirement of training, since the [VEPs](#) are inherent responses of the brain ([BIN et al., 2009](#); [VIALATTE et al., 2010](#)). An [SSVEP-BCI](#) system (Figure 20) enables the user to select among several commands that depend on the application, for example, moving a cursor on a computer screen ([ZHU et al., 2010](#)). The [SSVEP](#) response depends on a great extent on the characteristics of the stimulation source. The stimulation source color, intensity, duty cycle and especially flickering frequency all modulate the response. Software stimulation sources running on a computer consisting of alternate chessboard patterns or dedicated stimulation sources can be used to control intensity and waveform of stimulation signals. [SSVEP](#) patterns can be automatically detected through a series of signal processing steps including preprocessing (e.g., band-pass filtering), artifact detection/correction, feature extraction (e.g., spectral content at the stimulation frequencies), and feature classification. [BCI](#) performance is usually assessed in terms of classification accuracy, classification speed, number of available choices, and bit rate. In [SSVEP-BCI](#) systems, the classification accuracy is primarily influenced by the strength of the evoked response, the [SNR](#), and the differences in the properties of the stimuli. The classification speed depends on the time it takes for the [SSVEP](#) to be of sufficient strength. Increasing the number of targets offers a higher number of possible commands but can decrease classification accuracy and speed ([PASTOR et al., 2003](#)).

2.1.5.2 SSVEP-BCI and the Selective Attention

Although the traditional [SSVEP-BCI](#) systems are becoming robust systems, they are not suitable for patients with paralysis who does not have reliable control of eye

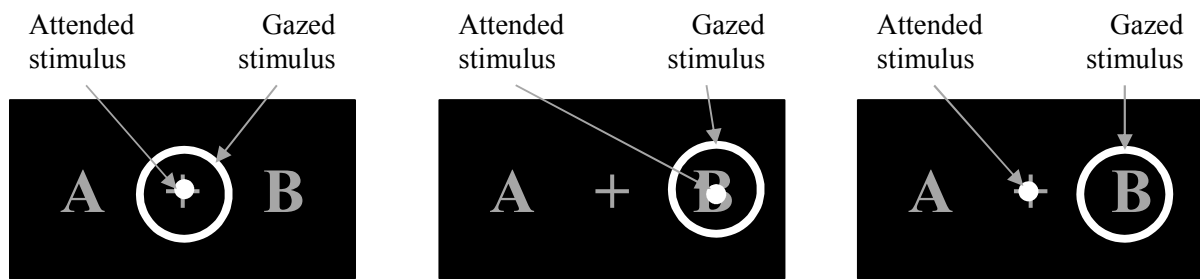


Figure 21 – Covert versus overt attention. (Left) Starting stage where gazing and attention are in the plus symbol. (Middle) Overt attention where both attention and gazing shift from plus symbol to letter B. (Right) Covert attention where only the attention shifts from plus symbol to letter B; Gazing directions does not change.

movements. Due to these systems demands muscular activity to attend a stimulus, they are called muscular dependent systems. Visual-spatial attention refers to the ability to selectively process the relevant events in the visual surroundings and ignore the irrelevant events. Attention can be directed to visual events in two ways; 1) head and eye movements can be employed to gaze directly to an object. This is often referred to as an overt shift of attention, and 2) alternatively, spatial attention can be directed towards the relevant object or event without movement of the eyes, often referred to as a covert shift of attention. Covert spatial attention allows an observer to attend events independent of eye movements. [Posner & Petersen \(1990\)](#) conclude that covert and overt attention shifts utilize different neural mechanisms.

Shift of attention is the mechanism that is employed in [SSVEP-BCI](#) to select one of a set of stimuli. It occurs when directing attention to a stimulus increased the efficiency of processing decreasing the processing of irrelevant stimulus. Figure 21 illustrates this mechanism, in which white circles and points were placed on the gazed and attended objects, respectively. First figure (left) represents an initial stage, in which an object is gazed and attended. The second figure (middle) illustrates the overt attention, in which the attention and gaze was shifted together. Due to, in the third figure (right), only the attention was shifted, it is called gaze-independent selection because muscular movements are not required to shift attention.

2.2 Current State of Gaze-independent SSVEP-BCI Research

[BCI](#) research has focusing on developing communication and control technologies for people with severe neuro-muscular disorders that could cause partial or complete paralysis. [BCIs](#) are using different technologies as [EEG](#), [magnetoencephalographic \(MEG\)](#) ([MELLINGER et al., 2007](#)), [electrocorticographic \(ECoG\)](#) ([POTES et al., 2012](#); [SCHALK](#);

LEUTHARDT, 2011), or intracortical recordings to measure the brain activity with high spatial resolution. Also, other signals as functional magnetic resonance imaging (fMRI) are being used to record information with high spatial resolution.

In BCI research area, the most common non-invasive method employed in BCI is based on EEG. In 1929, Hans Berger speculates about the possibility of reading the thoughts from EEG signals (BERGER, 1929 apud BIRBAUMER, 2005). Then, in 70's, the term BCI was coined by Vidal (1973). In almost 80's, the first SSVEP-BCI was proposed (REGAN, 1989 apud VIALATTE et al., 2010) and it was published studies demonstrating control of slow cortical potentials (SCP) (BIRBAUMER; KIMMEL, 1979 apud BIRBAUMER; COHEN, 2007). In 1988, a P300 speller based on event related potentials (ERP) was designed (FARWELL; DONCHIN, 1988). Late last century, applications of SSVEP-BCI was retook (CHENG; GAO, 1999 apud CHENG et al., 2002) and the basic principles of event related to desynchronization (ERD) and event related to synchronization (ERS) was described (PFURTSCHELLER; SILVA, 1999). Middendorf et al. (2000) develop a non-invasive SSVEP-BCI with two commands. In 2002, sensorimotor rhythms (SMR) were used to control a device with a BCI (WOLPAW et al., 2002). Figure 22 shows a timeline of the BCI research, in which are indicated the year in which BCI systems were proposed or developed. In the past decade, experiments to evaluate the the number of people that

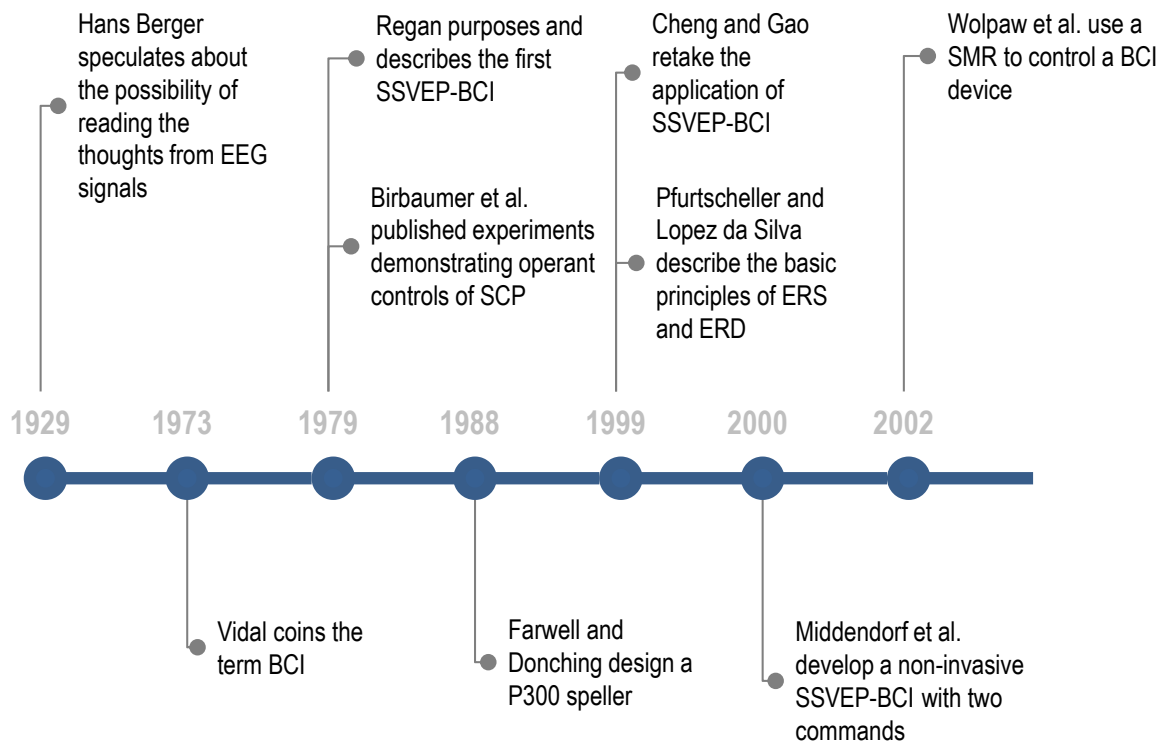


Figure 22 – Timeline of BCI research. It starts at 1929 when Berger speculated about the possibility of reading thoughts, and indicated when BCI systems based on SCP, ERD, P300, SMR and SSVEP was proposed or developed.

are able to operate BCI based on EEG. Regarding to BCI based on motor imagery and ERD, a demographic study conducted by Guger et al. (2003) achieved 93% of the subjects were able to achieve an classification accuracy above 60%. Regarding to BCI based on P300, a experiment conducted by Guger et al. (2009) achieved 72% of the subjects were able to spell with 100% accuracy. And, regarding to SSVEP-BCI, a demographic experiment conducted by Allison et al. (2010) it was achieved an accuracy average of 95%.

Although SSVEP-BCI is one of the systems presenting the best results, the disadvantage is given by its muscular dependence because subjects must to perform neck, head and/or eyeball to redirect their gaze direction making it not suitable for patients with deteriorated brain motor control. Notwithstanding, SSVEP-BCI systems that does not demands muscular movements are being proposed, for instance, exploring the covert attention as an alternative of stimulus selection. The representative studies in SSVEP-BCI that are not dependent of gaze movements are describe briefly below. To see how other BCI systems, such as P300 or motor imagery, are addressing the problem of gaze dependence please refer the study conducted by Riccio et al. (2012). Also, Marchetti & Priftis (2014) performs a meta analysis about BCI in ALS. Figure 23 shows a timeline of gaze-independent SSVEP-BCI research, in which systems based on spatial and non-spatial covert attention; and eye-closed systems are presented.

In a pioneer study, Kelly et al. (2004) showed that the transition from overt to covert attention in a SSVEP-BCI, allowing a binary decision, resulted in a reduction of classification accuracy by about 20% on average. In light of this performance decrease, the same authors redesigned the paradigm modifying the bilaterally displayed stimuli (visual angle) and obtained an average of binary accuracy of 70.3% (KELLY et al., 2005a).

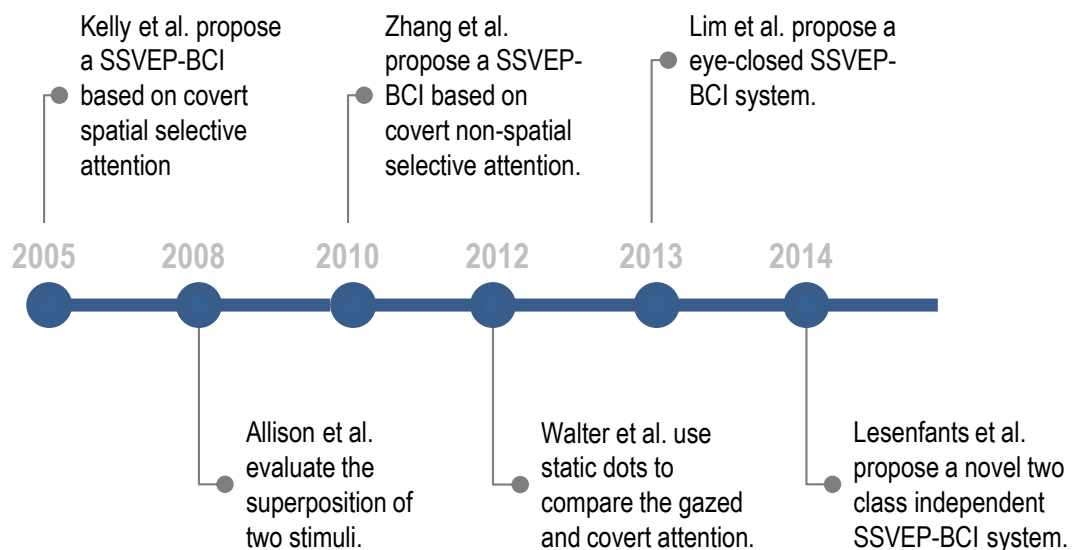


Figure 23 – Timeline of gaze-independent SSVEP-BCI research. Systems based on spatial and non-spatial covert attention; and eye closed are presented.

Allison et al. (2008) investigated the hypothesis that the superposition of visual stimulation patterns could evoke classifiable changes in SSVEP. They presented the subjects with two images each oscillating at a different frequency. The oscillating images could be presented either in a superimposed or separated condition, in order to explore the role of gaze function on the system performance. In half of the 14 involved healthy subjects the overlaid condition induced differences in SSVEP activity elicited by the visual stimulation patterns that were robust enough to predict an online BCI control. The authors demonstrated that such SSVEP differences depend on the selective attention paid to one of two superimposed stimulation patterns.

Zhang et al. (2010) proposed a covert non-spatial visual selective attention paradigm to operate a SSVEP-BCI. Two sets of dots with different colors and flickering frequencies were used to induce the perception of two superimposed transparent surfaces. A group of 18 healthy subjects was asked to selectively attend to one of the two surfaces in order to control the BCI system to perform a binary decision task during a three day training program. An average of accuracy of 72.6% was achieved in the last training session. As reported in Table 1 the system would achieve an ITR of 2.17 bits/min.

Lesenfants et al. (2014) proposed a novel two-class independent SSVEP-BCI based on covert attention. The influence of feature extraction algorithms and the number of harmonics frequencies were studied. Also a test with online communication on healthy volunteers and patients with LIS was performed. A newly developed portable light emitting diode-based “interlaced squares” stimulation pattern was employed. Mean offline and online accuracies on healthy subjects (H) were respectively $85 \pm 2\%$ and $74 \pm 13\%$, with eight out of twelve subjects succeeding to communicate efficiently with $80 \pm 9\%$ accuracy. Two out of six LIS patients (End Users) reached an offline accuracy above the chance level, illustrating a response to a command. One out of four LIS patients had success in online communication.

Walter et al. (2012) compared the modulation of SSVEP amplitudes when subjects directly gazed at a flickering array of static dots (overt attention) and when they covertly shifted attention to the dots keeping their eyes at central fixation. A discrimination task was performed at the attended location to ensure that subjects shifted attention as instructed. Horizontal eye movements (allowed in overt attention but to be avoided in covert attention) were monitored by an electrooculogram. It was demonstrated that overt and covert attention differ in their effect on SSVEP amplitudes and behavior. The lower amplitude modulation by covert attention was considered for both development and application of classification procedures in covert SSVEP-BCIs.

An additional study conducted by Lim et al. (2013), which was not identified in under the search criteria, performs a classification of binary intentions for individuals with impaired oculomotor function: “eyes-closed” SSVEP-BCI, allowing users to express

their binary intentions without needing to open their eyes. A pair of glasses with two light emitting diodes flickering at different frequencies was used to present visual stimuli to participants with their eyes closed, and recorded EEG patterns were classified in offline/online experiments conducted with eleven healthy participants and one patient with severe ALS. Through offline experiments it was confirmed that SSVEP could be modulated by visual selective attention to a specific light stimulus penetrating through the eyelids. The online experiment conducted with the ALS patient showed a classification accuracy of 80%.

Table 1 summarizes the results achieved by these studies that includes the accuracy and ITR. It can be seen that only the two more recent studies performed experiments with end-users. All of them tested their systems with two commands and the highest accuracy rate attained was 80%. The average of the reported ITR was 3.794. In general, results of this Table provide a true overview of the state-of-the-art concerning gaze-independent SSVEP-BCIs. In traditional SSVEP-BCI systems, it is achieved high accuracy rates; however subjects must to perform muscular movements to redirect their gaze. In SSVEP-BCI systems based on covert attention, subjects do not perform muscular movements; however the accuracy rates are not high. Furthermore, a previous training stage is necessary because subjects must learn to maintain they covert attention on the target stimulus. In this context, this Thesis proposes a novel paradigm, in which subjects select the target stimulus by shifting of focus that does not demand an exhausted training stage because focusing is an optical mechanism that is used naturally by humans throughout life. Also, focusing mechanism does not demand neck, head or eyeball movements, although these may or may not happen. Patients with paralysis that cannot control muscular movements; however, in patients with neurodegenerative diseases as ALS, the sense of sight is not affected, retain minimal eye movements, including pupil and accommodation reflex mechanisms; making focus control possible even in the end stages of these pathologies. Therefore, it is worth investing in other methodology.

Table 1 – Comparison of the accuracy and ITR of gaze-independent SSVEP-BCI. **H**: Healthy, **End**: End user, **on**: online, and **off**: offline.

Study	Class.	Acc. %	ITR bits/min	Analysis	popul.	Subj.	Eye Mov
Kelly et al. (2005a)	2	70.3	0.91	off	H	10	<1°
Allison et al. (2008)	2	74	4.18	on	H	14	
Zhang et al. (2010)	2	72,6	2.17	on	H	18	< 1μV
Walter et al. (2012)	2	70.3	0.91	off	H	14	< 25μV
Lim et al. (2013)	2	80	10.8	off/on	H/End	11/1	
Lesenfants et al. (2014)	2	80		off/on	H/End	12/6	nothing

3 The Novel Stimulation Setup

In traditional **SSVEP-BCI** systems a set of stimuli flickering at different frequencies are used. In this systems, users must to redirect their gaze direction that demands neck, head or eye movements to make a selection of an stimulus. Due to each stimulus are associated to any command, muscular movements are present each time that user wants to send a command. In this chapter, the novel **SSVEP-BCI** stimulation setup proposed in this Thesis is described, in which two **SSVEP** stimuli are presented in field of view of the **BCI** user but at different distances from him. This setup that is based on the optical phenomenon called Depth-of-field allow users to make a stimulus selection by shifting their eye focus instead of performing neck, head or eyeball movements.

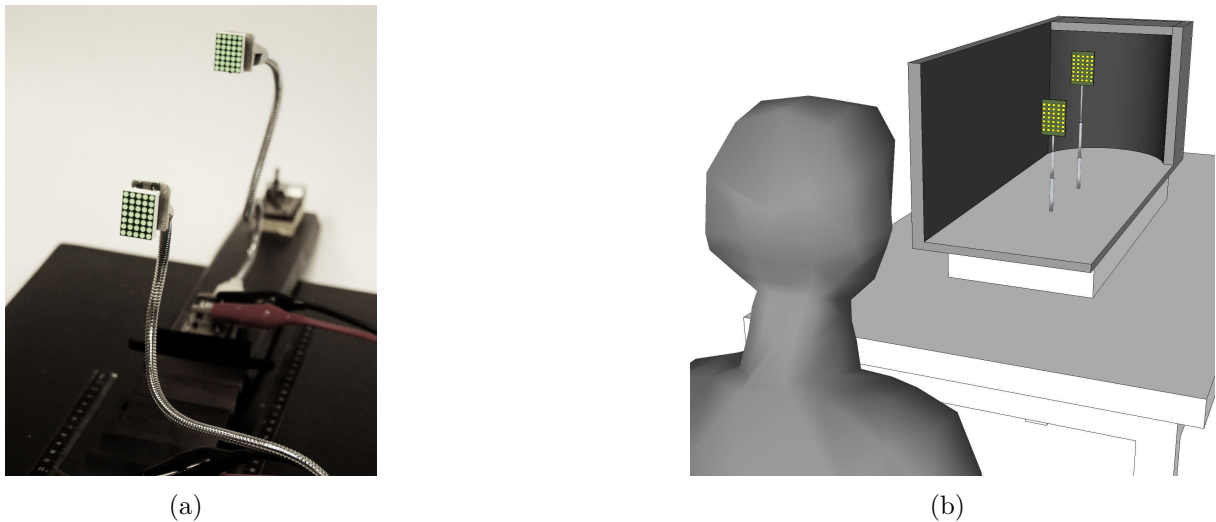


Figure 24 – The novel stimulation setup based on Depth-of-Field. a) Stimulation unit composed by two green **LED** arrangements that are presented together in the field of view of the user but at different distances. b) Subject, the stimulation unit and the stimulation box. Stimuli were adjusted to 0.1 lumen for both stimuli, measure at a distance of 15cm.

The setup is shown in Figure 24. Figure 24a shows the stimulation unit that is composed of two green **LED** arrangements (7×5 matrix) connected to two analog signal generators. The dimension of each arrangement is $18 \times 13 \text{ mm}^2$ and the luminous flux was adjusted to 0.1 lumen for both stimuli, measure at a distance of 15 cm. Stimuli were programmed to flicker at 5.6Hz and 6.4Hz with 50% of duty cycle (**BASTOS et al., 2014; MULLER; BASTOS; SARCINELLI, 2010**). These frequencies were chosen to be out of range between 15Hz and 25Hz that can provoke photosensitivity epileptic seizures (**FISHER et al., 2005**). Both arrangements are separated 2mm from each other in a vertical plane in order to avoid overlapping into the users' field of view. Figure 24b shows the unit

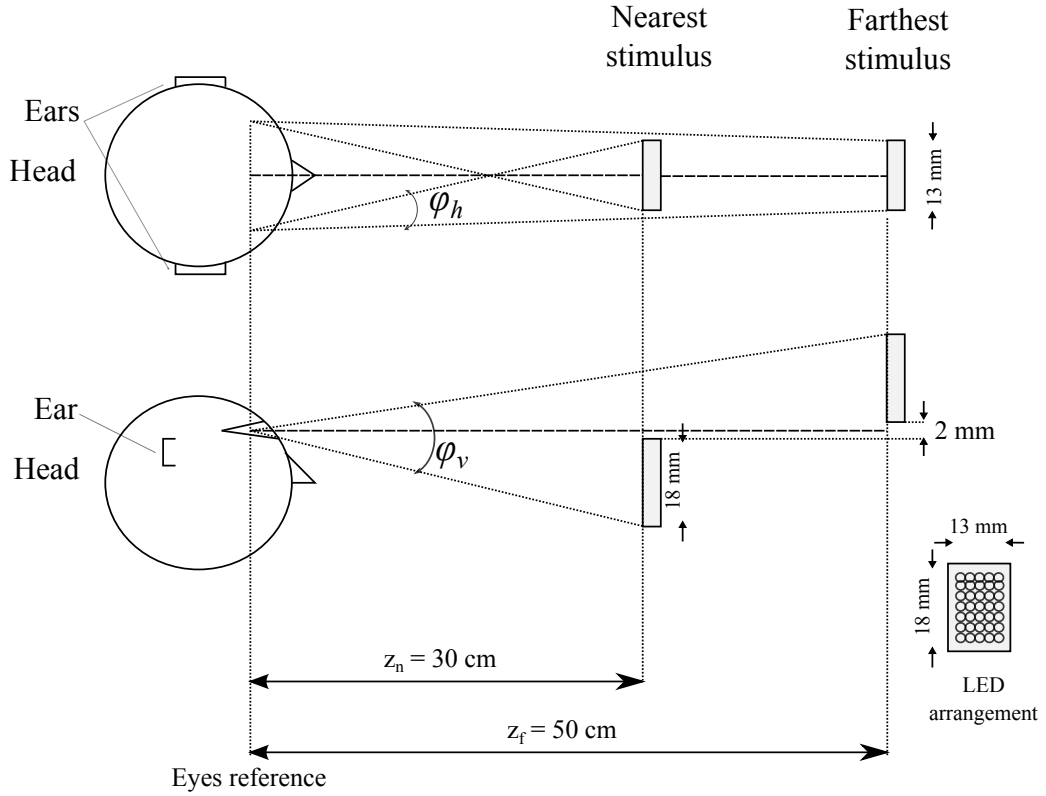


Figure 25 – Distances of placement of stimuli in the novel SSVEP-BCI setup. z_n and z_f denote the distances of the nearest and the farthest stimuli, respectively. ϕ_v and ϕ_h denote the horizontal and the vertical visual angles, respectively.

placed into a stimulation box, which in turn was placed next to the subject's head, ensures that only both stimuli were in the user's field of view avoiding the presence of other light sources. Also, the interior of the box was painted in black to eliminate the reflection of lights.

Figure 25 shows the distances where stimuli are placed. Due to two stimuli located at different distances are used, they are denoted as nearest and farthest. The nearest stimulus is placed at $z_n = 30\text{ cm}$ from the user, while the farthest one is placed at $z_f = 50\text{ cm}$ from him. These distances that were computed in the same way of Vishwanath & Blaser (2010) was adopted in this work because they satisfy the condition in that if one stimulus is focused on, then the other one is non-focused and vice versa. Horizontal and vertical visual angles can be observed, respectively, in the top and bottom insets of Figure 25. Then taking into account the distances of both stimuli and the dimension of the LED arrangements, the horizontal (ϕ_h) and the vertical (ϕ_v) angles of the stimulation unit can be computed as

$$\phi_h = 2 \tan^{-1}(h_L/2z_n), \quad (3.1)$$

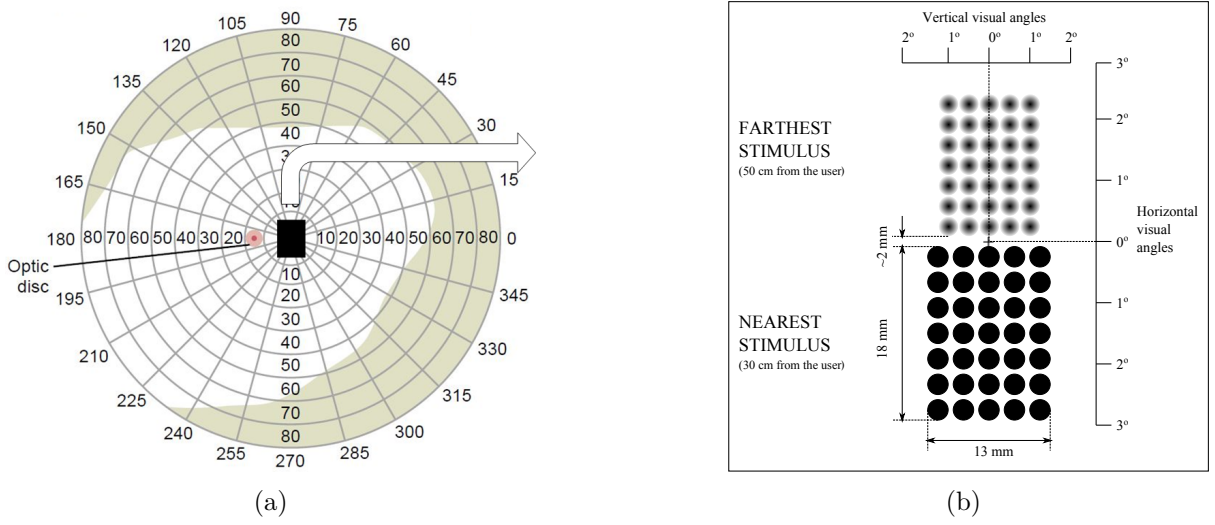


Figure 26 – Projections of focused and non-focused stimulus in the field of vision. a) Perimeter chart of the field of vision with a black rectangle that represent the projection area of both stimuli. b) Subjective view focused (nearest) and non-focused (farthest) stimuli with vertical and horizontal angles.

and

$$\varphi_v = \tan^{-1}(h_L/z_n) + \tan^{-1}(h_L/z_f), \quad (3.2)$$

where $h_L = 18\text{mm}$ and $w_L = 13\text{mm}$ are the dimensions of the LED arrangements. As a result, the angles are given by $\varphi_v = 5.49^\circ$ and $\varphi_h = 2.48^\circ$.

Figure 26a shows the perimeter chart of the field of vision of the eye described in Section 2.1.1, in which the black rectangle in the center of the chart represents an approximated area in which both stimuli of the novel setup are projected, considering the horizontal and vertical angles computed with (3.1) and (3.2), respectively. In Figure 26b it is represented how both stimuli are projected in the subjects' field of view when the nearest stimulus is focused on. Also, it is included the vertical and horizontal angles and the dimension of the LED arrangements. Note that the vertical and horizontal angles do not exceed the limits of the perimeter of vision, ensuring that both stimuli will be appear together in the field of view. Furthermore, due the angles are very small both stimuli are projected in the region with high density of photoreceptors of the retina. Hence, the setup here proposed does not demand neck, head and/or eyeball movement to choice the nearest or the farthest stimulus, but demands shifting of eye focus.

In the following sections, Depth-of-field, a function that describe blurriness, and the retinal blurry model are described. Also, the accommodation mechanism that that adjusts the shape of the lens in order to focus an objects is explained.

3.1 Non-focused Objects and Depth-of-field

An object is imaged sharp by optical systems when it is placed at the point of focus, then, objects that share the same distance with the point of focus are named as focused objects and also are imaged sharp. In contrast, objects placed at different distances are imaged blurred and are called non-focused objects. In general, a natural scene is composed by a set of focused and non-focused objects, as shown in Figure 27a. It can be seen that objects behind and in front of the point of focus are perceived blurred. When an object is out of focus, or non-focused, there is a reduction of contrast in its projected image and it is perceived blurred (ATCHINSON; SMITH, 2000). In photography, the blurriness of the object's image depends on the distance of the object from the fixation point, the diameter of aperture and the distance of the lens from the sensor surface. For instance, the picture of Figure 27a was taken with diaphragm aperture, exposure time and ISO speed of 5.6, 1/250s and 3200, respectively. The fixation point was at the label of the electrode O1. In human eyes, blurring effect occurs because the lens only converges a bundle of light rays from each point on the focused object to a discrete point in the retinal image, but it

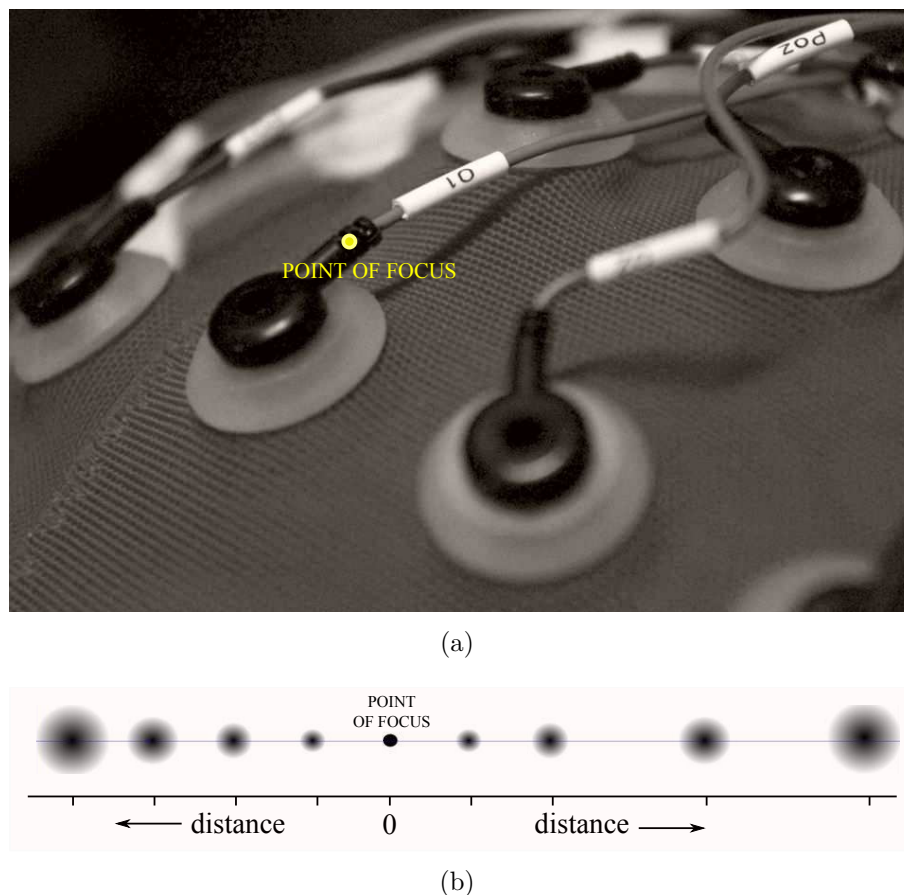


Figure 27 – Blurriness of non-focused objects. a) Picture took with diaphragm aperture, exposure time and ISO speed of 5.6, 1/250 seconds and 3200, respectively. The point of focus was at label of the electrode O1. b) Blurriness of non-focused points for different distances from a point of focus.

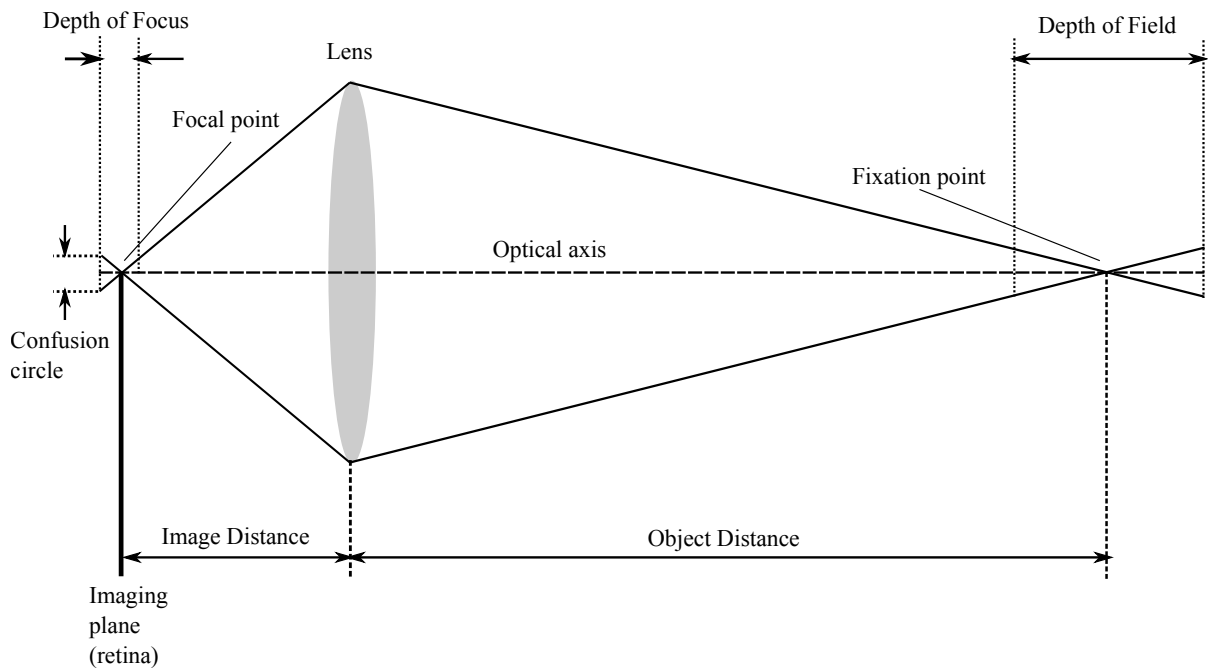


Figure 28 – Schematic diagram of Depth-of-field and depth-of-focus. The variation of blurriness is very slightly and points projected under the circle of confusion are assumed in sharp. The circle of confusion are related to the lens size, the distance of the lens from the point of focus (or fixation point), and the distance from the imaging plane. Adapted from [Songnian et al. \(2014\)](#).

diverges rays from points of the non-focused object ([GREGORY, 1997](#); [EBENHOLTZ, 2001](#)). Blurriness also depends of the distance of the non-focused objects from the focus point. In the picture, it can be seen that the far objects are more blurred than the objects near it. If the picture was composed by points, non-focused points could be perceived as blurred circles, as illustrated in Figure 27b, and the diameter of a nearest circles is larger than diameter of a farthest circle ([DAI, 2008](#); [MAHAJAN, 1991](#); [WILSON](#); [DECKER](#); [ROORDA, 2002](#)).

Notwithstanding, objects that are not placed at the same distance of the focus point but are placed very near it also can be perceived sharp. Depth-of-field is defined as the range of distances near the point of focus where the eye imaged an object as sharp. Then, objects placed out of the Depth-of-field are perceived blurred ([ATCHINSON](#); [SMITH, 2000](#)). It happens because there is a small region in the sensor surface of visual systems (the retina in human eyes), in which the variation of blurriness is very slightly and points projected under this region are assumed in sharp. This region is names as circle of confusion. Such the variation may be small enough that it is not noticed, and thus there is a small amount of “tolerance” As shown in Figure 28, the circle of confusion are related to the lens size, the distance of the lens from the point of focus (or fixation point), and the distance from the imaging plane. The range of the tolerance is termed the depth-of-focus ([WANG](#); [CIUFFREDA, 2006](#))

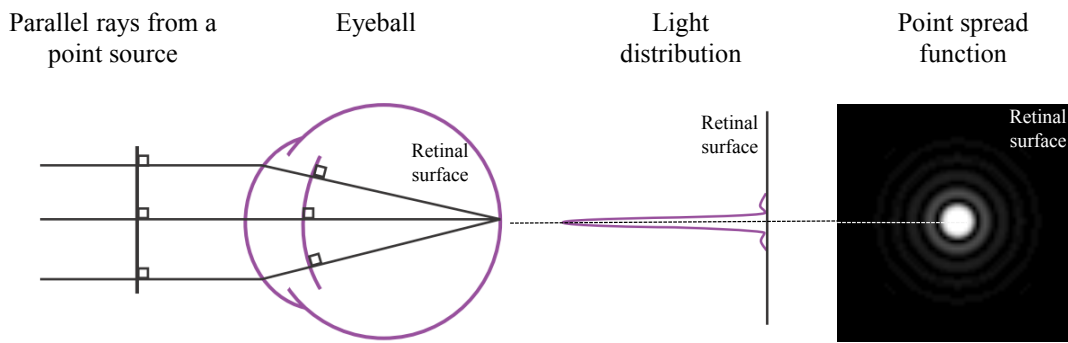


Figure 29 – PSF caused by diffraction. The light distribution caused by a point source forms the Airy disk pattern on the retina due to the diffraction at the pupil. Adapted from Shevell (2003).

3.2 Optical PSF

Optical PSF, or simply PSF describes the response of an imaging system to a point source or point object. Ideally, the image of a point source is a point image. However, even in a properly focused system, diffraction and the aberrations cause the illuminance to spread out around the point image position. It is defined as a relative measure of the luminous flux at the positions around the ideal point image that transform the image of the point in a spread function that can be given by a blur circle (KEATING, 2002). PSF can be understood as the impulse response of an optical system. Figure 29 illustrates this concept, in which the light distribution on the retinal surface that response to a point source is given by a function named as Airy disc pattern. This pattern is formed on the retina from a point source due to the diffraction at the pupil (PACKER; R.WILLIAMS, 2003). Due to PSF is the distribution of light across the photoreceptors surface, it can be used to measure the quality of an imaging system. Then, if it is assumed that an object is composed by a set of points, all points will be affected by the PSF in the projection image in a visual system. By this reason, in ophthalmology, PSF is used as diagnostic tool (DAI, 2008). Aberrations of human eye wavefront that cause some distortions of the projected images in the retinal surface also can be addressed with this spread function. Aberrations can be caused by defects of the cornea or the lens, or simply by the defocus (MAHAJAN, 1991). The image of an object can be simulated as the convolution of the true object and the PSF. Figure 30 shows some convolution examples and in which the effects of optical aberrations in the projected images are described by some spreading functions. Also, it can be seen that the PSF due to defocus aberration is concentric and symmetric; in addition the image of points of non-focused objects can be modeled as blurred circles, whose diameters vary with the distance (MAHAJAN, 1991).

In optical systems that are limited only by defocusing, the PSF for a specific point $\mathbf{x} = (x, y)$, could be expressed as

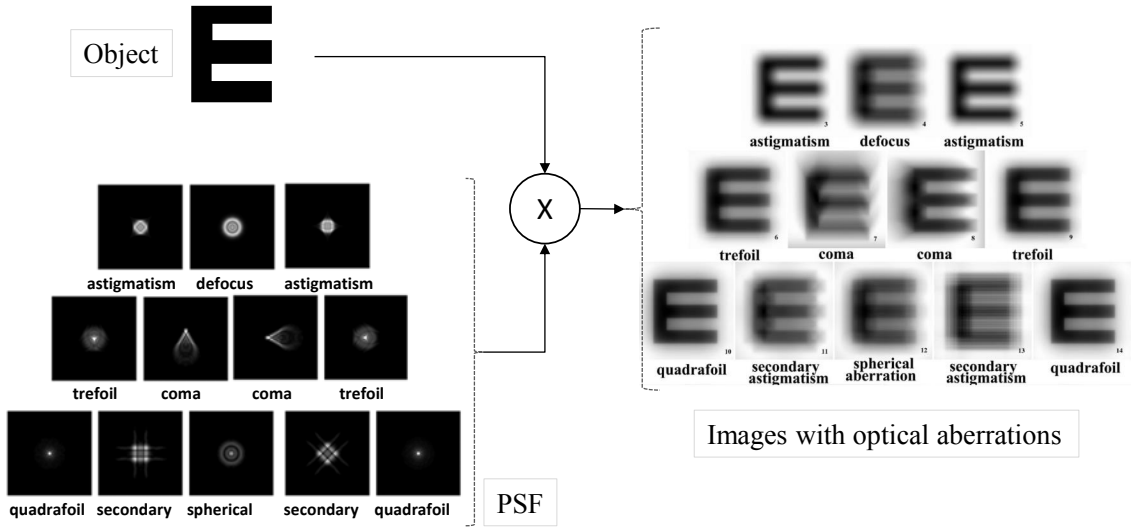


Figure 30 – Object, some PSF that describes some optical aberrations and their corresponding simulated images. The circle with “X” represents the convolution operation. Note that the PSF due to defocusing is symmetric. Adapted from (CHEN et al., 2005)

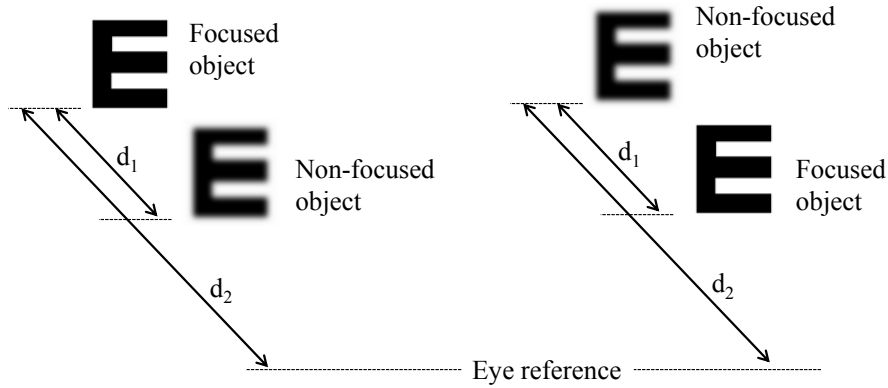


Figure 31 – Images of focused and non-focused objects when are presented together but at different distances. It is assumed that distances d_1 and d_2 are enough to the non focused object is out of Depth-of-Field of the focused one.

$$psf(\mathbf{x}, \Delta D) \quad (3.3)$$

where ΔD the defocusing degree or the optic power required to bring the object in focus (BURGE; GEISLER, 2011). Optical power is the degree to which an optical system converges or diverges light and its unit is given in diopters (m^{-1}). The defocus degree of a non-focused object can be defined as the difference between the lens system’s current power D_{focus} , and the power of the lens when this object is in focus D_{target} , as

$$\Delta D = D_{focus} - D_{target}. \quad (3.4)$$

Figure 31 illustrates the retinal images of two objects when are presented together but at different distances when it was assumed that the distances, d_1 and d_2 , are enough to ensure that the non-focused is out of the Depth-of-field of focused one. Then, when one of them is focused the other one is non-focused, and vice versa.

3.3 Retinal Blurry Model

The human eye, as any other optical system, has a limited sensitivity to optical blur. Retinal blurring effect occurs because the lens only converges a bundle of light rays from each point on the focused object to a discrete point in the retinal image, but it diverges rays from points of the non-focused object. Depth-of-field is the range of distances near the point of focus where the eye imaged an object as sharp. Hence, as illustrated in Figure 32, objects behind and in front of the point of focus are imaged blurred.

Blurriness caused by defocusing can be intended as concentric (MAHAJAN, 1991); and the image of a defocused point can be modeled as a blurred circle, whose diameters vary with the distance. Thus, the image of a defocused object can be simulated by convolving the image with a circular average spatial filter. In addition to the point of focus and the distance from the eye, the diameter of the blurry circle due to defocused point is related to the eye parameters such as pupil size or focal length. For example, the theoretical model introduced in (GRAND; HAGE, 1980) and adapted by (VISHWANATH; BLASER, 2010),

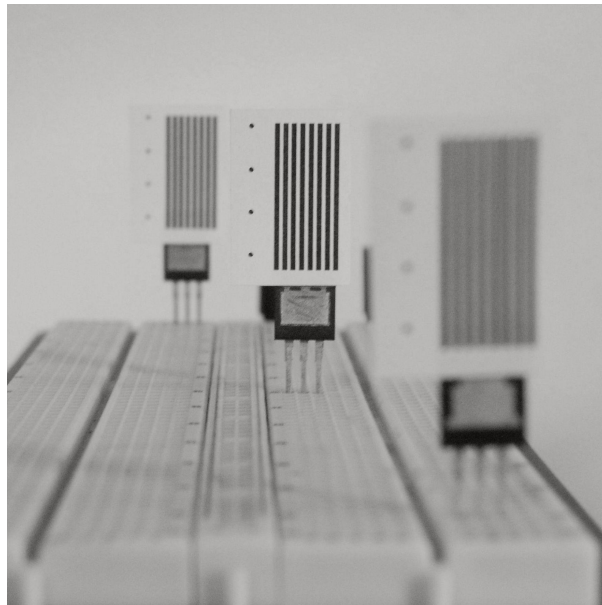


Figure 32 – Picture with three cards spaced by 8cm in which there are eight stripes with approximated dimensions of 25mm (length) and 1mm (width) and four dots of 1mm of diameter. It was shot at 1/40 seconds, f/7.1 and ISO 1600.

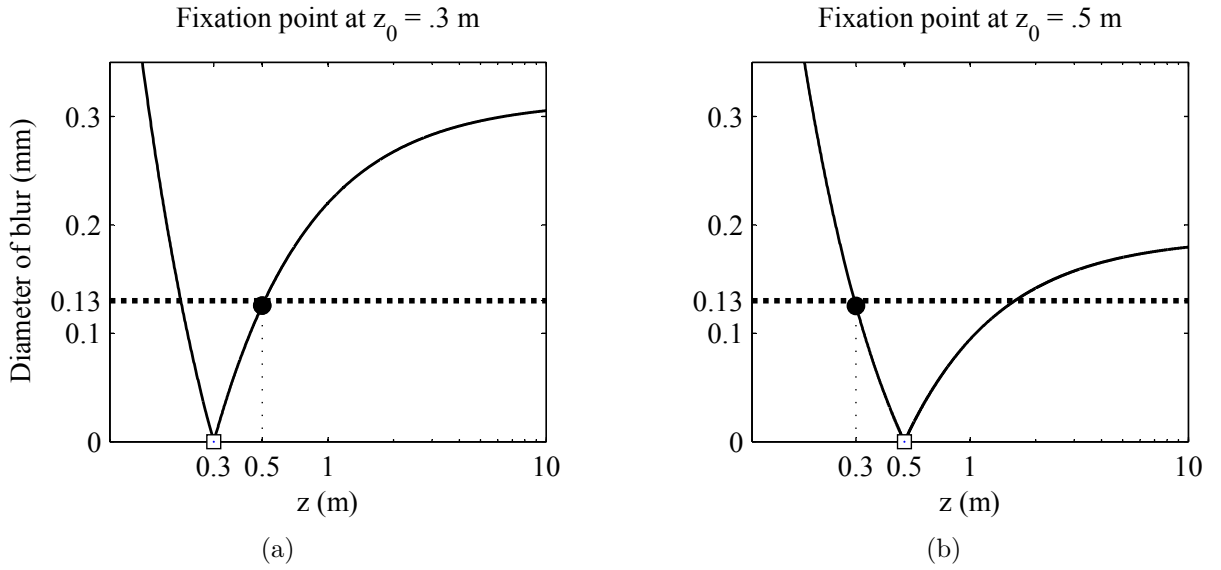


Figure 33 – Retinal blur and distance. The fixation point is at distance z_0 and is imaged sharply on the retina at b_0 , but appear blurred for other distances from the eye. The degree of blur is determined by z_0 .

the diameter can be summarized as

$$d(z)|_{z_0} = f(D, P, b_0, f_a, z_0, z), \quad (3.5)$$

where D is the pupil size and P is a pupil factor, b_0 is the distance from the lens to the retina, f_a is the focal length of the lens, z_0 is the distance of the fixation point, and z is the distance of the defocused point. In this simplified model, the image of defocused points projected on the retinal surface are modeled as blurred circles. Then, the diameter d of the blurred circle of a non-focused point located at z when the fixation point is located at z_0 can be estimated as

$$d(z)|_{z_0} = \frac{D |b - b_0|}{b + (P - 1)f_a}, \quad (3.6)$$

where f_a is the accommodated focal length; D is the pupil size and P is a pupil factor, assumed in the original model as 5mm and 0.9, respectively. b_0 is the distance between the retina and the lens; and b is the distance from the lens to the place where the non-focused point would be projected sharp, and they can be computed as

$$\frac{1}{f_a} = \frac{1}{b_0} + \frac{1}{z_0} \quad \text{and} \quad \frac{1}{f_a} = \frac{1}{b} + \frac{1}{z}.$$

Figure 33a and 33b show the curves of the diameter of blur circle d as a function of distance z computed with (3.6) for point of focus placed at $z_0 = 0.3$ m and $z_0 = 0.5$ m, respectively. Note in Figure 33a that the diameter at $z = 0.3$ m is zero (white square) while the diameter at $z = 0.5$ m is around 0.13mm (black marker). In the same way, in

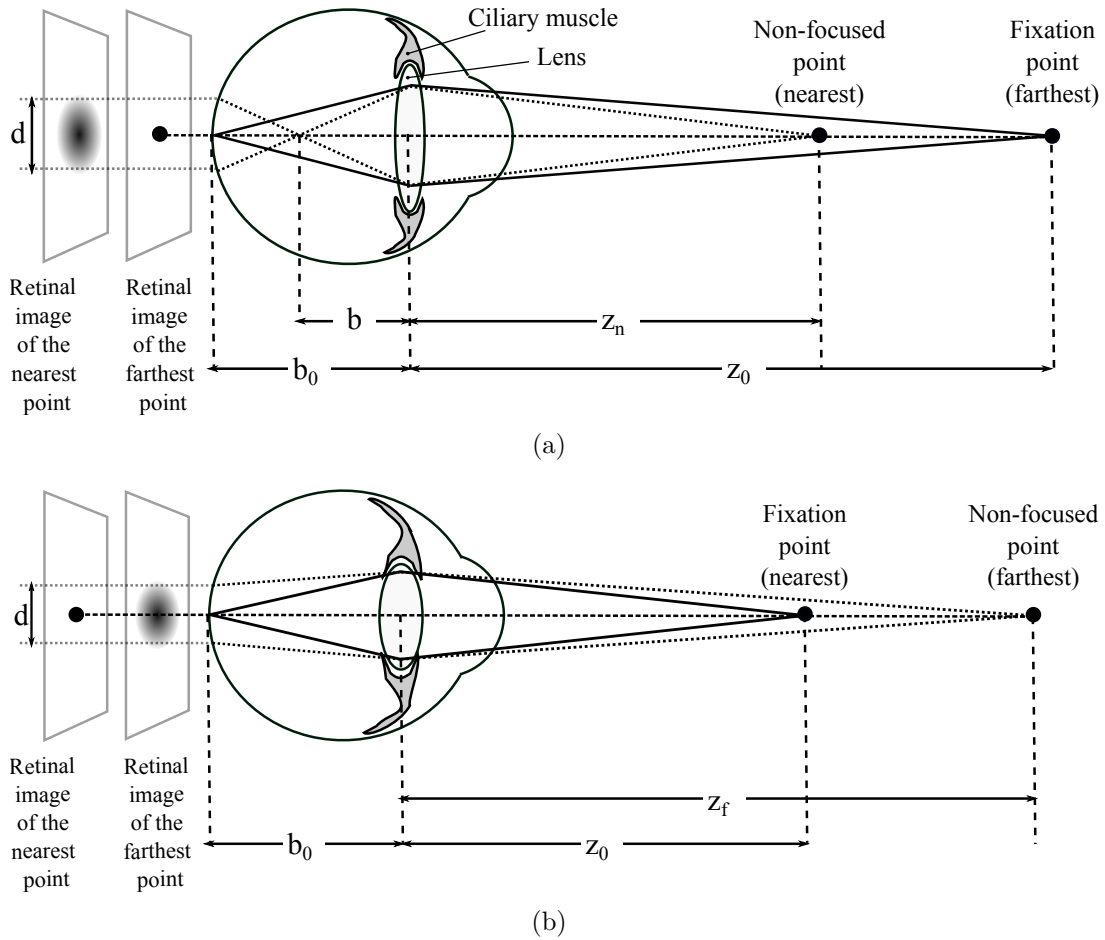


Figure 34 – Depth-of-field and defocusing. (a) Retinal blurring effect caused by a non-focused point placed nearer, $z = z_n$, than the fixation point, z_0 ; d is the diameter of the blurry circle; b_0 is the distance between the lens and the retina; and b is the distance from the lens to the point where the non-focused point would be imaged sharp. (b) Retinal blurring effect caused by a non-focused point placed farther, $z = z_f$, than the fixation point z_0 ; distance b not shown because it is outside the figure.

Figure 33b the diameter at $z = 0.5\text{m}$ (white square) is zero while the diameter at $z = 0.3\text{m}$ approximately 0.13mm (black marker).

This model satisfies facts as (i) points placed nearer and farther than fixation points are imaged blurred; (ii) the diameter of the blurred circle increases as defocused point approaches the eye; and (iii) the diameter increases asymptotically when the unfocused point is moving to infinite. Also, in the presence of two objects properly placed, the model shows the extraordinary situation when one of them is in focus, the other one is defocused and vice versa. For example, as represented in Figure 34a, if a point placed at $z_0 = 50\text{cm}$ is focused on, a blurred circle due to a non-focused point being placed at $z_n = 30\text{cm}$ is projected in retinal plane. Figure 34a represents the blurred circle due to the non-focused point placed at z_f , when the focused point was located at z_0 .

The diameter of blurry circle in Figures 34a and 34b are 0.129mm and 0.132mm, respectively. The human's eye is able to refocus an object when its distance changes, sharpening the projected image on the retinal surface (GREGORY, 1997). Focusing does not require eyeball movement because it is performed by an accommodation mechanism that modifies the shape of the lens making it a variable refractive element. The lens becomes more rounded to focus on near objects and more elongated (or stretched) to focus on objects that are far away (EBENHOLTZ, 2001).

3.4 Accommodation of the Eye

The human eye, as any other optical instrument, has a limited sensitivity to optical blur (HOWARD, 2012). If there is a little difference between the power and length, then the image that is formed on the retina will be very slightly out of focus. However, such a discrepancy may be small enough that it is not noticed, and thus there is a small amount of "tolerance" in the system such that a range of focus is considered to be acceptable, that is called circle of confusion. This range is termed the depth-of-focus of the eye (WANG; CIUFFREDA, 2006). In the case of human eyes, the defocusing degree is related to the lens size, pupil aperture and the distance between the fixation point and the defocused object. Accommodation of the eye is the mechanism that adjusts the shape of the lens in order to focus an object modifying the angle of refraction for impinging light rays. It minimizes the defocusing degree and maximize image quality. Accommodation for a near target occurs when the eye accommodates and the lens forms a more spherical shape to bring the near target into the focus. On the other hand, lens is elongated (stretched) for focusing distant objects (Figure 35). This is because lens only converges the bundle of light rays from each point on the focused object to a discrete point in the retinal image,

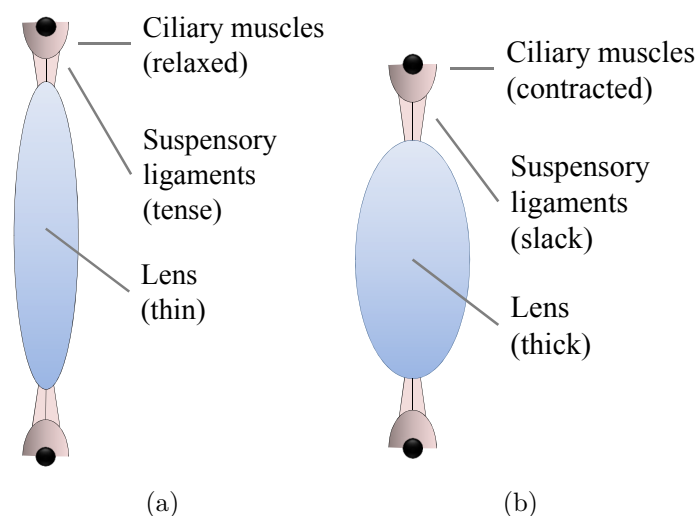


Figure 35 – Accommodation of the lens. Lens are elongated or rounded to focus distant or near objects, respectively. Modified from (EBENHOLTZ, 2001)

but it diverges rays from a point of non-focused object forming instead of a point, a blurry circle. Accommodation is a reflex response of the nervous system and appears to be under negative biofeedback control so as to automatically minimize blur in the retinal image. When the blur exceeds some threshold a neural signal is sent to the ciliary muscle to either stimulate or inhibit it, depending on what is needed to correct the focusing error (EBENHOLTZ, 2001), (GREGORY, 1997), (GRUSSER; GRUSSER-CORNEHLS, 1986).

3.5 Summary

In this chapter, Defocusing and Depth-of-field are defined before to describing the SSVEP-BCI stimulation setup. Also, point spread function and accommodation mechanism are presented. The retinal blur model introduced by and employed by Vishwanath & Blaser (2010) to compute a convenient distances for two objects are explained. Distances computed by Vishwanath and Blaser was adopted in this work because they satisfy the condition if one object is focused on the other one is non-focused and vice versa. Depth-of-Field of the human's eyes is the range of distances near the point of focus where the eyes perceive the image as sharp. Thereby if a stimulus located at z_0 from the lens is focused on, then another stimulus located nearer than this at z_n will be projected blurred in the retinal image; as well, if the near stimulus is focused on, then the far stimulus is projected blurred, as shown in Figure 34. The mechanism by which lens can be shaped in its geometry by the ciliar muscle is therefore a variable refractive element known as accommodation of the eye. The lens becomes more rounded to focus on near objects and more elongated (or stretched) to focus on objects that are far away. The human's eye is able to refocus an object when its distance changes, sharpening the projected image on the retinal surface. Thus, focusing does not require eyeball movement because it is performed by an accommodation mechanism. Focused points are sharply projected, but points away from focus point increasingly defocused are projected as blurry circles.

4 Statistical Evaluation

Rather than on subjective evaluation of response of nervous system, ORD that is based on well-defined statistical criterion can be used to automate the stimuli response identification (SIMPSON *et al.*, 2000). For instance, Infantosi, Lazarev & Campos (2005) applied an ORD based on SFT method to detect photic effects, testing the hypothesis of absence evoked responses, caused by intermittent photic stimulation. Testing is performed using EEG signals during and before the stimulation. A model of evoked potential generation is described by Melges, Sa & Infantosi (2012) that consider the electrical activity during the stimulation is the result of evoked potentials embedded in the spontaneous EEG.

In this Thesis a novel setup is being proposed (Chapter 3) based on the hypothesis that the focused stimulus is able to evoke a visual potential although a non-focused stimulus is also present together in the center of field of view. Then, the hypothesis testing of absence of responses (INFANTOSI; LAZAREV; CAMPOS, 2005) can be adapted to validate our hypothesis, as follows,

- first, expanding the model of the evoked responses for an isolated stimulus (MELGES; SA; INFANTOSI, 2012) in order to describe the neural response when two flickering stimuli are being used together;
- then, adapting the ORD based on SFT that was described for one stimulus (INFANTOSI; LAZAREV; CAMPOS, 2005; SA *et al.*, 2006; MELGES; SA; INFANTOSI, 2012) in order to describe the response for two stimuli presented together;
- finally, conducting a hypothesis test to evaluate how the stimulation composed by a focused stimulus and a non-focused one affects the spontaneous EEG.

Figure 36 shows the novel stimulation setup when any stimulus is on, when only one stimulus is on, and when both stimuli are on, in which unpainted rectangles represent stimuli off, while painted rectangles correspond to stimuli on. f_1 and f_2 are the flickering frequencies, and d_1 and d_2 are the distances of stimuli from the subject. In Figure 36a, the response is given by the spontaneous EEG because there is no stimulation. In Figure 36b, the target stimulus is given by the isolated stimulus and an evoked response arises at the frequency of the target stimulus. In Figure 36c where two stimuli are on, the target stimulus is given by the focused stimulus, and it is expected that an evoked potential arises at the frequency of the focused stimulus, even if the non-focused one is present.

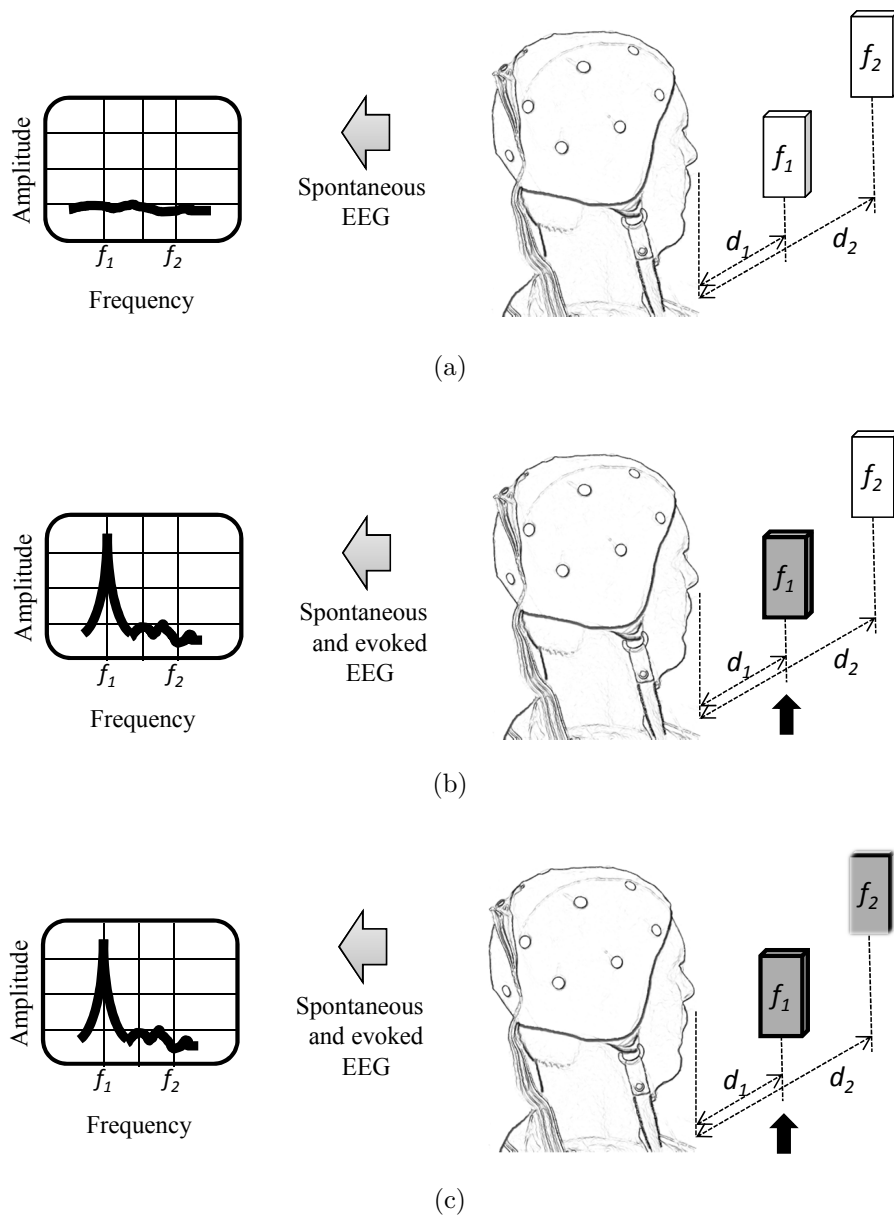


Figure 36 – Illustration of spectral EEG responses for three cases. Unpainted rectangles represent stimuli off, while painted rectangles corresponds to stimuli on. a) Spontaneous EEG response for no stimulation; b) Spontaneous and evoked responses for stimulation with one stimulus; and c) response for stimulation with two stimuli, a focused and a non-focused. The black arrow indicates the target stimulus, f_1 and f_2 denote the flickering frequencies, and d_1 and d_2 denotes the distances.

In the following sections of this chapter, the model of VEP generation with the ORD based on SFT is described. Then, a model of VEP generation for two stimuli is proposed, and the hypothesis test of absence of evoked potentials due to focused stimulus is evaluated.

4.1 Model of VEP generation and the ORD based on SFT

The generation of evoked potentials such as VEP can be modeled by employing the linear model showed in Figure 37 (MELGES; SA; INFANTOSI, 2012); in which the input caused by the target stimulus is represented by $u[n]$, $v[n]$ denotes the evoked potential that arises in response to the stimulus, $b[n]$ designates the background spontaneous EEG signal, and $H(f)$ represents the transfer function of the visual pathway. During the visual stimulation the output signal $y[n]$ that can be measured in the scalp is composed by evoked and background activities. This model that suggests the evoked potentials are embedded into the background activity can be expressed as

$$y[n] = v[n] + b[n]. \quad (4.1)$$

Observe that in absence of the visual stimulus ($u[n] = 0$), the scalp electrical activity only reflects the spontaneous activity. It also happens when the neural activity is not affected ($H(f) = 0$) by the stimulus and consequently the output signal belongs to the same population of the the spontaneous EEG. Statistical techniques based on ORD can be applied to detect the response of flickering visual stimulation (SA et al., 2006). Infantosi, Lazarev & Campos (2005) employed the SFT based on the spectral power density of the EEG recorded before and during the stimulation. They uses this statistical test based on Power spectral density (PSD) to analyze whether two sample spectra belong to the same population making it sensitive in detecting spectral changes.

The PSD of a signal $y[n]$ was calculated by using its Discret Fourier transform (DFT), $Y(f)$, as follows

$$P_{yy}(f) = Y(f) \cdot Y^*(f), \quad (4.2)$$

where $Y^*(f)$ is the complex conjugated of $Y(f)$ in the frequency domain. Also, they assumed the EEG segments as samples of Gaussian process of mean and variance of zero

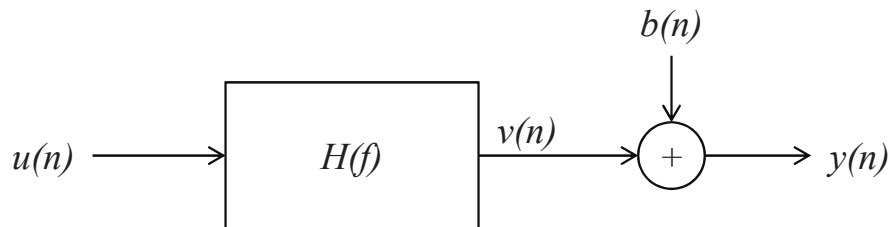


Figure 37 – Conventional linear model of the EEG signal during visual stimulation. $u[n]$, $v[n]$, $b[n]$ and $y[n]$ represent the input caused by the light stimulus, the evoked potential, the spontaneous EEG and the output signal, respectively. $H(f)$ represents the transfer function of the visual pathway. Adapted from Melges, Sa & Infantosi (2012).

and one, respectively; $P_{yy}(f)$ are distributed as Chi-square distribution with two degrees of freedom, χ_2^2 . Bartlett periodogram was employed to compute the PSD in order to increase the statistical significance

$$\hat{P}_{yy}(f) = \frac{1}{M} \sum_{m=1}^M P_{yy}^{(m)}(f), \quad (4.3)$$

where M is the number of disjoint independent segments with the same duration and $\tilde{P}_{yy}^{(m)}(f)$ is the estimated PSD on the m -th segment. Then, $\hat{P}_{yy}(f)$ is distributed as Chi-squared distribution with $2M$ degrees of freedom, χ_{2M}^2 .

The SFT is given by the ratio between the Bartlett periodogram of EEG during visual stimulation and the background EEG activity. If $y[n]$ is EEG the segment recorded during stimulation and $b[n]$ is EEG the segment immediately preceding segment, SFT that is symbolized as $\hat{\phi}_{yb}(f)$ is computed as

$$\hat{\phi}_{yb}(f) = \frac{\hat{P}_{yy}(f)}{\hat{P}_{bb}(f)}, \quad (4.4)$$

where $\hat{P}_{yy}(f)$ and $\hat{P}_{bb}(f)$ are the Bartlett periodogram of $y[n]$ and $b[n]$, respectively; that is,

$$\hat{\phi}_{yb}(f) = \frac{\frac{1}{M_y} \sum_{m=1}^{M_y} P_{yy}^{(m)}(f)}{\frac{1}{M_b} \sum_{m=1}^{M_b} P_{bb}^{(m)}(f)}. \quad (4.5)$$

$P_{yy}^{(m_y)}(f)$ and $P_{bb}^{(m_b)}(f)$ are, respectively, the DFT of the m -th EEG of $y[n]$ and $b[n]$; and M_y and M_b are the number of epochs recorded during and before the visual stimulation.

The assumption of absence of evoked response leads $y[n]$ and $b[n]$ to be independent, Gaussian distributed signals and belongs to the population with the same theoretical spectra. Then, both numerator and denominator are correspondingly distributed as Chi-squared distribution with $2M_y$ and $2M_b$ degrees of freedom, $\chi_{2M_b}^2$ and $\chi_{2M_y}^2$ respectively. Consequently, $\hat{\phi}_{xy}$, that follows the Fisher (F) distribution, is expressed as:

$$\frac{M_y}{M_b} \hat{\phi}_{yb}(f) \sim F_{2M_y, 2M_b}, \quad (4.6)$$

where $F_{2M_y, 2M_b}$ is the F distribution with $2M_y$ and $2M_b$ degrees of freedom. This reflects a null hypothesis H_0^{yb} of absence of cortical response caused by visual stimulation,

$$\left. \frac{M_y}{M_b} \hat{\phi}_{yb}(f) \right|_{H_0} \sim F_{2M_y, 2M_b}, \quad (4.7)$$

that compare it with a critical value. If $\hat{\phi}_{yb}(f)$ is higher than a critical value, it is rejected, otherwise, it is non-rejected. The critical value for $M = M_y = M_b$ and a significance level α can be expressed as

$$\phi_{yb}(f)_{crit} \sim F_{2M,2M,\alpha}. \quad (4.8)$$

In contrast, if $\hat{\phi}_{xy}$ is lower than the critical value, there is no statistical evidence to reject the null hypothesis H_0^{yb} . Results achieved by [Infantosi, Lazarev & Campos \(2005\)](#) show the existence of evoked responses at stimulation frequencies (and harmonics) for which the null hypothesis could be rejected.

4.2 Model of VEP generation for two stimuli and the ORD based on SFT

The linear model identifying a evoked response described above is used when only a visual stimulus is presented in the subjects' field of view, and does not include cases wherein a set of stimulus are presented together in the field of view. This model can be used in conventional [SSVEP-BCI](#) due to only one stimulus is presented in the center of the subject's field of view. However, this model can not be used in systems in which two stimuli are presented in the field of view and subject is asked to attend one of a them. In this sense, a more general model is proposed.

The proposed model for two stimuli that was obtained by expanding the linear [VEP](#) generation model described above, is shown in [Figure 38](#). The target and non-target

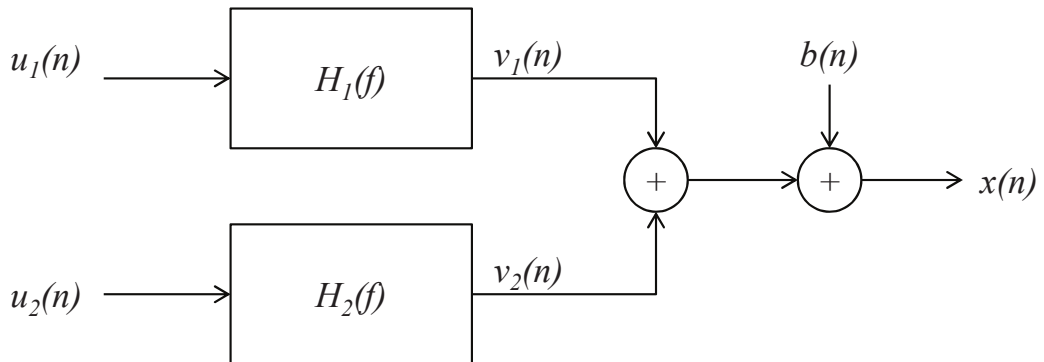


Figure 38 – Linear model of VEP generation for two stimuli. $u_1[n]$ and $u_2[n]$ denote the inputs caused by the target and non-target stimuli, respectively; $v_1[n]$ and $v_2[n]$ denote the evoked potential obtained by filtering the stimuli by using $H_1(f)$ and $H_2(f)$, respectively; b_0 denotes the spontaneous [EEG](#); and $x[n]$ is the output given by the [EEG](#) signal measured in the scalp.

stimuli are denoted as $u_1[n]$ and $u_2[n]$, respectively; the evoked responses $v_1[n]$ and $v_2[n]$ are obtained by filtering the stimuli inputs using $H_1(f)$ and $H_2(f)$, respectively; and $b[n]$ designates the spontaneous EEG. The output that is the measured EEG is composed by evoked potentials of target and non-target stimulus, and the background activity and can be expressed as

$$x[n] = v_1[n] + v_2[n] + b[n]. \quad (4.9)$$

It can be seen that

- when both stimuli are off, $u_1 = u_2 = 0$, potentials are not evoked, $v_1 = 0$ and $v_2 = 0$, consequently the output is given by the background spontaneous EEG;
- and when only the target stimulus is presented and the non-target is off, $u_1 \neq 0$ and $u_2 = 0$, the non-target stimulus does not evoke any potential, and the model is reduced to (4.1); in which the output is composed by evoked and background activities. Then, for purposes of explanation, in this section $y[n] = x[n]$ will be used to name the response of the model only to the target stimulus.

However, the output of the model is not known when $u_1 \neq 0$ and $u_2 \neq 0$; hence, some scenarios that can be evaluated are following

- the target and the non-target stimulus do not evoke any potential, $v_1 = v_2 = 0$, then, $H_1(f) = H_2(f) = 0$;
- both, the target and the non-target stimuli, evoke potentials, $v_1 \neq 0$ and $v_2 \neq 0$, then, $H_1(f) \neq 0$ and $H_2(f) \neq 0$;
- the target evokes and the non-target stimulus does not evoke potentials, $v_1 \neq 0$ and $v_2 = 0$, then, $H_1(f) \neq 0$ and $H_2(f) = 0$.

Recall that in the novel stimulation setup proposed in this work, two stimuli flickering at different frequencies are presented together in the user's field of view, but at different distances. It causes that if the target stimulus is selected by focusing the eye, then the non-target is defocused. This setup was proposed under the hypothesis that the focused stimulus is able to elicit a distinguishable evoked potential regardless the defocused stimulus is also present in the field of view.

In the same manner of [Infantosi, Lazarev & Campos \(2005\)](#), the ORD based on SFT was applied to detect driving effects of the visual stimulation for two stimuli, and hence for testing an absence of response. Therefore, since $b[n]$ is the model's output for non-stimulation; and $y[n]$ and $x[n]$ are the output when only the target stimuli, and both

stimuli (target and non-target) are presented, respectively; three null hypothesis can be conducted,

- first, the null hypothesis, H_0^{yb} , of absence of evoked potentials due to the isolated target stimulus evaluating SFT with $y[n]$ and $b[n]$, denoted as $\hat{\phi}_{yb}(f)$ and given by (4.4);
- The null hypothesis, H_0^{xb} , of absence of evoked potentials due to target and/or non-target stimulus evaluating the SFT between $x[n]$ and $b[n]$, given by

$$\hat{\phi}_{xb}(f) = \frac{\hat{P}_{xx}(f)}{\hat{P}_{bb}(f)}, \quad (4.10)$$

where $\hat{P}_{xx}(f)$ and $\hat{P}_{bb}(f)$ are the Bartlett periodogram of $x[n]$ and $b[n]$, respectively.

- The null hypothesis, H_0^{xy} , of absence of effects due to non-target stimulus evaluating the SFT between $x[n]$ and $y[n]$, given by

$$\hat{\phi}_{xy}(f) = \frac{\hat{P}_{xx}(f)}{\hat{P}_{yy}(f)}, \quad (4.11)$$

where $\hat{P}_{xx}(f)$ and $\hat{P}_{yy}(f)$ are the Bartlett periodogram of $x[n]$ and $y[n]$, respectively.

In order to follow (4.6) - (4.8) to find the critical value, the EEG signals $b[n]$, $y[n]$, and $x[n]$ were assumed zero-mean Gaussian distributions with proportional variance.

4.3 Materials

Subjects

Four healthy subjects participated in the study (age range 23-36 years). All of them showed normal or corrected to normal vision. The experiments were undertaken with the understanding and written consent of the subjects. This study was approved by the Ethics Committee of the Federal University of Espirito Santo.

Signals

EEG signals were recorded with a device for clinical purposes BrainNet36 together with a cap of integrated electrodes positioned according the international 10/10 system. Passive electrodes at locations P1, P2, P3, P4, Pz, PO3, PO4, PO7, PO8, POz, O1, O2, and Oz (see Figure 73), referenced to Cz were employed. The ground electrode was placed on the AFz position. All signals were recorded with a sampling frequency of 200 Hz.

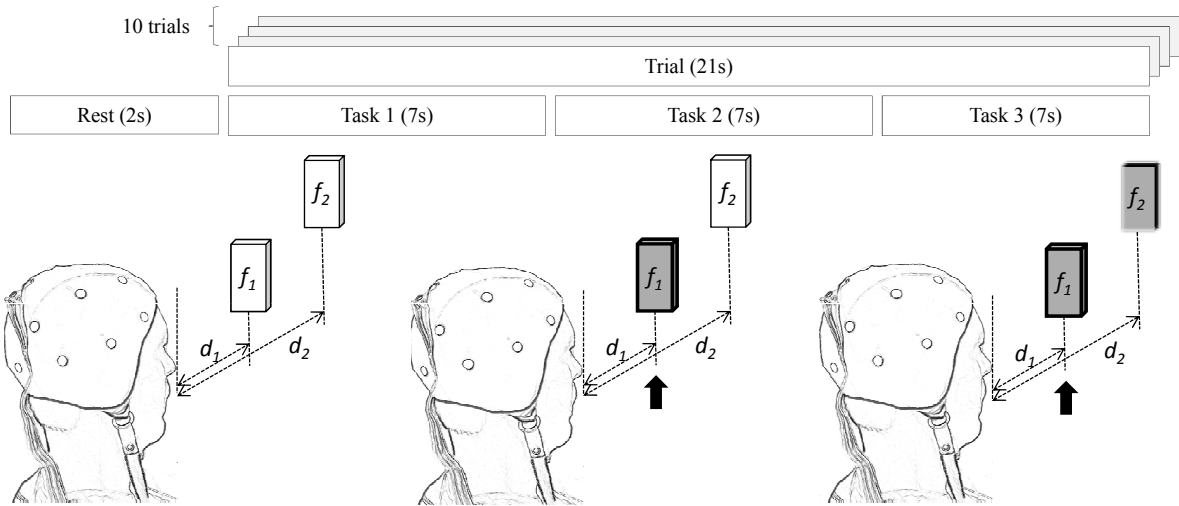


Figure 39 – Protocol of an experiment that includes ten trials of three tasks of 7s. Painted rectangles represent stimuli on, while unpainted rectangles corresponds to stimuli off, f_1 and f_2 denote the flickering frequencies, and d_1 and d_2 denote the distances. In Task 1 there is no stimulation, in Task 2 one stimulus is on, and in Task 3 both stimuli are on. The black arrow indicates the target stimulus. There is a resting time of 2s between trials.

Protocol

Figure 39 shows the protocol of an experiment. Painted rectangles represent stimuli on, while unpainted rectangles corresponds to stimuli off, f_1 and f_2 denote the flickering frequencies, and d_1 and d_2 denote the distances. The black arrow indicates the target stimulus. Two experiments were conducted, in which

- $f_1 = 5.6$ and $f_2 = 6.4$ Hz, and target stimulus placed at $d_1 = 30\text{cm}$; and
- $f_1 = 5.6$ and $f_2 = 6.4$ Hz, and target stimulus placed at $d_2 = 50\text{cm}$.

All experiment were composed by ten trials of 21s. In order to evaluate the three hypothesis tests described in previous section, each trial was composed by three tasks of 7s each one. In Task 1, both stimuli were turned off and spontaneous EEG was recorded ($b[n]$); in Task 2, one stimulus was turned on, subjects was asked to gaze it, and EEG activity due to a stimuli was recorded ($y[n]$); and in Task 3, both stimuli was turned on, subjects were asked to maintain their focus on the same stimulus of the Task 2 even if the other stimulus was turned on, and EEG signals due to joint (focused and non-focused) stimulation was recorded ($x[n]$). To preserve the same experimental conditions, the three tasks were carried out consecutively, as shown in Figure 39. There was 2s breaks between trials.

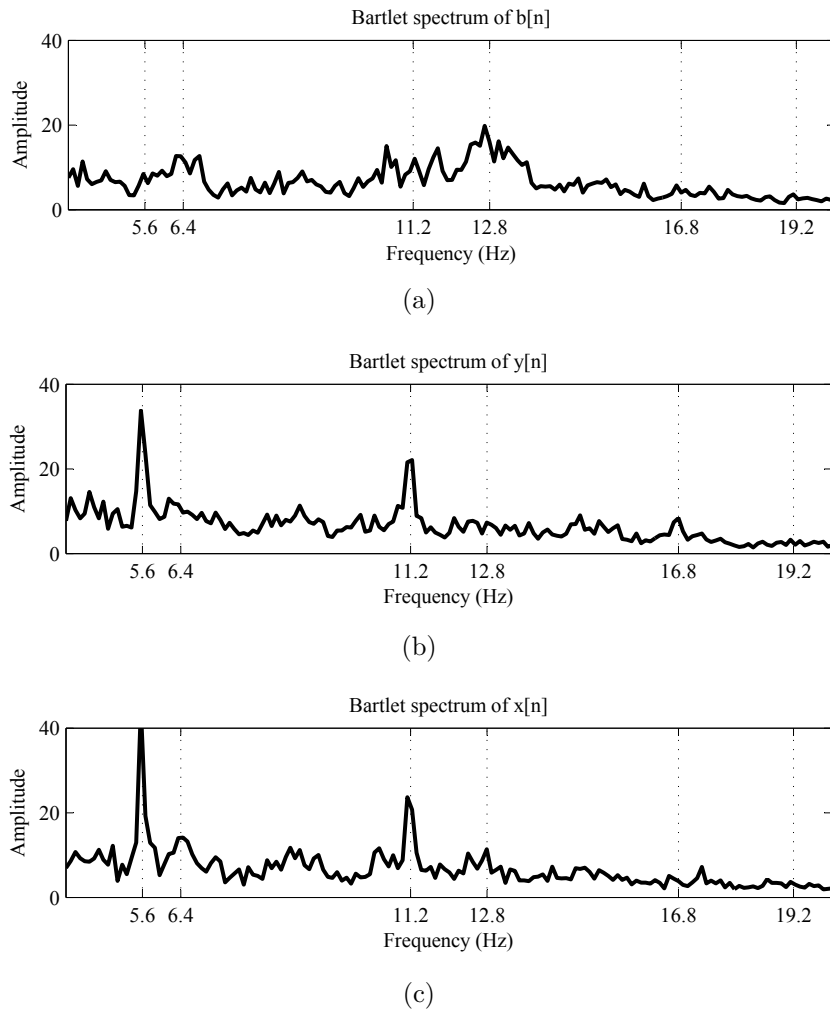


Figure 40 – Bartlett periodogram of signals recorded at electrode Oz of one subject; a) for spontaneous EEG signal, $b[n]$, with no visual stimulation; b) for EEG signals due to isolated stimulus flickering at 5.6 Hz, $y[n]$; and c) for EEG signals caused by focused and non-focused stimuli flickering, respectively, at 5.6 and 6.4 Hz, $x[n]$.

4.4 Results

Figure 40 shows the Bartlett periodogram at frequency range of 4-20 Hz of the EEG signals of a subject. Signals were recorded at electrode Oz when the target stimulus was flickering at 5.6 Hz during the three tasks described in Figure 39. Periodograms of $b[n]$, $y[n]$, and $x[n]$ signals that were recorded in each task are shown in Figure 40a, Figure 40b and Figure 40c, respectively. It can be seen that the amplitude of the Bartlett periodogram of $b[n]$ increases for frequencies between 10 and 13 Hz, possibly due to alpha rhythm. In the periodogram of $y[n]$, the amplitude presents strong peaks at fundamental (5.6 Hz) and second harmonic (11.2 Hz) frequencies of the flickering stimulus. And, in the case $x[n]$, the amplitude also presents strong peaks at fundamental (5.6 Hz) and second harmonic (11.2 Hz) frequencies of the focused stimulus. Weak peaks are observed at fundamental

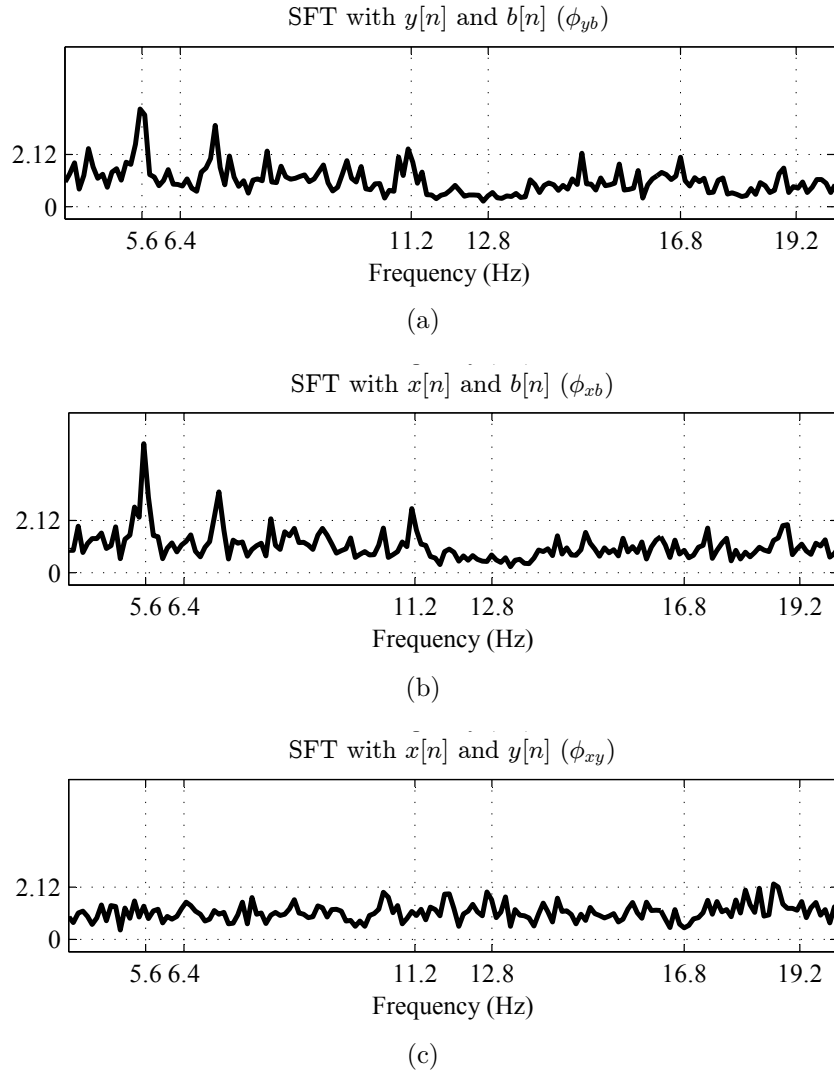


Figure 41 – SFT results and Hypothesis test evaluation a) H_0^{yb} between isolated stimulus response $y[n]$ and background activity $b[n]$; b) H_0^{xb} between focused stimulus response when non-focused one is present $x[n]$ and background activity $b[n]$; and c) H_0^{xy} between focused stimulus response $x[n]$ and isolated stimulus response $y[n]$. Critical values for all cases are $\hat{\phi}_{yb}(f)_{crit} = \hat{\phi}_{xb}(f)_{crit} = \hat{\phi}_{xy}(f)_{crit} = 2.12$.

(6.4 Hz) and second harmonic (12.8 Hz) frequencies of non-focused stimulus.

Figure 41 shows the SFT computed according (4.4), (4.10) and (4.11), respectively, for EEG signals recorded at electrode Oz. Note that due to every signals were recorded in ten trials, then $M_b = M_y = M_x = 10$. Hence, the critical value for evaluating null hypothesis computed using (4.8) for degrees of freedom given by the number of segments and for a significance level of $\alpha = 0.05$ is

$$\hat{\phi}_{yb}(f)_{crit} = \hat{\phi}_{xb}(f)_{crit} = \hat{\phi}_{xy}(f)_{crit} = 2.12. \quad (4.12)$$

Hypothesis test, H_0^{yb} , that evaluates if $y[n]$ and $b[n]$ belong the same population are

shown in Figure 41a. Hypothesis test, H_0^{xb} , that evaluates $x[n]$ and $b[n]$; and Hypothesis test, H_0^{xy} , that evaluates $x[n]$ and $y[n]$, are shown in Figure 41b and Figure 41c, respectively. In three cases, a dotted line was draw to indicate the critical value. Then,

- in Figure 41a, it can be seen clearly that $\hat{\phi}_{yb}(f) < \hat{\phi}_{yb}(f)_{crit}$ at every frequency except at the fundamental frequency of flickering stimulus, 5.6 Hz; thus, H_0^{yb} was rejected at this frequency showing that there is a evoked response due to visual stimulus into the EEG response $y[n]$. Also, H_0^{yb} can be rejected at second and third harmonic, because the $\hat{\phi}_{yb}(f)$ are close to the critical value. These results are coherent to those obtained by [Infantosi, Lazarev & Campos \(2005\)](#);
- in Figure 41b, H_0^{xb} was rejected at fundamental frequency of focused stimulus, $\hat{\phi}_{xb}(f = 5.6) > \hat{\phi}_{xb}(f)_{crit}$, and it was not rejected at fundamental frequency of non-focused stimulus, $\hat{\phi}_{xb}(f = 6.4) < \hat{\phi}_{xb}(f)_{crit}$. These results are too important in this evaluation, because indicate that would have an evoked potential due to focused stimulus that is not affected by non-focused stimulus. Apparently, this last stimulus does not evoke any potential in the response. Results of second harmonic frequencies, 11.2 and 12,8 Hz, of both stimuli reinforce this statement; and
- in Figure 41c, H_0^{xy} was not rejected at every frequency domain ($\hat{\phi}_{xb}(f) < \hat{\phi}_{xb}(f)_{crit}$), indicating that there responses of isolated stimulus and responses of focused stimulus (when non-focused one is present) could belong to the same distribution.

Bartlett periodogram of EEG signals recorded at thirteen electrode positions (Figure 73) at frequency range of 4-13 Hz for all subjects considered in this evaluation (gray curves) and their averages (black curves) are shown in Figure 42, Figure 43 and Figure 44. Figure 42 shows the periodogram of spontaneous EEG signals recorded when no stimuli was on, $b[n]$. Note that the amplitude increases in the frequency range 10-12 Hz than can be related to the alpha rhythm in all channels. Figure 43 shows the periodogram of EEG signals recorded when subjects was asked to gaze an isolated stimulus flickering at 5.6 Hz, $y[n]$. Note in the average curves that peaks at fundamental frequency of the attended stimulus are present in all channels. Amplitude of peaks at occipital channels are higher than parietal channels. Peaks at second harmonic of the attended stimulus are observed, which are clearly distinguishable in occipital channels. In parietal channels, an increasing of frequency in the frequency range 10-12 Hz is also observed. Figure 44 shows the periodogram of EEG signals recorded when subjects was asked to focus on the stimulus flickering at 5.6 Hz while the non-focused one was flickering at 6.4 Hz, $x[n]$. Note that in the same way of Figure Figure 43, peaks at fundamental and second harmonic of the attended stimulus are observed in all channels. However, peaks at fundamental frequencies of the non-focused stimulus also are observed; and even if peaks due to non-focused stimulus are weak, they are present in all channels.

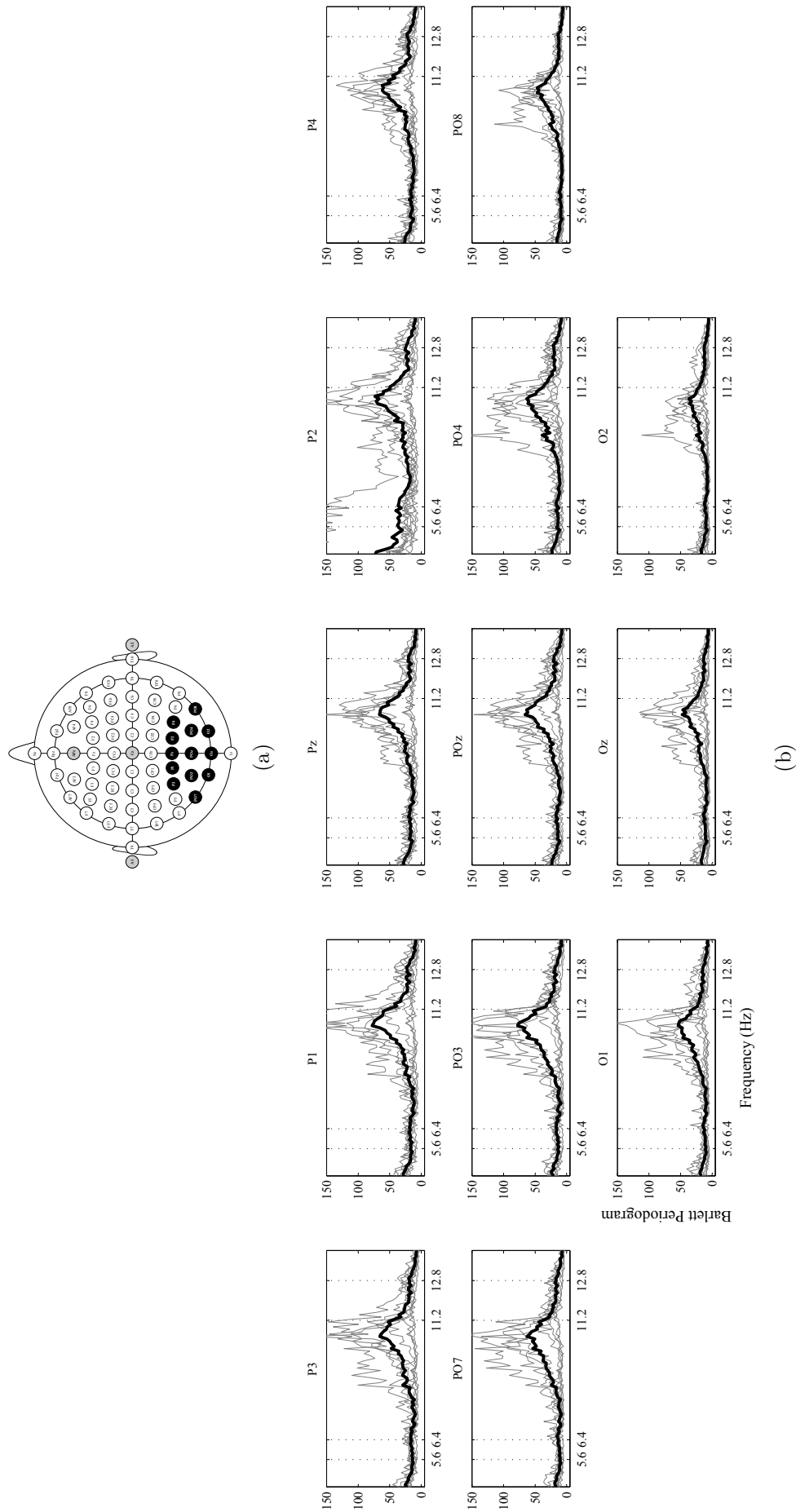


Figure 42 – Bartlett periodogram of spontaneous EEG signals, $b[n]$. a) Extended 10/20 international system; black circles are the P1, P2, P3, P4, Pz, PO3, PO4, PO7, PO8, POz, O1, O2 and Oz positions, and gray circles are the A1, A2, Cz and AFz positions. b) Bartlett periodogram at frequency range of 4-13 Hz for thirteen electrodes corresponding to four subjects (gray curves) and their grand average (black curves).

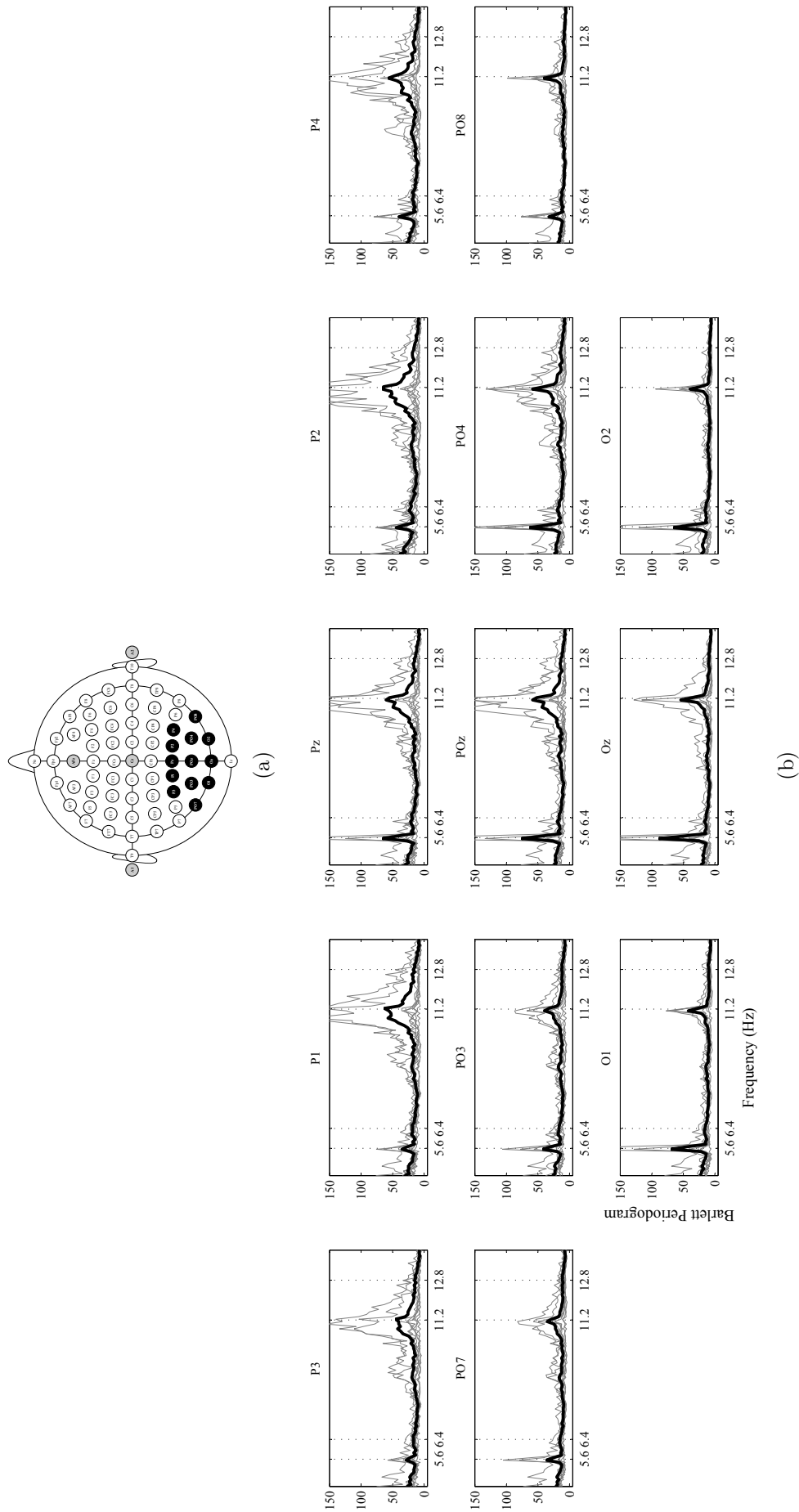


Figure 43 – Bartlett periodogram of EEG signals due to isolated stimulus flickering at 5.6 Hz, $y[n]$. a) Extended 10/20 international system; black circles are the P1, P2, P3, P4, Pz, PO3, PO4, PO7, PO8, POz, O1, O2 and Oz positions, and gray circles are the A1, A2, Cz and AFz positions. b) Bartlett periodogram at frequency range of 4-13 Hz for thirteen electrodes corresponding to four subjects (gray curves) and their grand average (black curves).

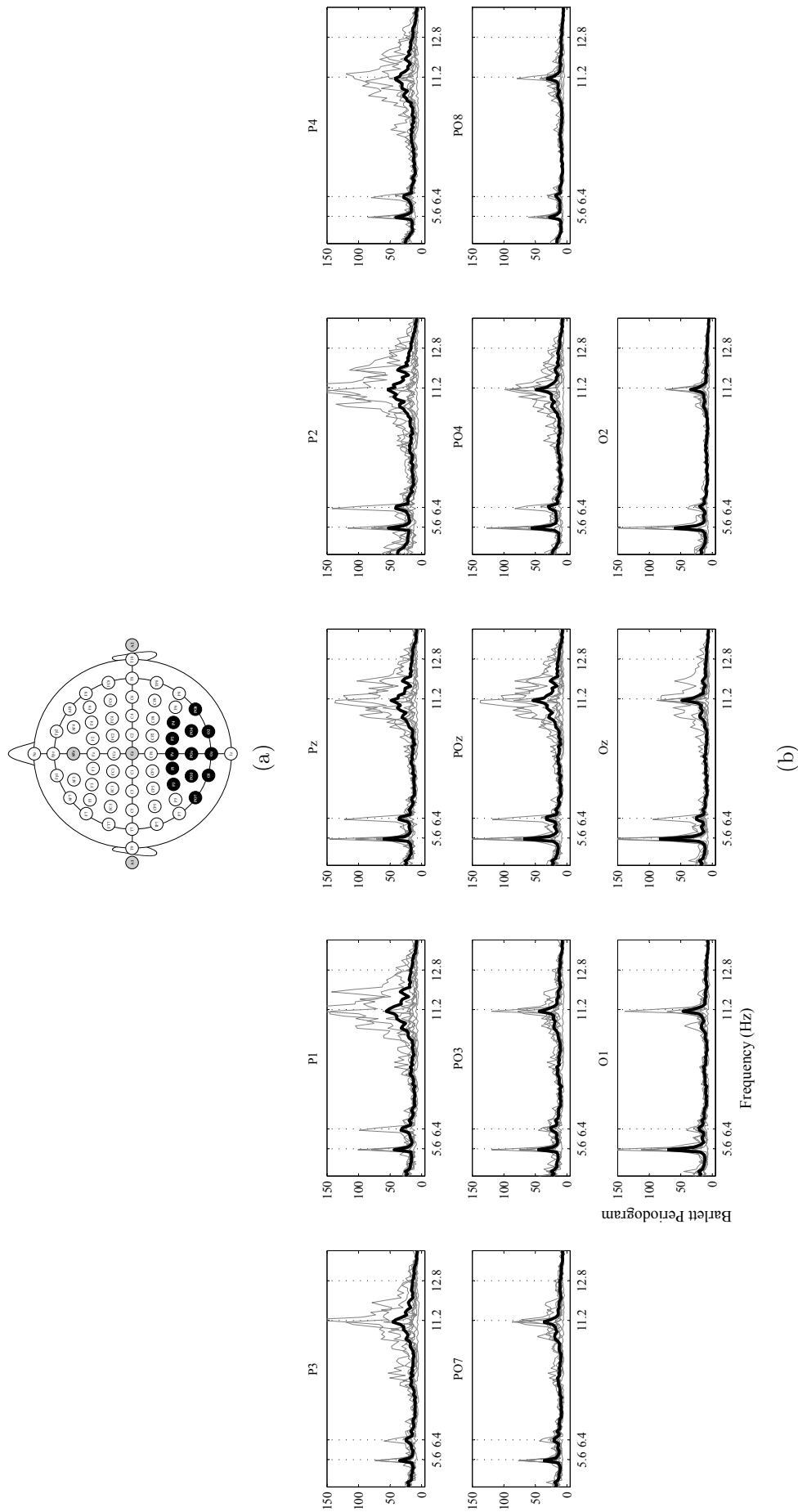


Figure 44 – Bartlett periodogram of EEG signals caused by focused and non-focused stimuli flickering at 5.6 Hz and 6.4 Hz, respectively. a) Extended 10/20 international system; black circles are the P1, P2, P3, P4, Pz, PO3, PO4, PO7, PO8, POz, O1, O2 and Oz positions, and gray circles are the A1, A2, Cz and AFz positions. b) Bartlett periodogram at frequency range of 4-13 Hz for thirteen electrodes corresponding to four subjects (gray curves) and their grand average (black curves).

To evaluate if the peaks due to the non-focuses stimulus observed in Figure 44 affects the response of the focused stimulus, hypothesis test of absence of response are conducted. Figure 45, Figure 46 and Figure 47 show, respectively, the $\hat{\phi}_{yb}(f)$, $\hat{\phi}_{xb}(f)$ and, $\hat{\phi}_{xy}(f)$ for thirteen channels and for all subjects (gray curves) together with average (thick black curves), and their confidence interval for 95% (thin black curves). The critical value that is used to evaluate the hypothesis test was the same in all cases, $\hat{\phi}_{yb}(f)_{crit} = \hat{\phi}_{yb}(f)_{crit} = \hat{\phi}_{yb}(f)_{crit} = 2.12$.

In Figure 45, $\hat{\phi}_{yb}(f)$ was computed according (4.4) using the Bartlett periodogram of $y[n]$ recorded when subjects were asked to gaze an isolated stimulus flickering at 5.6 Hz, and $b[n]$ recorded with no stimulation. Note that the null hypothesis, H_0^{yb} , of absence of evoked potentials due to attended stimulus is rejected at the fundamental frequency of the flickering stimulus, due to in the average $\hat{\phi}_{yb}(f = 5.6) > \hat{\phi}_{yb}(f)_{crit}$, in all electrodes but parietal electrodes P1, P2, P3 and P4. In contrast, $\hat{\phi}_{yb}(f = 5.6)$ achieves higher values in occipital and central electrodes, O1, O2, Oz, POz and Pz. On another hand, in the average H_0^{yb} is not rejected at the second harmonic frequency of the attended stimulus (11.2 Hz) in all electrodes ($\hat{\phi}_{yb}(f = 11.2) < \hat{\phi}_{yb}(f)_{crit}$). As expected in traditional systems where only a target stimulus are presented to subjects, there is evoked potentials at the frequency of the target stimulus (INFANTOSI; LAZAREV; CAMPOS, 2005), principally in occipital electrodes.

In Figure 46, $\hat{\phi}_{xb}(f)$ was computed according (4.10) using the Bartlett periodogram of EEG signals recorded when subjects were asked to focus on the target stimulus flickering at 5.6 Hz, $x[n]$, while the non-focused stimulus was flickering at 6.4 Hz; and signals recorded when subjects were in rest time with no stimulation, $b[n]$. In this case, the null hypothesis, H_0^{xb} , evaluates the absence of evoked potentials due to focused or non-focused stimuli. Note that H_0^{xb} in the average is rejected at the fundamental frequency of focused stimulus $\hat{\phi}_{xb}(f = 5.6) > \hat{\phi}_{xb}(f)_{crit}$ in all electrodes but P1, P2, P3 and P4. $\hat{\phi}_{xb}(f = 5.6)$ achieves higher values in occipital electrodes. Regarding the non-focused stimulus, even some individual values of $\hat{\phi}_{xb}(f)$ are higher than critical value in its fundamental frequency, in the average H_0^{xb} is not rejected ($\hat{\phi}_{xb}(f = 6.4) < \hat{\phi}_{xb}(f)_{crit}$) in all electrodes. H_0^{xb} also is not rejected at the second harmonic frequencies of focused and non-focused stimuli (11.2 and 12.8 Hz). Therefore, it can be seen that (a) although the non-focused stimulus is present in the subjects' field of view, there are distinguishable evoked potentials due to focused stimulus; and (b) it can not be affirmed that there is or there is not evoked potentials due to non-focused stimulus.

In Figure 47, $\hat{\phi}_{xy}(f)$ was computed according (4.11) using the Bartlett periodogram of signals recorded when subjects were asked to focus on the target stimulus flickering at 5.6 Hz, $x[n]$, while the non-focused stimulus was flickering at 6.4 Hz; and signals recorded when subjects were asked to gaze an isolated stimulus flickering at 5.6 Hz, $y[n]$. In this

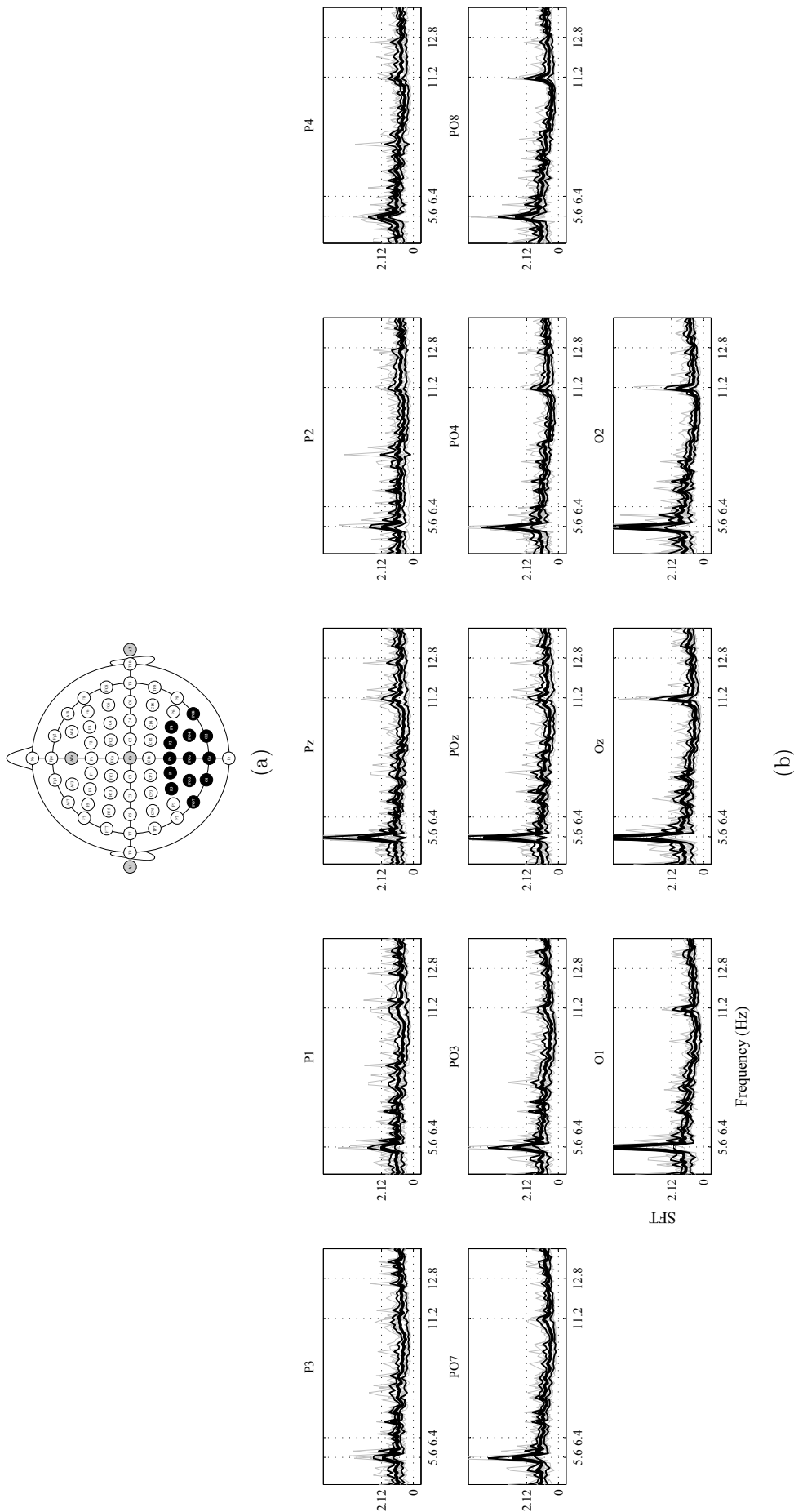


Figure 45 – H_0^{yb} evaluated with EEG signals due to isolated stimulus flickering at 5.6 Hz $y[n]$, and spontaneous EES $b[n]$. a) Extended 10/20 international system; black circles are the P1, P2, P3, P4, Pz, PO3, PO4, PO7, PO8, POz, O1, O2 and Oz positions, and gray circles are the A1, A2, Cz and AFz positions. b) $\hat{\phi}_{yb}(f)$ at frequency range of 4-13 Hz for thirteen electrodes corresponding to four subjects (gray curves), their average (thick black curves), and the 95% confidence interval (thin black curves). Critical value is $\phi_{yb}(f)_{crit} = 2.12$.

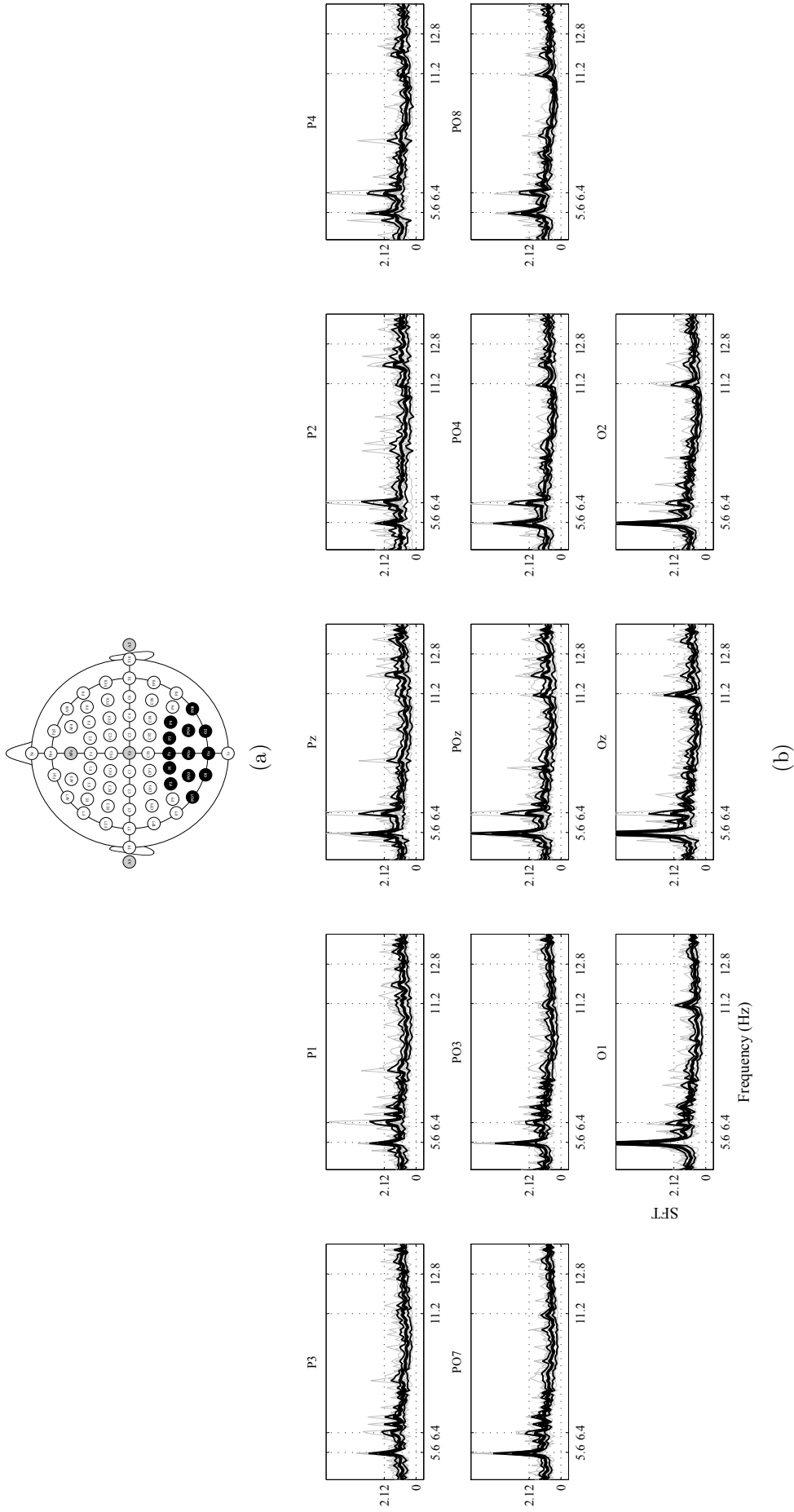


Figure 46 – H_0^{xb} evaluated with EEG signals recorded when focused (5.6 Hz) and non focused (6.4 Hz) stimuli were present in the subjects' field of view $x[n]$, and spontaneous EEG $b[n]$. a) Extended 10/20 international system; black circles are the P1, P2, P3, P4, Pz, PO3, PO4, PO7, PO8, POz, O1, O2 and Oz positions, and gray circles are the A1, A2, Cz and AFz positions. b) $\hat{\phi}_{xb}(f)$ at frequency range of 4–13 Hz for thirteen electrodes corresponding to four subjects (gray curves), their average (thick black curves), and the 95% confidence interval (thin black curves). Critical value is $\phi_{xb}(f)_{crit} = 2.12$.

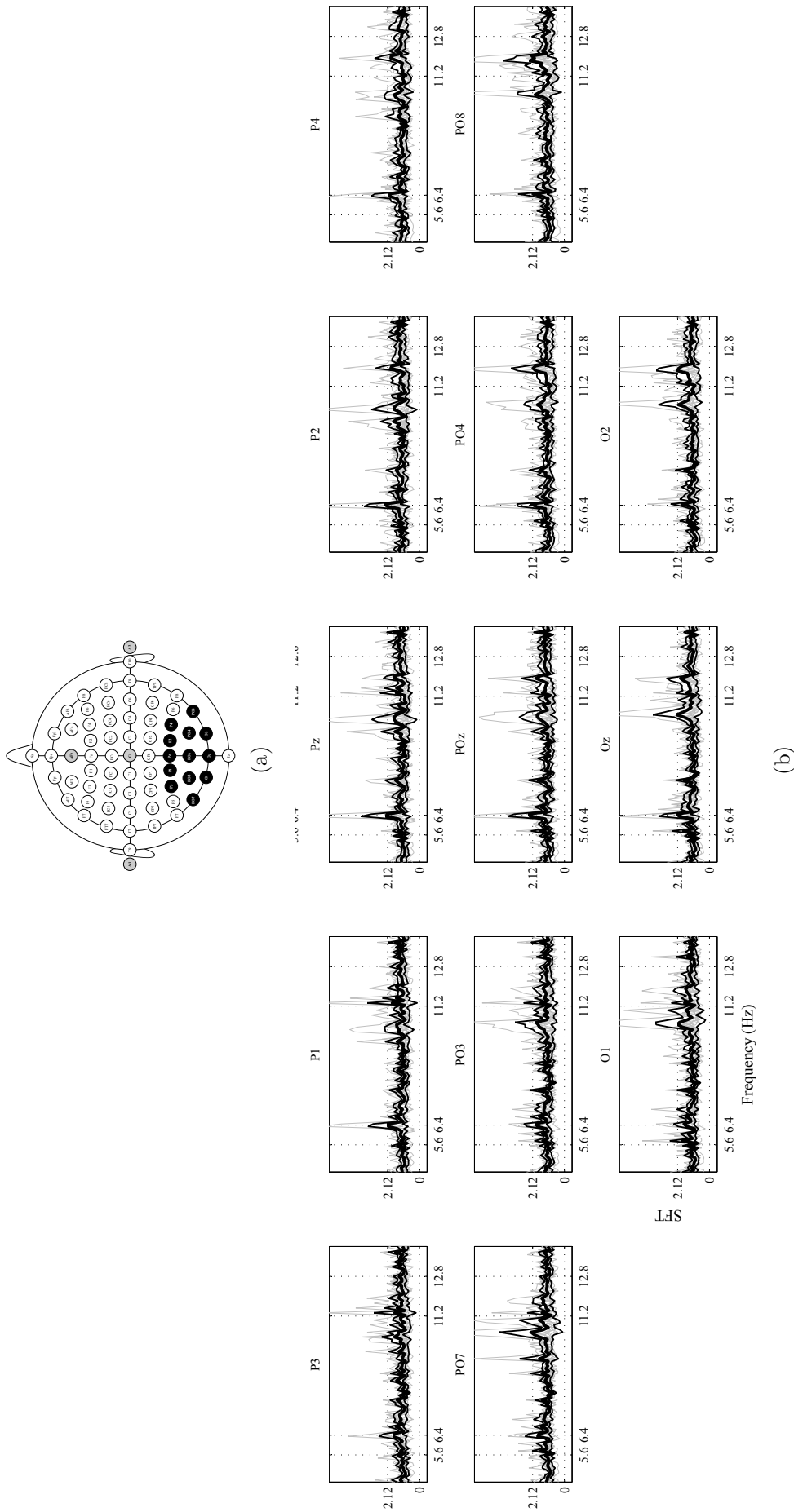


Figure 47 – H_0^{yb} evaluated with EEG signals recorded when focused (5.6 Hz) and non focused (6.4 Hz) stimuli were present in the subjects' field of view $x[n]$, and EEG signals due to isolated stimulus flickering at 5.6 Hz $y[n]$. H_0^{xy} between focused stimulus response $x[n]$ and isolated stimulus response $y[n]$. a) Extended 10/20 international system; black circles are the P1, P2, P3, P4, Pz, PO3, PO4, PO7, PO8, POz, O1, O2 and Oz positions, and gray circles are the A1, A2, Cz and AFz positions. b) $\hat{\phi}_{xy}(f)$ at frequency range of 4-13 Hz for thirteen electrodes corresponding to four subjects (gray curves), their average (thick black curves), and the 95% confidence interval (thin black curves). Critical value is $\phi_{xy}(f)_{crit} = 2.12$.

case, the null hypothesis H_0^{xb} is not rejected at all range of frequencies evaluated including the fundamental and second harmonic frequencies of focused and non focused stimuli ($\hat{\phi}_{xy}(f) > \hat{\phi}_{xy}(f)_{crit}$). It means that there is not sufficiently arguments to asseverate that signals recorded when the attended stimulus was isolated $y[n]$, and signals recorded when the attended stimulus was in focus while other stimulus was present in subjects' field of view $x[n]$, are different.

Bartlett periodogram of EEG signals when the attended stimulus, gazed or focused, was flickering at 5.6 Hz were shown in Figures 42, 43 and 44. Also, the evaluation of the null hypothesis for this frequency were described in Figures 45, 46 and 47. Following the same procedure, Figures 48, 49 and 50 show the Bartlett periodogram when the target stimulus was flickering at 6.4. And in Figures 51, 52 and 53 the null hypothesis are evaluated. In general, the results for frequency of target stimulus of 6.4 Hz are similar to results for frequency of 5.6 Hz. In Figure 48, the amplitude increases in the frequency band 10-12 Hz in all electrodes. In Figure 49, peaks at the fundamental and the second harmonic frequencies of the attended stimulus are observed in all electrodes. In Figure 50, strong peaks at the fundamental and the second harmonic frequencies of the focused stimulus are observed in all electrodes. Also, weak peaks are observed in the fundamental frequency of non-focused stimulus. In Figure 51, in the average the null hypothesis was rejected at the fundamental frequency of attended stimulus in all electrodes. Also, it was rejected at the second harmonic frequency in all electrodes but P1 and P3. In Figure 52, the null hypothesis was rejected at the fundamental frequency of the focused stimulus in all electrode but P2 where it is evident that the signal was not registered in right way. Also, it was rejected at its second harmonic frequency in all electrodes but P1, P2, P3 and P4. However, the null hypothesis was not rejected at the fundamental frequency of non-focused stimulus in electrodes P1, Pz and POz. And, in Figure 53, the null hypothesis was rejected at the fundamental frequency of the non-focused stimulus in electrodes P1, Pz and POz.

4.5 Discussion

ORD techniques that are based on statistical tests are being employed successfully in the detection of somatosensory (TIERRA-CRIOLLO; INFANTOSI, 2006), visual (SA et al., 2006; INFANTOSI; LAZAREV; CAMPOS, 2005) and auditory (FELIX et al., 2014) evoked potentials. In this chapter, the ORD based on SFT was used to evaluate the hypothesis of this Thesis that establishes that the focused stimulus is able to evoke a visual potential although a non-focused stimulus is also present together in the center of field of view. In this sense, a null hypothesis of the absence of effects of the non-focused stimulus in the response of the focused stimulus was tested. In Figures 46 and 52, it was observed that although the non-focused stimulus is present in the subjects' field of view,

there are distinguishable evoked potentials due to focused stimulus.

However it can not asseverate that there is or there is not evoked potentials due to non-focused stimulus because the non-rejection indicates that the null hypothesis can be kept in order to conduct some detection method, which can be based on the comparison of the SNR computed around the fundamental frequencies (and harmonic frequencies) of Focused and non-focused stimuli. Although it is recommended to repeat the fail experiments, they have not been disregarded of this work in order to present the full results of our experiments. Sometimes, even if hypothesis tests have two possible outcomes, rejection and non-rejection, they are considered as accepted instead of non-rejected (INFANTOSI; LAZAREV; CAMPOS, 2005; SA et al., 2006).

Finally, results of this chapter provide evidences that if two stimuli are presented simultaneously in the center of the field of view of the BCI's user, flickering at different frequencies and located at different distances from the user, then the focused stimulus will be able to elicit distinguishable SSVEP pattern regardless the non-focused stimulus is also present. To conduct the statistical evaluation based on SFT, it was assumed that the spontaneous EEG signal, the response to isolates stimulus and the response to the focused stimulus, $b[n]$, $y[n]$ and $x[n]$ were zero-mean Gaussian distributions with equal variance.

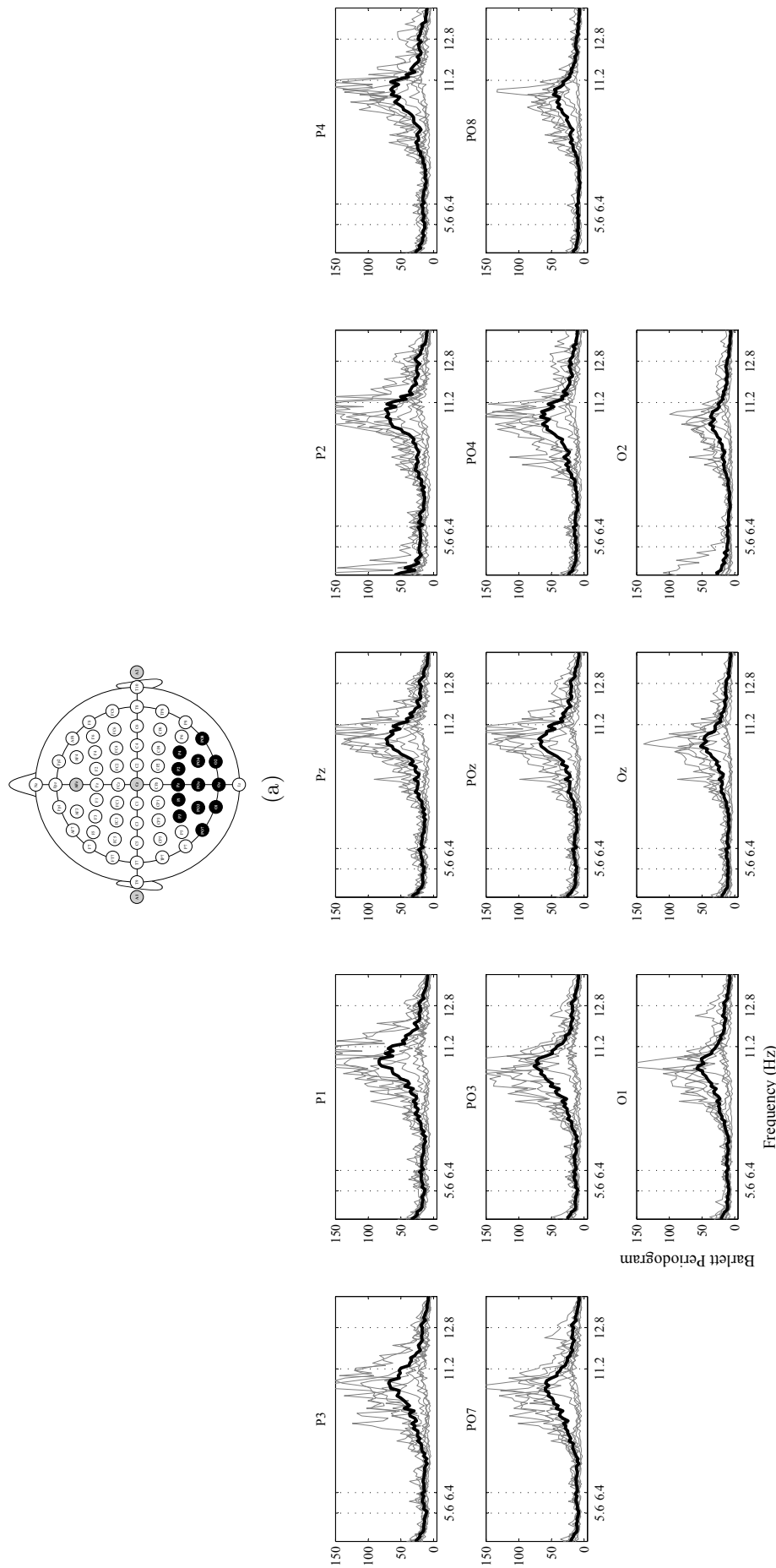


Figure 48 – Bartlett periodogram of spontaneous EEG signals, $b[n]$. a) Extended 10/20 international system; black circles are the P1, P2, P3, P4, Pz, PO3, PO4, PO7, PO8, POz, O1, O2 and Oz positions, and gray circles are the A1, A2, Cz and AFz positions. b) Bartlett periodogram at frequency range of 4-13 Hz for thirteen electrodes corresponding to four subjects (gray curves) and their grand average (black curves).

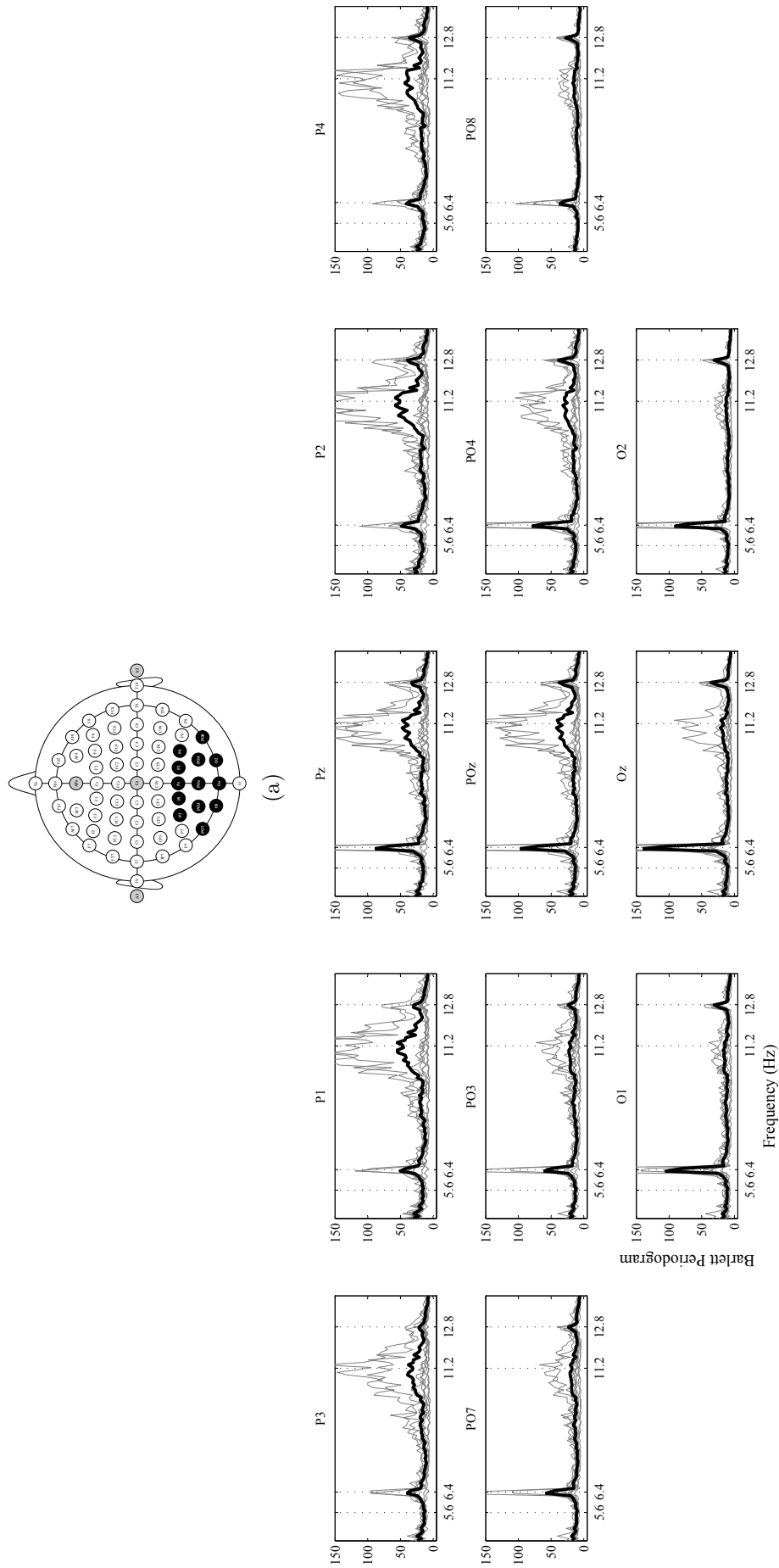


Figure 49 – Bartlett periodogram of EEG signals due to isolated stimulus flickering at 6.4 Hz, $y[n]$. a) Extended 10/20 international system; black circles are the P1, P2, P3, P4, Pz, PO3, PO4, PO7, PO8, POz, O1, O2 and Oz positions, and gray circles are the A1, A2, Cz and AFz positions. b) Bartlett periodogram at frequency range of 4-13 Hz for thirteen electrodes corresponding to four subjects (gray curves) and their grand average (black curves).

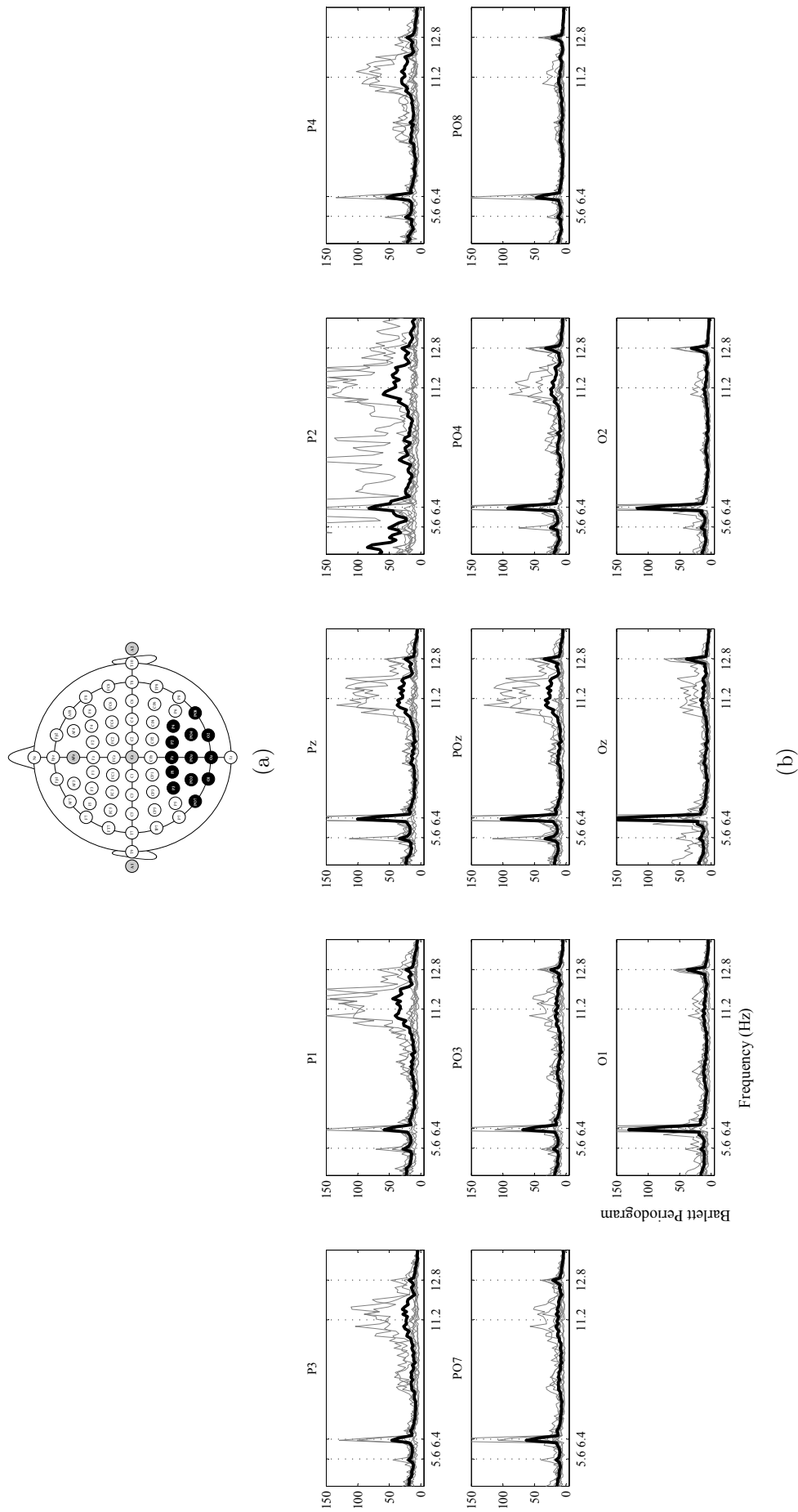


Figure 50 – Bartlett periodogram of EEG signals caused by focused and non-focused stimuli flickering at 6.4 Hz and 5.6 Hz, respectively. a) Extended 10/20 international system; black circles are the P1, P2, P3, P4, Pz, PO3, PO4, PO7, PO8, POz, O1, O2 and Oz positions, and gray circles are the A1, A2, Cz and AFz positions. b) Bartlett periodogram at frequency range of 4-13 Hz for thirteen electrodes corresponding to four subjects (gray curves) and their grand average (black curves).

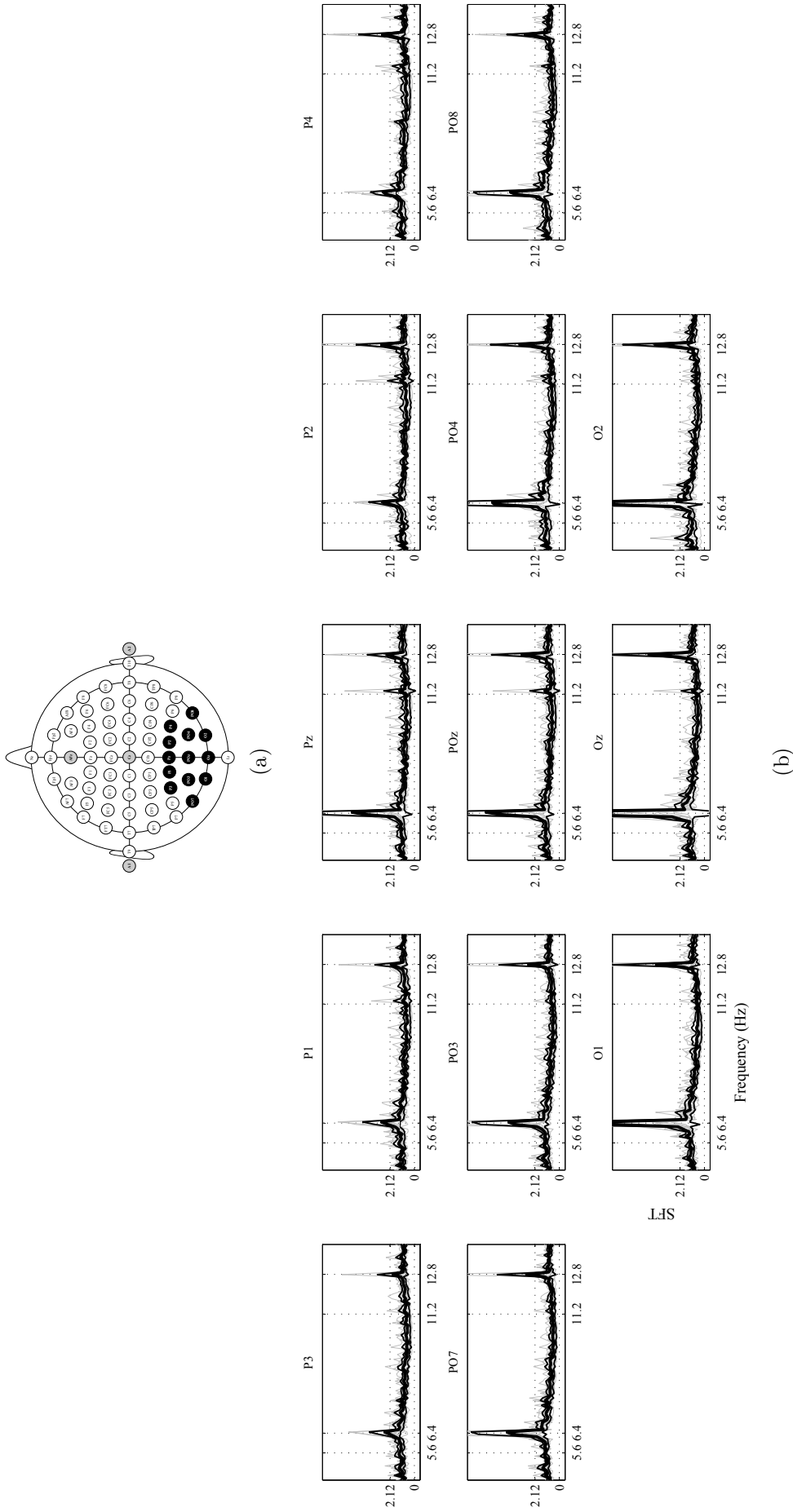


Figure 51 – H_0^{yb} evaluated with EEG signals due to isolated stimulus flickering at 6.4 Hz $y[n]$, and spontaneous EES $b[n]$. a) Extended 10/20 international system; black circles are the P1, P2, P3, P4, Pz, PO3, PO4, PO7, PO8, POz, O1, O2 and Oz positions, and gray circles are the A1, A2, Cz and AFz positions. b) $\hat{\phi}_{yb}(f)$ at frequency range of 4-13 Hz for thirteen electrodes corresponding to four subjects (gray curves), their average (thick black curves), and the 95% confidence interval (thin black curves). Critical value is $\phi_{yb}(f)_{crit} = 2.12$.

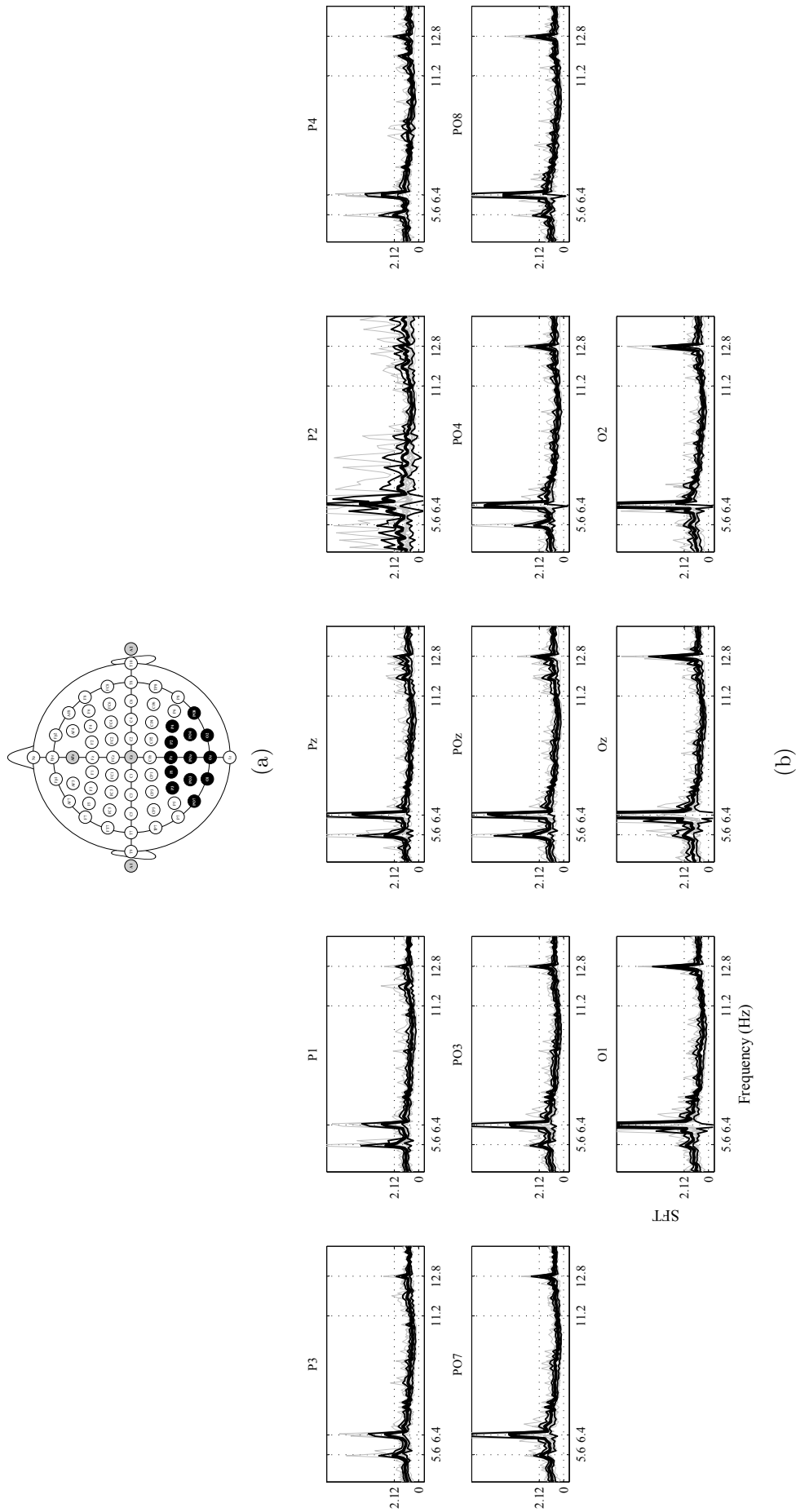


Figure 52 – H_0^{zb} evaluated with EEG signals recorded when focused (6.4 Hz) and non focused (5.6 Hz) stimuli were present in the subjects' field of view $x[n]$, and spontaneous EEG $b[n]$. a) Extended 10/20 international system; black circles are the P1, P2, P3, P4, Pz, PO3, PO4, PO7, PO8, POz, O1, O2 and Oz positions, and gray circles are the A1, A2, Cz and AFz positions. b) $\hat{\phi}_{zb}(f)$ at frequency range of 4–13 Hz for thirteen electrodes corresponding to four subjects (gray curves), their average (thick black curves), and the 95% confidence interval (thin black curves). Critical value is $\phi_{zb}(f)_{crit} = 2.12$.

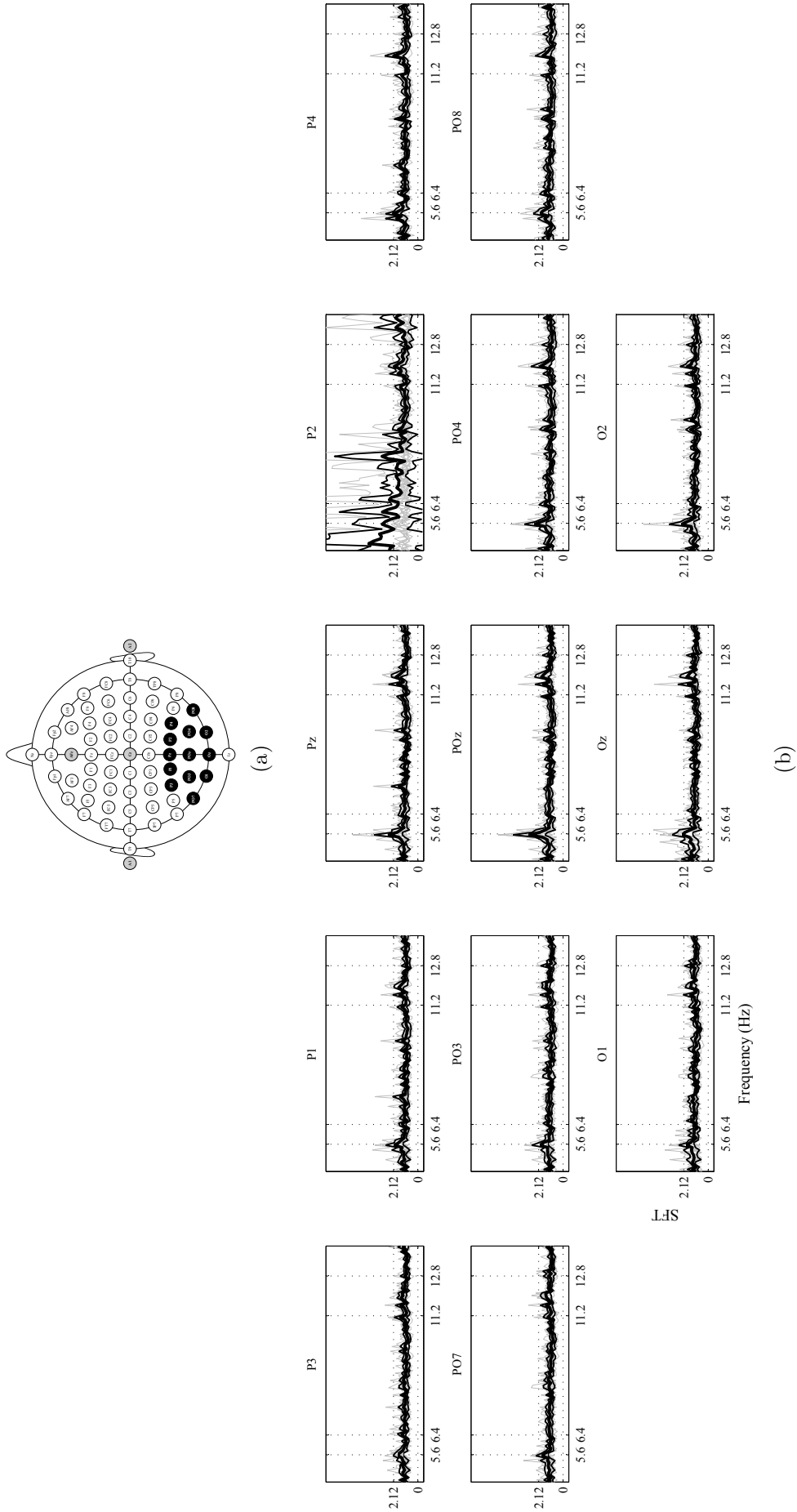


Figure 53 – H_0^{xy} evaluated with EEG signals recorded when focused (6.4 Hz) and non focused (5.6 Hz) stimuli were present in the subjects' field of view $x[n]$, and EEG signals due to isolated stimulus flickering at 6.4 Hz $y[n]$. H_0^{xy} between focused stimulus response $x[n]$ and isolated stimulus response $y[n]$. a) Extended 10/20 international system; black circles are the P1, P2, P3, P4, Pz, PO3, PO4, PO7, PO8, O1, O2 and Oz positions, and gray circles are the A1, A2, Cz and AFz positions. b) $\hat{\phi}_{xy}(f)$ at frequency range of 4-13 Hz for thirteen electrodes corresponding to four subjects (gray curves), their average (thick black curves), and the 95% confidence interval (thin black curves). Critical value is $\phi_{xy}(f)_{crit} = 2.12$.

5 Equation for SSVEP Demodulation

Traditional [SSVEP-BCI](#) systems only consider the response of one stimulus in the center of the field of view against several stimuli located in the peripheral vision. Thus, not encompassing the general situation in which several stimuli are placed in the center of the field of view. In addition, although a set of stimulus are projected in the retinal surface, demodulation analysis are performed taking into account only the target stimulus and ignoring the other stimuli. Hence, currently modulation/demodulation methods are proposed taking into account only one stimulus at a time. For instance [Wang et al. \(2010\)](#) describe two ways of demodulating based on analytical signals and based on spectral peak detection. However, in the setup proposed in this Thesis two stimuli are presented together in the field of view. In this sense, traditional methods must be reviewed and evaluated in order to determine thier ability in demodulating the signals recorded using the novel setup.

In the present chapter, the modulation/demodulation method are described. Then, the demodulation methods described by [Wang et al. \(2010\)](#) are modified so that they can be applied in the extraction of the frequency of the focused stimulus. Both methods based on analytical and spectral were evaluated and modified. A requirement for applying these methods is that the power of the focused stimulus is higher than the non-focused stimulus. Although this requirement seems obvious, the discussion leaping to such conclusion is based on a different approach thatis the eye focusing and accommodation mechanism, which play a key role in the novel setup. Traditional systems visually do not evaluate if the power of the focused stimulus is higher than the non-focused one because the changing of gaze direction ensures that only one stimulus is the center of the field of view. In this sense the retinal response is studied. First, the spatio-temporal response of the retina is described for an isolated flickering stimulus as well as its power spectrum amplitude. Next, the retinal response was described for two stimuli; both for traditional and the novel setups. To evaluate the amplitude of the response of targeted and non targeted stimuli, an expression to denote the spatio-temporal retinal response was elaborated, based on visual perception parameters as wavelength, distance of the stimulus or photoreceptors density.

Finally, some experiments are conducted evaluating and comparing the spectral power of attended and non-attended stimuli in order to verify if the amplitude of the retinal response to focused stimulus is higher than the amplitude response to the non-focused one.

5.1 Traditional Modulation/Demodulation

Modulation

In **SSVEP-BCI** systems, the modulation of brain signals is performed by selective attention. In these systems, a set of stimuli flickering at different frequencies is presented and users are asked to choose one of them. A **SSVEP** pattern that is an increase of the amplitude at the attended stimulus frequency arises in the **EEG** signals recorded at the occipital brain areas (**MIDDENDORF et al., 2000**). The amplitude of this pattern increases significantly as the attended stimulus is moved to the center of the visual field (**WANG et al., 2010**). Due to any stimulus are able to be selected, users' brain signals can be modulated with different frequencies. Then, the frequency modulation is the basic principle of implementing **BCIs** using **SSVEP** patterns to detect the users' gaze direction.

Figure 54 shows a **SSVEP-BCI** based on the modulation of two frequencies. Gray rectangles represent two stimuli flickering at different frequencies, dot lines represent the visual field, and the big and the small circles represent the user's head and the occipital electrode, respectively. In modulation of brain signals, the subject can choose one stimulus changing his gaze direction. Then, a **SSVEP** pattern that arises in f_1 or f_2 can be observed as a peak in the power spectrum of the modulated signal. Thus, **SSVEP-BCI** systems are

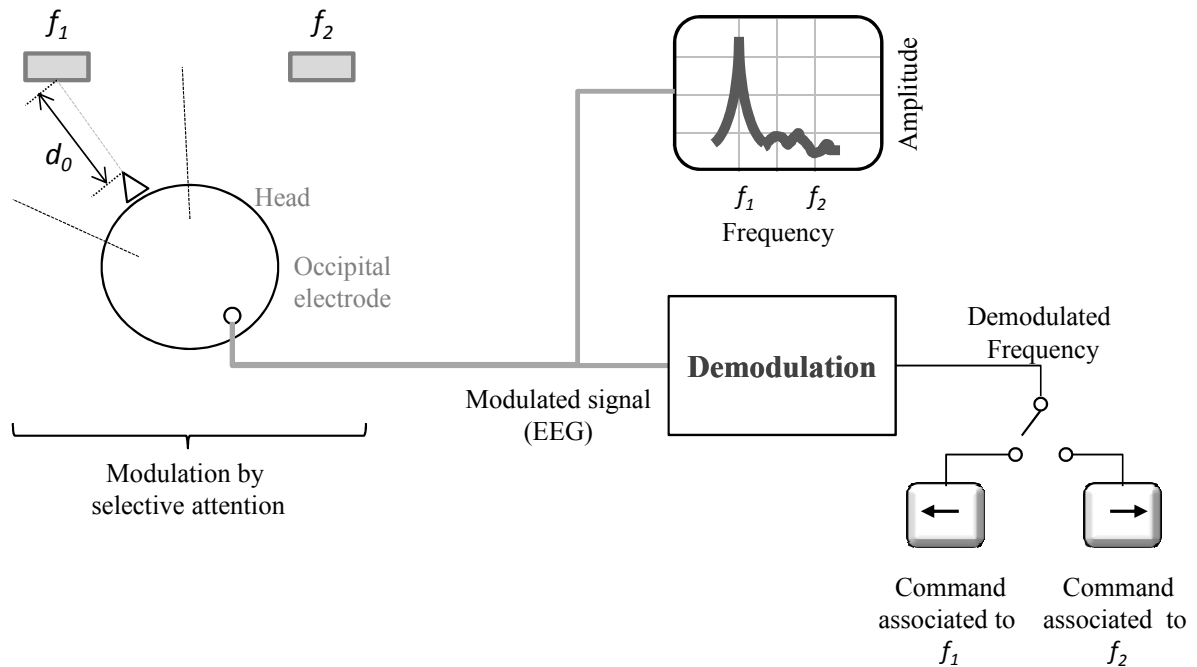


Figure 54 – Traditional **SSVEP-BCI** modulation/demodulation. Modulation is performed by selective attention when subject gazes the stimulus flickering at f_1 and placed at d_0 . Modulated signals was recorded at occipital electrode and showed at spectral analyzer. Demodulation is performed by decoding the attended frequency that is associated to a command.

frequency coded as the frequency of each stimulus is associated to a specific command. In these sense, a computational demodulation process is needed to decode the gazed direction. The aim of the demodulation process is to extract embedded information to be converted into a control signal. In this kind of systems, users could send a sequence of commands by alternating the stimulus attention.

Demodulation

In Figure 54, stimuli are separated enough to ensure that the non-attended stimulus is outside of visual field when the attended one is in the center of the visual field. This information is highlighted and it is worth mentioning it because traditional systems do not encompass the presence of a non-attended stimulus also in the field of view. For instance, Wang et al. (2010) describe two ways of performing demodulation in traditional SSVEP-BCI systems based on analytical signals and based on the peak detection.

In the demodulation based on analytical signals, signals are described as complex functions defines as

$$g(t) = s(t) + j\hat{s}(t) = A(t)e^{j\phi(t)}, \quad (5.1)$$

where $s(t)$ is the EEG modulated signal, $\hat{s}(t)$ is the Hilbert transform of $s(t)$. In the exponential form, it can be seen that $A(t)$ and $\phi(t)$ are the envelope of the signal and the instantaneous phase, respectively. Then, the instantaneous frequency of the attended stimulus can be found by deriving the phase as

$$\omega_i = \frac{d\phi_i(t)}{dt}, i = 1, 2 \dots N, \quad (5.2)$$

where ω is the instantaneous angular frequency, N is the number of visual stimuli and $\omega_i = 2\pi f_i$. Although the demodulation based on analytical signals can be used to demodulate tasks associated to motor imagery using the $A(t)$ or tasks based on phase-coded; it is not commonly used to demodulate frequency in SSVEP-BCI.

For real systems, Wang et al. (2010) adopts the approach of demodulation by detecting the peak value in the power spectrum for frequency recognition. Due to the attended stimulus will induce a peak in the amplitude spectrum at its flickering frequency, the aim of the demodulation is to search for the peak value in the power spectrum and determine the corresponding frequency. In this sense, the frequency can be identified as

$$\omega_i = \arg \max_{\omega_i} P_{ss}(\omega), i = 1, 2 \dots N, \quad (5.3)$$

where $P_{ss}(\omega)$ represents the power spectrum of the modulated EEG signal $s(t)$, N is the number of visual stimuli and $\omega_i = 2\pi f_i$.

5.2 Proposed Modulation/Demodulation

Modulation

In the novel **SSVEP-BCI** setup proposed in this Thesis, the modulation process is performed by selective attention but based on focused mechanism instead changing of gaze direction. Figure 55 illustrates the novel setup in which gray rectangles represent the two stimuli flickering at different frequencies and dotted lines delimit the visual field. Stimuli are presented together in the visual field and separated conveniently so that if one is in focus the other one is defocused. Rectangle with border represents the focused stimulus. In the case that two stimuli are present simultaneously in the central field of view the output will be affected by two stimuli; then, the **EEG** signal could be modulated by both frequencies.

Analytical Demodulation

When two stimuli are presented together in the field of view, it can not be assumed *a priori* that each stimulus evokes a potential at its flickering frequency. However, in order to see how each frequency affect the **EEG** signal, it can be decomposed in two signals, one that includes only the frequency of the focused stimulus and other one that only includes the frequency of the non-focused stimulus, as shown in Figure 55. Hence, a **LPF** and a

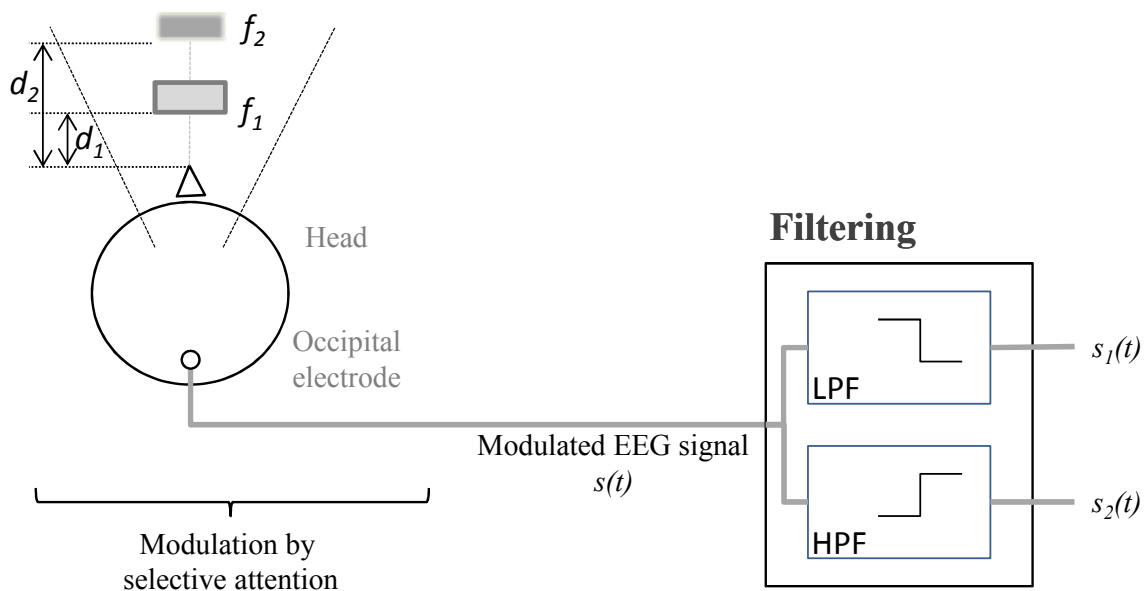


Figure 55 – Modulation/demodulation for the Novel **SSVEP-BCI** Setup. Modulation is performed by selective attention when subject focus on the target stimulus that is flickering at f_1 and placed at d_1 . Modulated signals were recorded at occipital electrode. Demodulation is performed by filtering the modulated signal $s(t)$ in order that $s_1(t)$ only includes the frequency of the focused stimulus, and $s_2(t)$ only includes the frequency of the non-focused one.

HPF can be both used with a cut frequency of $\omega_c = (\omega_1 + \omega_2)/2$, in which $\omega_i = 2\pi f_i$.

If $f_1 < f_2$, then the LPF and the HPF attenuate the frequencies f_2 and f_1 , respectively; consequently the analytical signals for f_1 and f_2 , respectively, are given by

$$g_1(t) = A_1(t)e^{j\phi_1(t)}, \quad (5.4)$$

and

$$g_2(t) = A_2(t)e^{j\phi_2(t)}; \quad (5.5)$$

where $A_i(t)$ is the amplitude and $\phi_i(t)$ is the instantaneous phase. Note that if stimuli were presented isolated, the instantaneous frequency ω_i (for $i = 1, 2$) could be computed by using (5.2). In this sense, a more general expression can be proposed to find the frequency of the attended stimulus that includes responses of both stimuli as

$$\omega_a = a_1\omega_1 + a_2\omega_2, \quad (5.6)$$

or

$$\omega_a = a_1 \frac{d\phi_1(t)}{dt} + a_2 \frac{d\phi_2(t)}{dt}, \quad (5.7)$$

in which a_i (for $i = 1, 2$) is used to find analytically the instantaneous frequency ω_a of the stimulus that is being attended. Then, if the amplitude of focused stimulus is assumed higher than the amplitude of the non-focused stimulus, the instantaneous value of a_i can be computed as

$$a_1 = \frac{\text{sgn}(A_1(t) - A_2(t))}{2} + 0.5, \quad (5.8)$$

and

$$a_2 = \frac{\text{sgn}(A_2(t) - A_1(t))}{2} + 0.5, \quad (5.9)$$

where $A_i(t)$ for $i = 1, 2$ is the amplitude of the analytical signal. Finally, combining (5.7), (5.9), and (5.8) the demodulation using analytical signals can be expressed as

$$\omega_a = \left(\frac{\text{sgn}(A_1(t) - A_2(t))}{2} + 0.5 \right) \frac{d\phi_1(t)}{dt} + \left(\frac{\text{sgn}(A_2(t) - A_1(t))}{2} + 0.5 \right) \frac{d\phi_2(t)}{dt}. \quad (5.10)$$

Recall that 5.10 describes analytically the response of the focused stimulus, if and only if, the amplitude at its frequency is greater than the amplitude at the frequency of the non attended one. Due to harmonics frequencies can be also evoked (MULLER-PUTZ et al., 2005), a Band-pass filter (BPF) can be used before the HPF and LPF filters.

Demodulation based on Spectral Peak Detection

In demodulation based on the peak detection, signal decomposition is not necessary because the frequency values can be compared directly in the spectral domain. Therefore, according to (5.3), the frequency of the focused stimulus can be found by

$$\omega_a = \arg \max_{\omega_i} P(\omega_i | P_{ss}(\omega)), \quad (5.11)$$

where $\omega_a = 2\pi f_a$ and $P_{ss}(\omega)$ represents the power spectrum of the EEG signal $s(t)$, which is computed by using Fast Fourier transform (FFT) over a finite TW. In practical systems, it can be reduced to

$$\omega_a = \arg \max_{\omega_i} P_{ss}(\omega_i). \quad (5.12)$$

Analogously to analytical demodulation, in peak based detection (5.12) can be applied with success if, and only if, the amplitude of the power spectrum at the frequency of attended stimulus is greater than the amplitude of the power spectrum at the frequency of the non-attended one.

In the following sections, the retinal response are described in order to address a possible coherent explanation for the relative low power frequency observed for the non-focused regarding the focused one. A principle that underlies the development of the new setup here proposed.

5.3 Spatio-temporal Retinal Response for a Flickering Stimulus

The idealized retinal image $I(x, y)$ is the projection of an object $O(x, y)$ on the retinal surface, which does not take into account optical conditions of the visual system as lens shape or pupil size that affects the projected images. In general, projected idealized images are associated to an object as

$$I(x, y) = O(x/M, y/M) \quad (5.13)$$

where M is the magnification coefficient between object and image planes (SHEVELL, 2003). Figure 75 of Appendix E shows a scene with two objects, in which the lower is focused and the object above is non-focused. In human eye, the projection of both objects on the retina are affected by optical conditions of the visual system. The non-focused object are projected blur because lens are not accommodated for it. The color of objects are given by the wavelength, then a more complete way to express a point of the idealized image is $I(x, y, \lambda)$ or $I(\mathbf{x}, \lambda)$, in which $\mathbf{x} = (x, y)$ is a bidimensional point and λ is its wavelength.

Optical

The projected image of a non-focused object, as described in Section 3.2, can be expressed as the convolution of the idealized image and the PSF,

$$I(\mathbf{x}, \lambda) * psf(\mathbf{x}, \lambda, \Delta D). \quad (5.14)$$

The PSF is computed for each point \mathbf{x} and its wavelength λ ; ΔD is the power required to bring in focus a non focused object (BURGE; GEISLER, 2011). Regarding to the focused object, although its image is projected sharp on the retina, it is also affected by optical conditions of visual system (PACKER; R.WILLIAMS, 2003). In general, all images projected the retinal surface are affected, for instance by the pupil aperture and optical variation such as aberrations (MAHAJAN, 1991). Because of this, a more general form of PSF that also depends on aperture system, the transmittance of the pupil or wave aberration function can be found in Appendix E.

Neural

Other visual eye condition that affects the retinal response is the non-uniform density of the photoreceptors at the retinal surface. Thibos & Bradley (1995) defined the NPSF as the neural image formed by an array of neurons in response to a point of light on the retina. As seen in Figures 7 and 8 of Section 2.1.1, the density of the photoreceptors on the retina varies with its eccentricity; density is high at the fovea that is the region on the center of the retina and is low in the peripheral regions. Then, the response of the retinal surface can be expressed as the convolution of projected image and the NPSF,

$$I(\mathbf{x}, \lambda) * npsf(\mathbf{x}, \lambda, \epsilon). \quad (5.15)$$

The NPSF is computed for each point \mathbf{x} and its wavelength; ϵ denotes the eccentricity of the retinal surface. In Appendix E is shown that the NPSF also is affected by the phenomenon named Stiles–Crawford effect (PACKER; R.WILLIAMS, 2003), where light entering the eye near the edge of the pupil produces a lower photoreceptor response compared to light of equal intensity entering near the center of the pupil.

Spatial response

Due to optical and neural characteristics of visual systems affects the projected image of objects, either focused or non-focused, the spatial response of the retina can be expressed as the convolution of idealized image and the PSF, and NPSF;

$$r(\mathbf{x}, \lambda, \Delta D, \epsilon) = I(\mathbf{x}, \lambda) * psf(\mathbf{x}, \lambda, \Delta D) * npsf(\mathbf{x}, \lambda, \epsilon), \quad (5.16)$$

where \mathbf{x} , λ , ΔD and ϵ are a point of the projected image, its wavelength, the optical power required to bring it focus and their eccentricity, respectively (BURGE; GEISLER, 2011; THIBOS; BRADLEY, 1995).

Spatial-temporal response

When the projection of an object is changing in time, the neural response will also depends on time (MALLOT, 2013). Then, the projected image $I(\mathbf{x}, \lambda)$ in a time t can be expressed as $I(\mathbf{x}, \lambda, t)$. In the particular case, in which the object is given by a flickering stimulus, all points of a light stimulus is oscillating periodically due to it is connected to a function generator. In this case, the projected image can be expressed as the product of every points of the projected image with sinusoidal function,

$$I(\mathbf{x}, \lambda, t) = I(\mathbf{x}, \lambda) \cos(\omega_0 t), \quad (5.17)$$

where $\omega_0 = 2\pi f_0$, and f_0 is the flickering frequency of the light stimulus. Then, the spatio-temporal of the retinal response due to a flickering stimulus can be denoted as

$$r(\mathbf{x}, \lambda, \Delta D, \epsilon, t, \omega_0) = [I(\mathbf{x}, \lambda) \cos(\omega_0 t)] * p s f(\cdot) * n p s f(\cdot), \quad (5.18)$$

where \mathbf{x} , λ , ΔD , ϵ , ω_0 and t represents the points of the stimulus, the wavelength, the power required to bring the object in focus, the eccentricity of the retinal surface, the flickering frequency and the time, respectively.

EEG Signal at Cortex V1

It was shown in Section 2.1.1 that there are regions at visual cortex that are related to regions of the retinal surface. For instance, the activity of the cortex V1 corresponds to the fovea (Figure 10), after passing through the visual pathway (Figure 9). In this sense, the response of the visual cortex is associated to \mathbf{x} , λ , ΔD , ϵ , ω_0 and t can be expressed as

$$r_v(\mathbf{x}, \lambda, \Delta D, \epsilon, \omega_0, t), \quad (5.19)$$

this is a very relevant expression because the evoked response r_v that arise in response to an external light stimulus, depends on its flickering frequency, its color, its shape, its blurriness degree and on the retinal surface where it is projected. Then, the EEG signal is composed by an evoked signal and the spontaneous background EEG,

$$s(t) = r_v + \xi, \quad (5.20)$$

as indicated by [Infantosi, Lazarev & Campos \(2005\)](#). Note that r_v does not include the physiological parameters due to visual pathway and skull. Therefore, the temporal response registered at occipital region can be summarized as

$$s(t) = s(\mathbf{x}, \lambda, \Delta D, \epsilon, \omega_0, t, \xi). \quad (5.21)$$

5.4 Power Spectrum of the Retinal Response

Isolated Stimulus

Figure 56a represents a subject attending a stimulus flickering at f_1 and placed at distance d_0 ; and Figure 56b illustrates the projection of the stimulus on the retinal surface give by the gray rectangle. Gazed objects are projected onto the fovea, which is the central region of the retina possessing high density of photoreceptors. Concentric circles are used to indicate the distance from the center of the surface to the peripheral region. The dark gray circle represents the blind point due to the optic nerve (11 of Section 2.1.3). The curve of density of photoreceptors was plotted below the fovea depiction to indicate that the center of the retinal surface has high density of photoreceptors compared to the peripheral regions, and there is no photoreceptors in the blind point (Figure 7 of Section 2.1.1).

As Figure 56b shows, the image will excite a high number of photoreceptors when projected on the center of the fovea, corresponding to an null eccentricity ($\epsilon = 0$). Otherwise, when the image is projected out of the center ($\epsilon \neq 0$) a low number of photoreceptors will be excited, then showing the fundamental role of the eccentricity in the neural response. In addition, when a stimulus off center, a change of orientation $\Delta\theta$ is required to bring the stimulus to the center of the field of view in order to obtain a better neural response. Then, the response $s(t)$ of (5.22) can be expressed as

$$s(t) = s(\mathbf{x}, \lambda, \Delta D, \epsilon(\Delta\theta), \omega_0, t, \xi)., \quad (5.22)$$

Its power spectrum in steady-state can be computed as

$$P_{ss}(\omega) = S(\omega)S^*(\omega), \quad (5.23)$$

where $S(\omega)$ is the Fourier transform of $s(t)$ computed with a temporal window $w(t)$. Then, the amplitude of the power spectrum for an isolated stimulus flickering at ω_0 is given by

$$P_{ss}(\omega_0) = P_{ss}(\mathbf{x}, \lambda, \Delta D, \epsilon(\Delta\theta), \xi), \quad (5.24)$$

which achieves the maximum amplitude when $\Delta\theta = 0$.

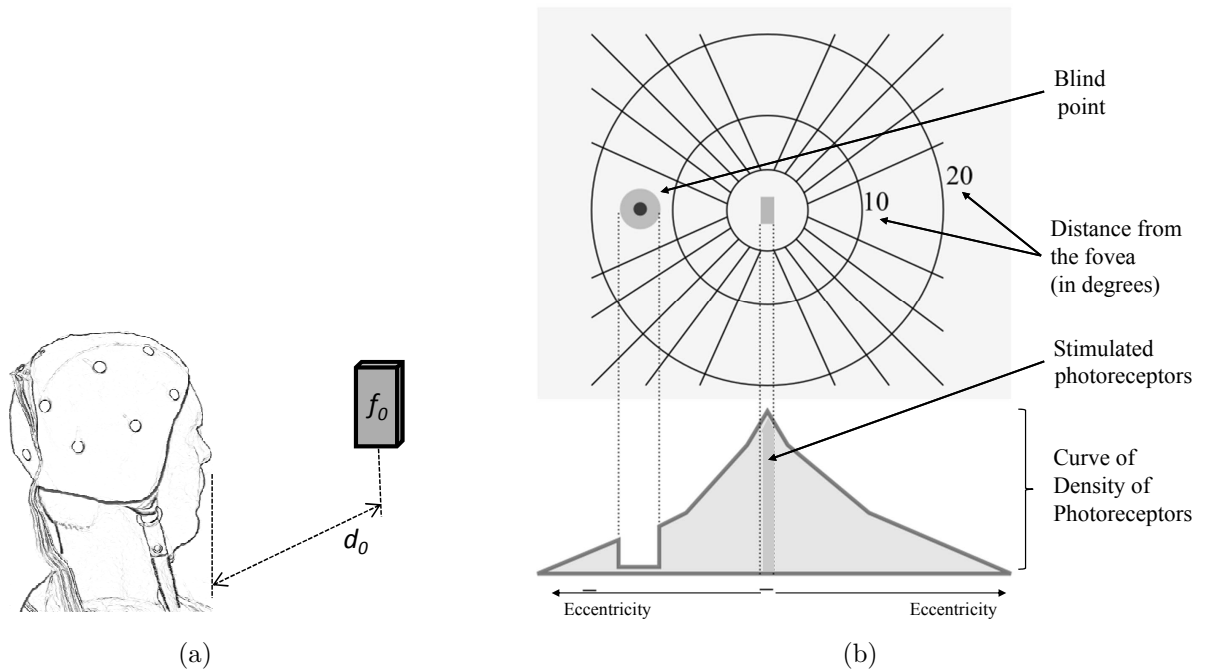


Figure 56 – Image projection due to an isolated stimulus. a) Setup with an stimulus flickering at f_0 . b) Retinal projection of the isolated stimulus together with the curve of density of photoreceptors. Gray rectangle and the central circle represent the stimulus and the fovea, respectively. Note that the density of photoreceptors is higher in the fovea, and that there is no photoreceptors in the blind point.

Two Stimuli for traditional SSVEP Systems

Figure 57a shows a conventional SSVEP with two stimuli placed in front of the user at a same distance (d_0), at orientations θ_1 and θ_2 and flickering at different frequencies f_1 and f_2 , respectively. In this setup, the separation between stimulus plays an important role because if it is greater than horizontal field of view ($\theta_1 + \theta_2 > 120^\circ$ for monocular vision), the demodulation problem is reduced to the case discussed in Section 5.3 for an isolated stimulus. This occurs because only the focused stimulus will be projected onto the retinal surface, as shown in Figure 56. Notwithstanding, if the separation is lower than 120° the non-attended stimulus is projected on the retina, while the attended one will be projected onto the center of the field of view. Figure 57b illustrates this situation for cases in which both stimuli are separated 20° . When the stimulus flickering at f_1 is gazed and projected on the center of the retinal surface ($\theta = 0$), the non-attended one is projected in the peripheral region. And the number of photoreceptors excited by the gazed stimulus is higher than the non-gazed one. Therefore, following (5.24) the power spectrum of gazed stimulus is given by

$$P_{ss}(\omega_1) = P_{ss}(\mathbf{x}, \lambda, \Delta D, \epsilon(\Delta\theta = 0), \xi) \quad (5.25)$$

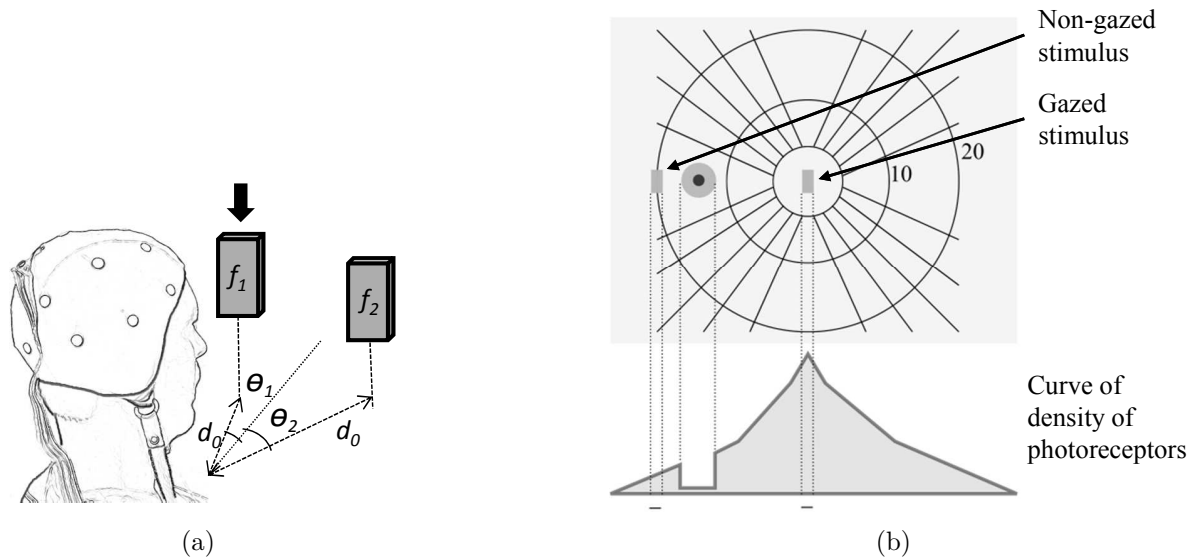


Figure 57 – Image projection of two stimuli placed in the traditional setup way when stimulus flickering at f_1 is gazed. a) Traditional setup with two stimuli flickering at f_1 and f_2 frequencies placed at the same distance (d_0) of the user and separated $\theta_1 + \theta_2$ degrees. b) Retinal projection of both stimuli. Gazed and non-gazed stimuli are projected in the center and in the peripheral region of the retina, respectively.

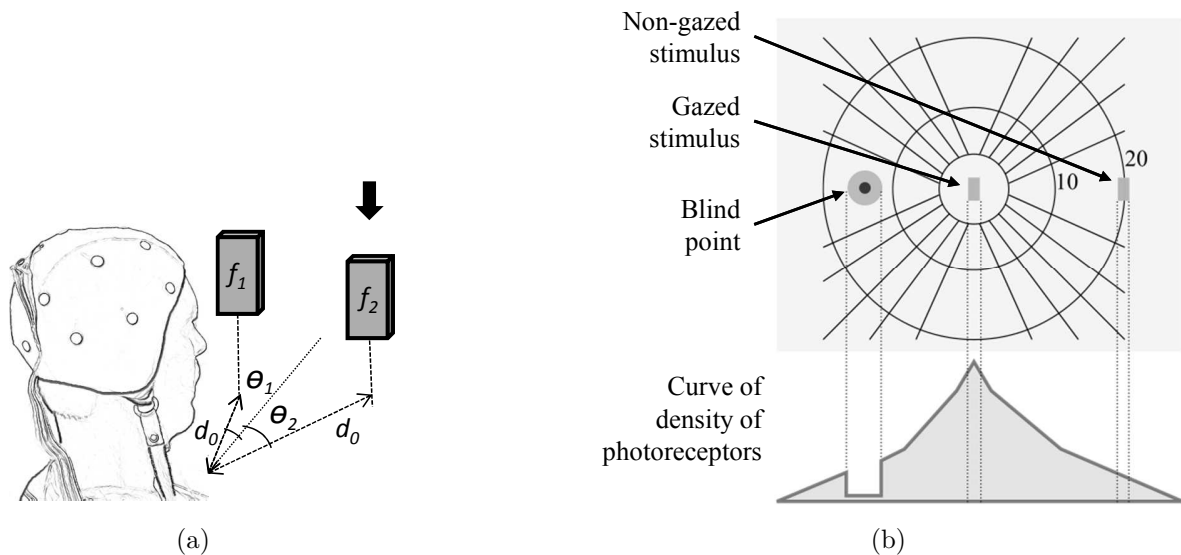


Figure 58 – Image projection of two stimuli placed in the traditional setup way when stimulus flickering at f_2 was gazed. a) Traditional setup with two stimuli flickering at f_1 and f_2 , frequencies placed at the same distance (d_0) of the user and separated $\theta_1 + \theta_2$ degrees. b) Retinal projection of both stimuli. Gazed and non-gazed stimuli are projected in the center and in the peripheral region of the retina, respectively.

were $\omega_1 = 2\pi f_1$. And the power spectrum of the non-gazed stimulus is

$$P_{ss}(\omega_2) = P_{ss}(\mathbf{x}, \lambda, \Delta D, \epsilon(\Delta\theta = \theta_1 + \theta_2), \xi), \quad (5.26)$$

were $\omega_2 = 2\pi f_2$. Due to both attended and non-attended stimuli have the same shape, the same color and are placed at the same distance; \mathbf{x} , λ , and ΔD are the same for (5.25) and (5.26). In consequence, the power spectrum principally depends on the eccentricity; since the maximum value is achieved when $\epsilon(0)$, then,

$$P_{ss}(\mathbf{x}, \lambda, \Delta D, \epsilon(0), \xi) > P_{ss}(\mathbf{x}, \lambda, \Delta D, \epsilon(\theta_1 + \theta_2), \xi). \quad (5.27)$$

Note that due to the high SNR of the evoked response (WANG et al., 2010), it is assumed that the spontaneous EEG (ξ) should not affect significantly the measured response. Finally, the power spectrum of target stimulus flickering at f_1 should be higher than the stimulus flickering at f_2

$$P_{ss}(\omega_1) > P_{ss}(\omega_2), \quad (5.28)$$

where were $\omega_1 = 2\pi f_1$ and were $\omega_2 = 2\pi f_2$. The same analysis is true when the target stimulus is flickering at f_2 , what is shown in Figure 58a and 58b.

Two Stimuli for the novel SSVEP Setup

Figure 59a shows the novel setup with two stimuli flickering at f_1 and f_2 and placed in front of the user so that they are projected together in the center of the retinal surface. To avoid the dependence of large muscular movements, they are placed conveniently in the same line of view with the same θ and at different distances from the subject's eye (d_1 and d_2 , respectively). In this setup the separation between stimuli plays an important role, because the defocusing degree is related to this distance, as shown in Section 3.3. Figure 59b shows the projection of both stimuli on the retinal surface, in which the the projection of the focused stimulus that is flickering at f_1 is represented sharp and the non-focused one is represented blur.

As shown in Section 3.2, every point of a non-focused stimulus are affected by the spreading function that project them as a blurry circles; so that the images of non-focused objects are projected with an expanded area. Nonetheless, although the area increases, the amount of light covering the photoreceptors of retinal surface remains the same. Recall that refraction of light causes the change of direction of the photons (CHARTIER, 2005), and as the luminous flux of both stimuli were adjusted to an equal and constant value of lumens (Figure 24), the larger projected image of the defocused one has lower intensity. It can be seen in Figure 59b, in which the number of photoreceptors covered by the focused and non-focused stimuli are different, because the light spreading would cause variation of

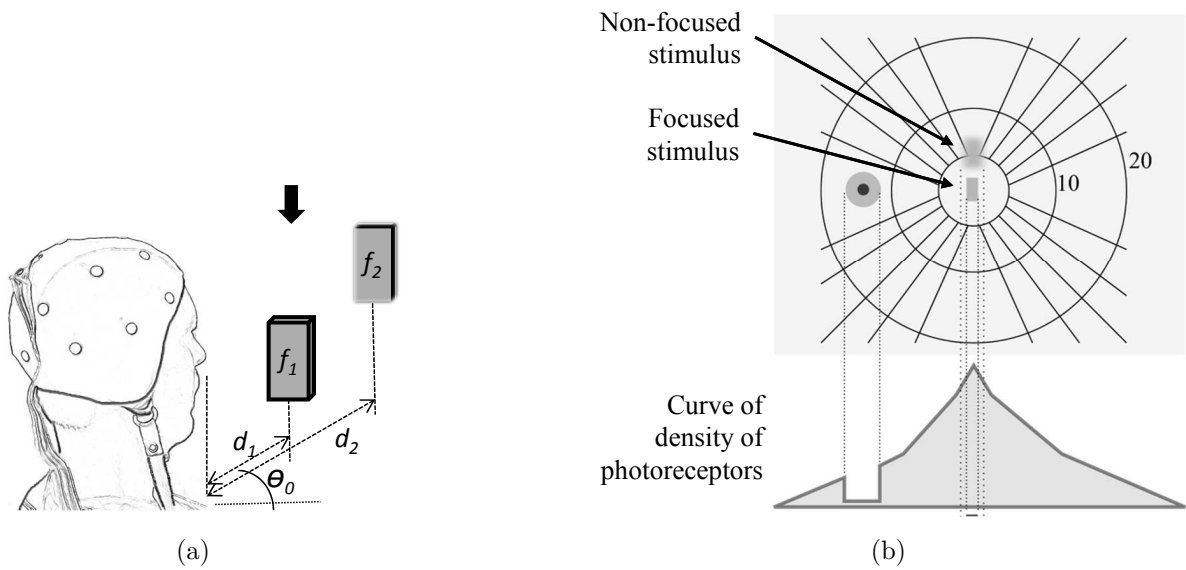


Figure 59 – Image projection of two stimuli placed in the novel setup way when stimulus flickering at f_1 was focused on. a) Novel setup with two stimuli flickering at f_1 and f_2 frequencies placed at the same angle (θ_0°) and at different distances d_1 and d_2 . b) Retinal projection of both stimuli. Focused and non-focused stimuli are projected in the center of the retina, sharp and blurred, respectively.

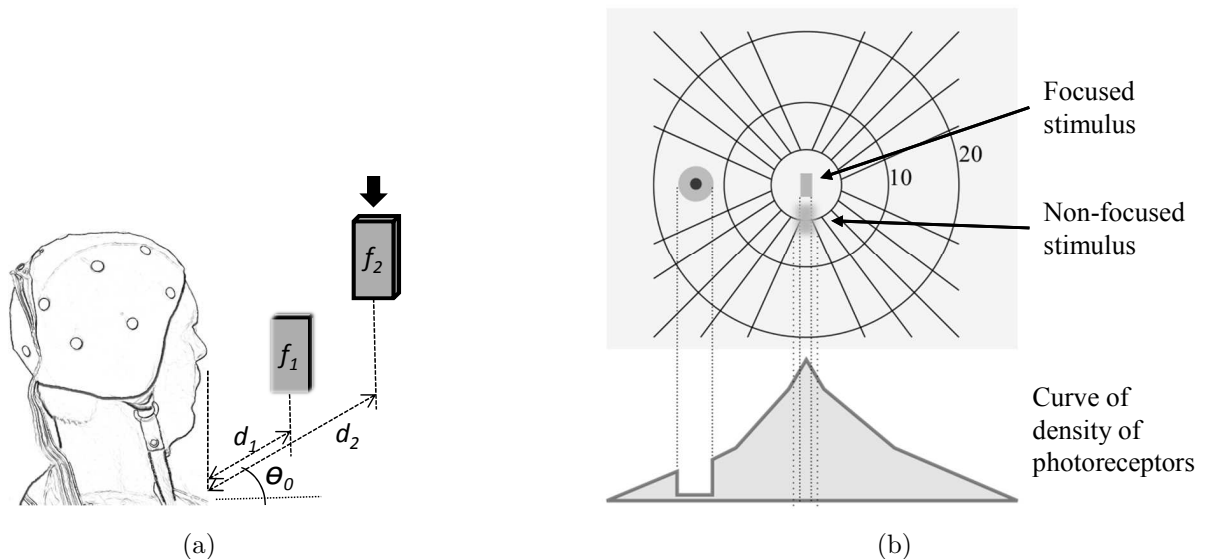


Figure 60 – Image projection of two stimuli placed in the novel setup way when stimulus flickering at f_2 was focused on. a) Novel setup with two stimuli flickering at f_1 and f_2 frequencies placed at the same angle (θ_0°) and at different distances d_1 and d_2 . b) Retinal projection of both stimuli. Focused and non-focused stimuli are projected in the center of the retina, sharp and blurred, respectively.

the neural response with the eccentricity. Due to the optical power required ΔD to bring an object in focus depends on its distance to the current focus, $\epsilon(\Delta D)$ can be expressed as $\epsilon(\Delta d)$.

When the stimulus flickering at f_1 is focused on, it is projected sharp in the center of the retinal surface and the non-focused one is projected blur. And the number of photo-receptors excited is higher than non-focused stimuli in general; therefore the power spectrum of focused stimulus is given by:

$$P_{ss}(\omega_1) = P_{ss}(\mathbf{x}, \lambda, \Delta_1 D, \Delta\theta_1, \epsilon(\Delta d = 0), \xi), \quad (5.29)$$

where $\omega_1 = 2\pi f_1$. And the power spectrum of the non-focused stimulus is

$$P_{ss}(\omega_2) = P_{ss}(\mathbf{x}, \lambda, \Delta_2 D, \Delta\theta_2, \epsilon(\Delta d = d_2 - d_1), \xi), \quad (5.30)$$

where $\omega_2 = 2\pi f_2$. Due to both focused and non-focused stimuli have the same shape, the same color and are placed at the same line; \mathbf{x} , λ , and θ are the same for (5.29) and (5.30). In consequence, the power spectrum principally depends on the eccentricity; since the maximum value is achieved when $\epsilon(0)$, then,

$$P_{ss}(\mathbf{x}, \lambda, \Delta D, \epsilon(0), \xi) > P_{ss}(\mathbf{x}, \lambda, \Delta D, \epsilon(d_2 - d_1), \xi). \quad (5.31)$$

Assuming that the spontaneous EEG (ξ) should not affect significantly the response due to high SNR of the evoked response (WANG et al., 2010). Finally, the power spectrum of target stimulus flickering at f_1 is higher than the stimulus flickering at f_2

$$P_{ss}(\omega_1) > P_{ss}(\omega_2), \quad (5.32)$$

where were $\omega_1 = 2\pi f_1$ and were $\omega_2 = 2\pi f_2$. This inequality can be supported by the fact that a different number of photoreceptors are excited by focused and non-focused stimuli. In addition, the activity of photoreceptors specialized in contrast detection is lower because blurred images have poor contrast (ATCHINSON; SMITH, 2000). The same analysis is true when the focused stimulus is flickering at f_2 , showed in Figure 60a and 60b.

5.5 Experimental Evaluation

As seen in (5.32), the amplitude of the power spectrum of the retinal response at the frequency of the focused stimulus is higher than the amplitude at the non-focused one. Then, the experimental evaluation of the amplitude of the power spectrum responses due to the focused and non-focused stimuli in the context of the novel setup is conducted in this section.

5.5.1 Materials

Subjects

Four healthy subjects participated in the study (age range 23-36 years). All of them showed normal or corrected to normal vision. The experiments were undertaken with the understanding and written consent of the subjects. This study was approved by the Ethics Committee of the Federal University of Espirito Santo.

Signals

EEG signals were recorded with a device for clinical purposes BrainNet36 together with a cap of integrated electrodes positioned according the international 10/10 system. Passive electrodes at locations P1, P2, P3, P4, Pz, PO3, PO4, PO7, PO8, POz, O1, O2, and Oz (Figure 73), referenced to Cz were employed. The ground electrode was placed on the AFz position. All signals were recorded with a sampling frequency of 200 Hz.

Protocol

Figure 61 shows the protocol of an experiment. Painted rectangles represent stimuli on, while unpainted rectangles corresponds to stimuli off, f_1 and f_2 denote the flickering frequencies, and d_1 and d_2 denote the distances. The black arrow indicates the target stimulus. In this protocol both stimuli are turned on sequentially while the user keeps focusing at just one of them. The first stimulus was turned on and subjects were asked to focus on it for 7s. The second stimulus was then also turned on, while subjects maintained

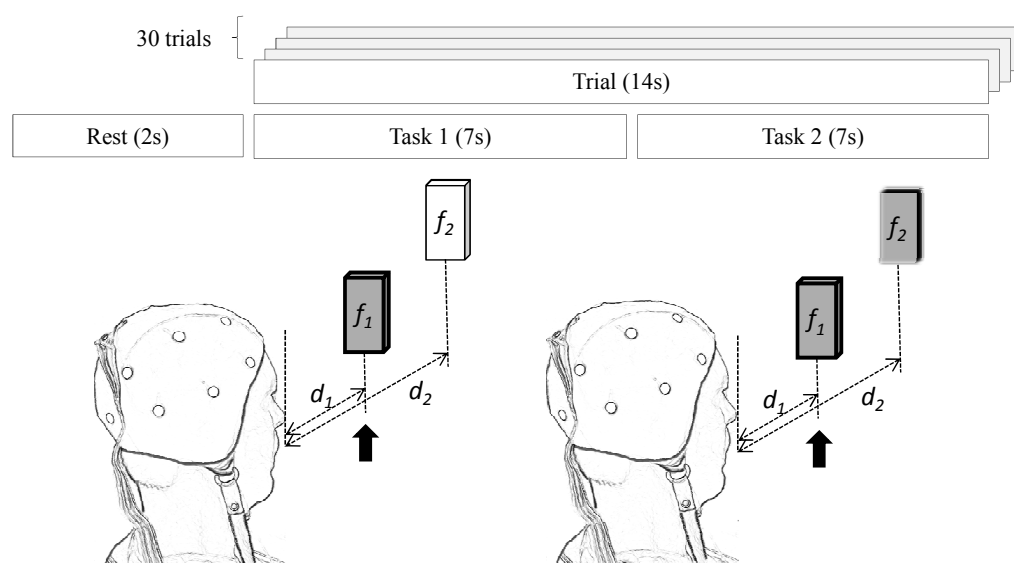


Figure 61 – Experimental procedure to evaluate the inequality of visual evoked response due to defocusing. Gray and white rectangles represent stimuli turned on and turned off, respectively. The arrow indicates which stimuli was being focused.

their focus on the first one during other 7s. To preserve the same conditions, signals of responses with isolated and focused stimulus were recorded in the same trial.

5.5.2 Results

Figures 62 and 63 show the spectral responses averaged over thirty trials of an isolated stimulus (black dotted curve) together with the response of two stimuli when one of them was focused (gray curve). Figure 62a shows the electrodes employed in experiments, and 62b shows responses for each electrode when the target stimulus was flickering at 6.4 Hz. Black dotted curves, labeled as **N6F_x** are the responses obtained from signals recorded when only the nearest stimulus, which was flickering at 6.4 Hz was turned on, and the farthest one was off, as shown in Figure 56a. As expected in traditional systems that presents isolated stimulus, it can be seen strong peaks at 6.4 Hz in all electrodes, which are higher in occipital electrodes (O1, O2 and Oz) than in parietal electrodes, specially P1, P2, P3 and P4. On the other hand, gray curves that were labeled as **N6F5** are the responses obtained from signals recorded when the nearest stimulus flickering at 6.4 Hz was focused on, and the farthest stimulus flickering at 5.6 Hz was non-focused, as shown in Figure 59a. Strong peaks can be observed at 6.4 Hz in all electrodes and they are higher at occipital electrodes (O1, O2 and Oz). Also it can be seen that the amplitude at the frequency of the non-focused stimulus is small. It can be perceived at electrodes O2, POz, PO4, PO8, P2 and P4.

Figure 63a shows the electrodes employed in experiments, and 63b show responses for each electrode when the target stimulus was flickering at 5.6 Hz. Black dotted curves, labeled as **N_xF5** are the responses obtained from signals recorded when only the farthest stimulus that was flickering at 5.6 Hz and the nearest one was off. As expected, it can be seen strong peaks at 5.6 Hz in all electrodes, which are higher in occipital electrodes and central (O1, O2, Oz, POz and Pz) than in parietal electrodes, specially P1 and P3. On the other hand, gray curves that were labeled as **N6F5** are the responses obtained from signals recorded when the farthest stimulus flickering at 5.6 Hz was focused on, and the nearest stimulus flickering at 6.4 Hz was non-focused, as shown in Figure 60a. Strong peaks can be observed at 5.6 Hz in all electrodes and they are higher at electrodes O1, O2, Oz, PO3, PO4 and POz. Unlike results showed in Figure 62b, in which peaks at the frequency of the non-focused stimulus are too small, in this case distinguishable peaks are observed at 6.4 Hz in all electrodes. Peaks due to the non-focused stimulus are smaller at occipital electrodes (O1, O2 and Oz) and are higher at electrodes PO3, PO4, POz, and Pz. Peaks due to the focused stimulus are weak at parietal regions, while peaks due to the non-focused stimulus are weak in both, occipital and parietal regions. Hence, evoked amplitudes of focused and non-focused stimulus measured in occipital area are clearly distinguishable ($p < 0.01$), whereas evoked amplitudes of focused and non-focused stimulus

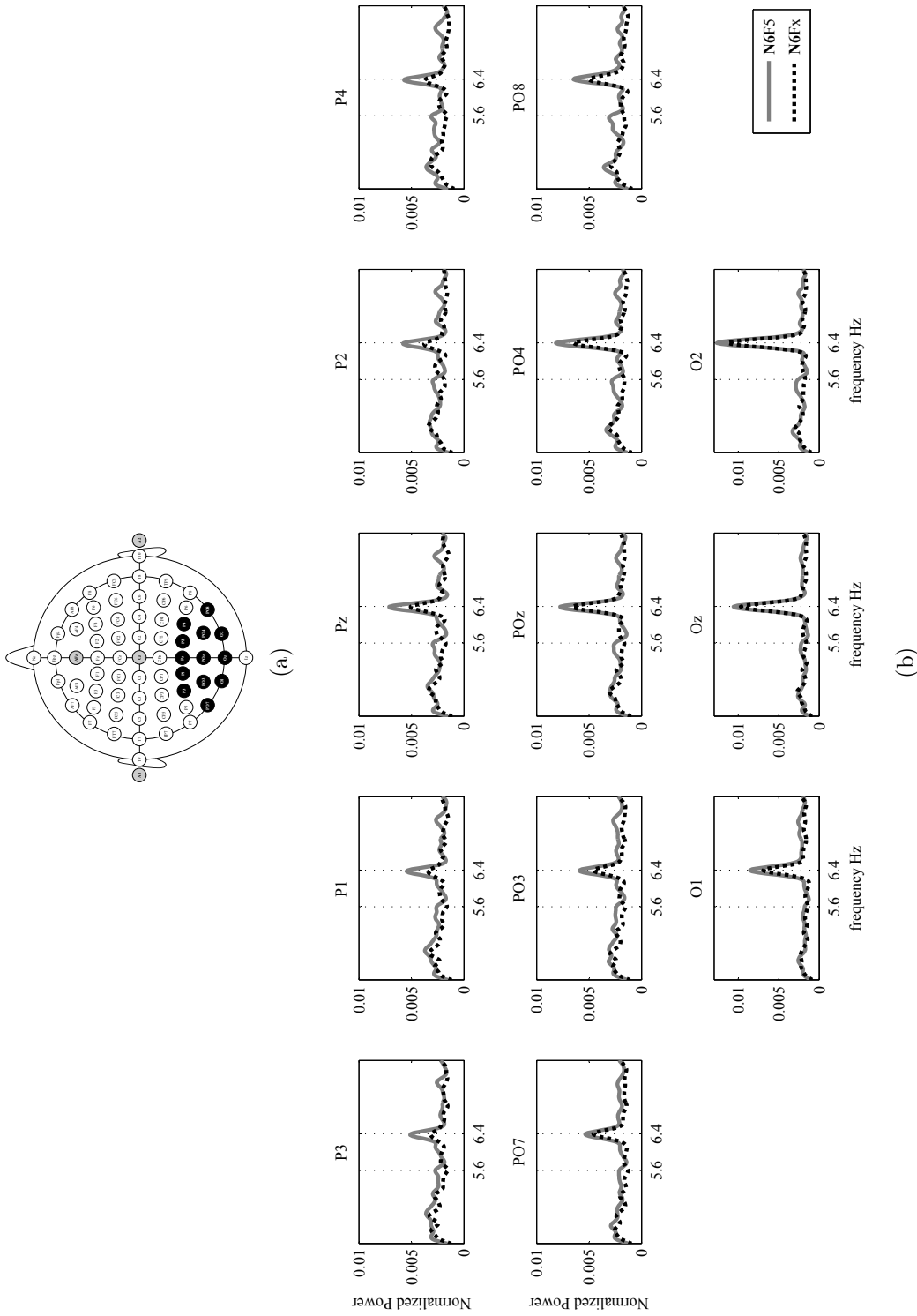


Figure 62 – Spectral response of occipital-parietal for Nx5 and N65 tasks. a) Extended 10/20 international system; black circles are the P1, P2, P3, P4, Pz, PO3, PO4, PO7, PO8, POz, O1, O2 and Oz positions, and gray circles are the A1, A2, Cz and AFz positions. b) Spectral response of occipital-parietal electrodes for isolated stimulus (black curves) and for focused stimulus (gray curves). Frequency of nearest and farthest stimuli at 6.4 and 5.6 Hz. N6Fx and N6F5 tasks.

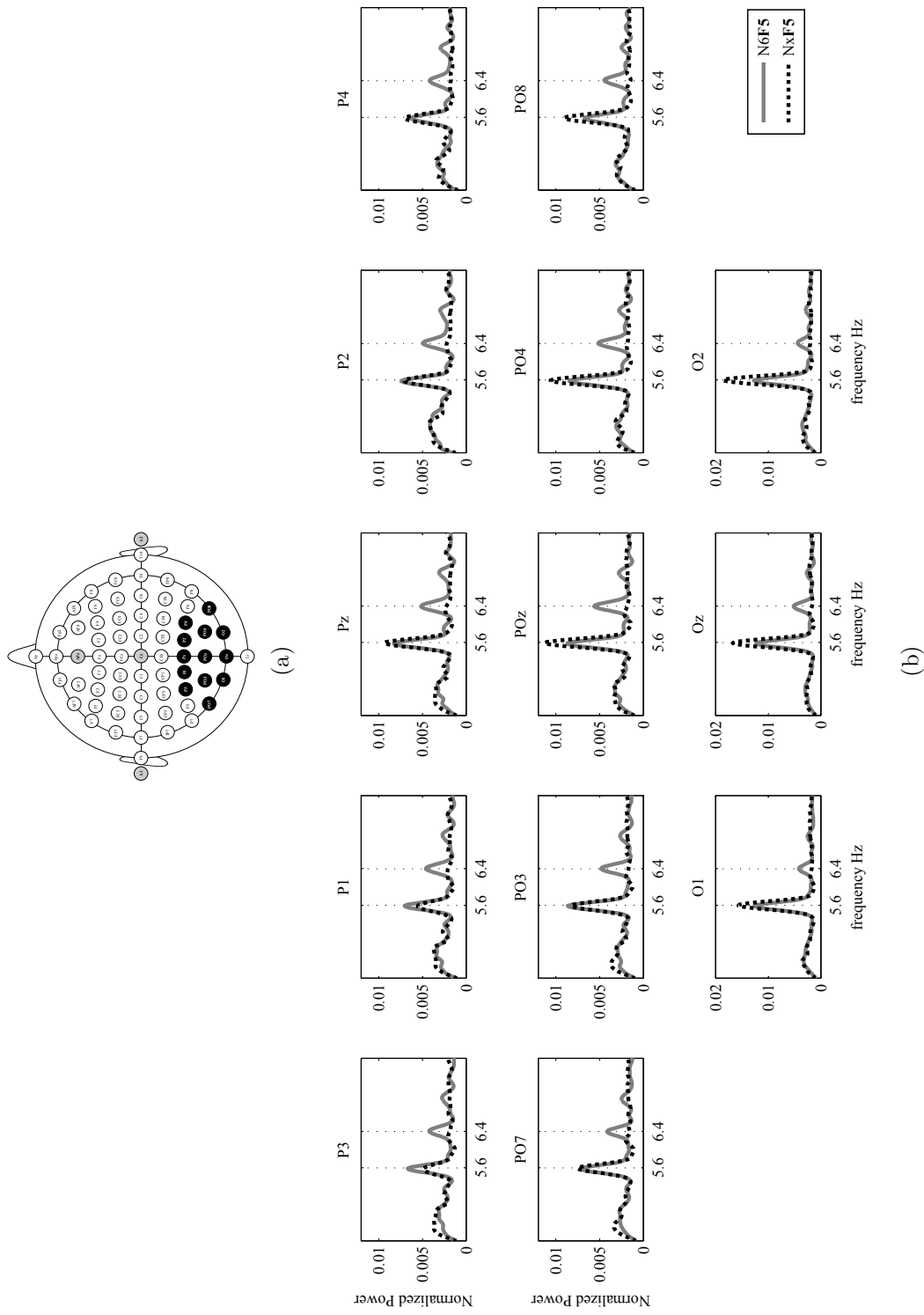


Figure 63 – a) Extended 10/20 international system; black circles are the P1, P2, P3, P4, Pz, PO3, PO4, PO7, PO8, POz, O1, O2 and Oz positions, and gray circles are the A1, A2, Cz and AFz positions. b) Spectral responses of occipital-parietal electrodes for isolated stimulus (black curves) and for focused stimulus (gray curves). Frequency of nearest and farthest stimuli at 6.4 and 5.6 Hz (Nx F5 and N6 F5 tasks).

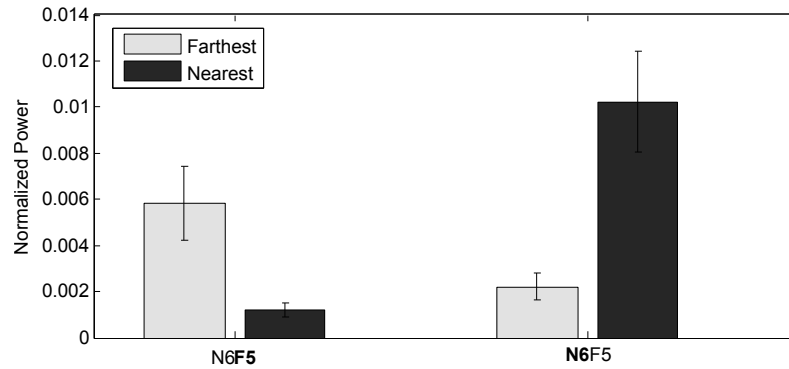


Figure 64 – Normalized spectral power at the flickering frequency of focused and non-focused stimuli ($p < 0.05$) for N6F5 and N6F5 settings. Black and gray bars correspond to the average of responses for nearest of farthest stimuli, respectively.

measured in parietal area are quite similar ($p < 0.05$).

Figure 64 shows the normalized spectral power of the amplitude of focused and non-focused stimuli for electrode Oz. Bars in the left and right sides correspond to N6F5 and N6F5 settings, respectively. Black and gray bars correspond to the average of responses for nearest of farthest stimuli, respectively. It can be noted that (1) the response due to focused stimulus is greater than the response due to the non-focused one; and (2) the response for the nearest focused stimulus is greater than the response for the farthest focused stimulus.

5.6 Discussion

Strong peak were observed at the frequency of the focused stimulus in all electrodes. Likewise, weak peaks were observed at the frequency of the non-focused stimulus in some electrodes. Also, it can be seen that the responses at frequencies of non-focused stimuli were higher when these were placed nearest than farthest, particularly in parietal electrodes. Although in parietal electrodes, responses at frequencies of focused and non-focused are quite similar ($p < 0.05$), in other brain regions, especially in the occipital region, the response of focused was high ($p < 0.01$).

These results are very important because enable those modulation/demodulation methods proposed in (5.10) and (5.12) to be used in the novel setup. On the other hand, results endorse the analysis of the retinal response conducted in Section 5.4, which discussed over the difference in amplitude of focused and non-focused stimuli, leading to a conclusion that amplitude responses of the attended stimulus should be higher than amplitude responses of the non-focused one, as shown in (5.28) and (5.32) for the traditional and the novel setups, respectively. Furthermore, it was seen that responses of both conventional and novel setups are associated directly with the eccentricity of the

density of the retinal surface. In conventional SSVEP-BCI setup the neck, head and/or eyeball movements, characterized by $\Delta\theta$, bring and place the target stimulus to the region with maximum density of photoreceptors. On the other hand, the response in the novel setup depends directly of blurred projection, which in turn depends on the distance between stimuli. The purpose of the focusing mechanism is to collimate the light rays of the focused stimulus in direction of the center of the retinal surface, while the rays of non-focused stimulus are spread, what is characterized by the defocusing degree ΔD .

The analysis of the retinal response for two stimuli in traditional SSVEP setups performed in Section 5.4 can be extended or generalized for system with a greater number of stimuli. Due to density of photo-receptors is high in the center of the retinal surface, only the gazed stimulus that was chosen from a set of stimuli will be projected in this region, and the other one will be projected out as show in Figures 57 and 58. It can be one reason because systems with a great number of stimuli are being developed in the traditional way (YIN et al., 2014). In the same manner, the demodulation method described in Figure 55 of Section 5.2 can be used for traditional systems in which more than one stimuli are present in the field of view, and the demodulation based on peak detection 5.12 can be employed successfully since the amplitude of attended stimulus is higher than the non attended stimuli. Finally, the demodulation based on analytical signal 5.10 could be used in systems with more than two stimuli, $N > 2$. In that case, a more general expression to compute values of a_i , for $i = 1, \dots, N$, must be proposed.

6 SSVEP Peak Detection

In Chapter 4 a the that the focused stimulus is able to evoke a visual potential although a non-focused stimulus is also present together in the center of field of view was tested. In Chapter 5, equations for SSVEP demodulation when two stimuli are presented together in the field of view of the user based on the retinal response to flickering stimuli was proposed and evaluated . In this Chapter, the performance of the SSVEP-BCI attained when the novel stimulation paradigm proposed in this Thesis is evaluated by using well-know SSVEP detection methods, such as CCA, LASSO and PSDA. Also, accuracy rate, AUC of Receiver operating characteristic (ROC), Cohen's Kappa coefficient and ITR, that are used in traditional SSVEP-BCI systems, are employed to evaluate the detection performance. Furthermore, EOG signals was employed to measure the eyeball movements when users are asked to shift their focus in order to select the target stimulus.

Results obtained in this Chapter are important because allow to compare the performance of the novel stimulation setup with gaze-independent SSVEP-BCI systems described in Section 2.2.

6.1 Analysis Methods

Two referenced methods were applied in this work. Raw signals originally referenced to Cz were re-referenced to Pz and CAR (MCFARLAND et al., 1997). EEG signals were preprocessed with a band-pass filter with cutoff frequencies of 4 and 45 Hz. From each 7s of attend period, segments with different TW from 1s to 7s were extracted using a hamming window starting at 0s. In order to evaluate the performance of the proposed setup, three state-of-the-art detection methods were employed: CCA, LASSO, and PSDA.

CCA Detection Method

In CCA, the frequency of the target stimulus is identified by finding the maximal correlation coefficient ρ between two multidimensional random variables given by the EEG signals X and a predefined sinusoidal reference signals Y (LIN et al., 2007; BIN et al., 2009). The canonical correlation is given by the maximum value of ρ as

$$\max_{W_x, W_y} \rho(x, y) = \frac{E[x^T y]}{\sqrt{E[x^T x]E[y^T y]}},$$

where $x = X^T W_x$ and $y = Y^T W_y$; and $E[.]$ is the expected value.

LASSO Detection Method

In **LASSO**, the target stimulus is detected by using the sparse regression model $X = Y\beta + \varepsilon$, where X is the EEG signals and Y is a set of reference signals; β and ε represent the regression coefficients and a noise vector with zero mean and unit variance, respectively (**ZHANG et al., 2012**). The method estimate is given by

$$\hat{\beta} = \arg \min_{\beta} \left(\|x - Y\beta\|_2^2 + \lambda_L \|\beta\|_1 \right),$$

where $\|\cdot\|_n$ denotes l_n norm. The penalty parameter λ_L controls the sparsity of solution $\hat{\beta}$. The contribution degree (CD) of the i -th stimulus frequency and its harmonic to the EEG signal can be calculated as follows:

$$CD_i = \frac{\sum_{j=1}^{N_c} \sum_{h=1}^{2N_h} |\beta_{i,h}^j|}{N_c},$$

where N_c is the number of channels, and N_h is the number of harmonic frequencies.

PSDA Detection Method

In **PSDA**, the amplitude of the power spectral density of the EEG signals is evaluated that is estimated by employing the fast **FFT**. The intensity of the response for each stimulus is defined as the sum of the amplitudes of the fundamental and the second harmonic frequencies (**CHENG et al., 2002**). Furthermore, in **PSDA** method the **SSVEP** response can be enhanced for detection by computing the the follow expression based on the **SNR** as:

$$S_{snr} = 10 \log_{10} \left(\frac{nP(f_i)}{\sum_{k=1}^{n/2} P(f_i + k\Delta f) + P(f_i - k\Delta f)} \right)$$

where f_i is the frequency of the flickering stimulus for $i = 1, 2$, n is the number of points around f_i , $P(f)$ is the **PSD** and Δf is the frequency step (**TANAKA; ZHANG; HIGASHI, 2012**).

In this work, the set of reference signals for **CCA** and **LASSO** was composed by sine and cosine signals with the fundamental and the second harmonic of the stimuli frequencies. **CCA** was evaluated in two ways: **CCA-8** that uses eight channels O1, O2, Oz, PO3, PO4, PO7, PO8, and POz and **CCA-12** that uses all channels of Figure 73 but Pz. **LASSO** was evaluated for $\lambda_L = 0.01$, with signals of electrodes O1, O2, and Oz. In **PSDA**, the frequency of the target stimulus was detected by comparing the response intensities of signals of electrodes O1, O2, and Oz. **FFT** was computed with of 4096 data points. The performance of the detection was evaluated by employing the accuracy of the detection, **AUC** under **ROC**, and the statistical Cohen's Kappa coefficient κ , which takes into account

the detections occurring by chance (JAPKOWICZ; SHAH, 2011). It can be computed as

$$\kappa = \frac{p_0 - p_e}{1 - p_e}, \quad (6.1)$$

where p_0 is the proportion of observations in agreement (or accuracy) and p_e is the proportion in agreement due to chance. Furthermore, the ITR that is an objective measure of BCI performance was computed (WOLPAW et al., 1998).

6.1.1 Experimental Procedure

Subjects

Eight healthy subjects participated in the study (six men and two women, age range 22-41 years; mean \pm SD: 28.7 \pm 6.8). All of them showed normal or corrected to normal vision. The experiments were undertaken with the understanding and written consent of the subjects. This study was approved by the Ethics Committee of the Federal University of Espirito Santo.

Signals

EEG signals were recorded with a device for clinical purposes (BrainNet36) together with a cap of integrated electrodes. EEG signals were recorded from passive electrodes at locations P1, P2, P3, P4, Pz, PO3, PO4, PO7, PO8, POz, O1, O2, and Oz, referenced to Cz, based on the international 10/20 system (Figure 73). The ground electrode was placed on the AFz position. Eye movements were measure by using EOG signals of two bipolar channels of the same device. All signals were recorded with a sampling frequency of 200 Hz. EEG signals were preprocessed with a Finite impulse response (FIR) band-pass filter with cutoff frequencies of 4 and 45 Hz. From each 7s of attend period, segments with different TW from 1 to 7s were extracted using a hamming window starting at 0 s.

Protocol

As shown in Figure 65, in this procedure two settings were used to test the proposed setup: the first one was named as “Nearest at 6.5 and Farthest at 5.6 Hz” (N6F5), in which frequencies of the nearest and farthest stimulus were set at 6.4 and 5.6 Hz, respectively. The second one, in which frequencies were exchanged, was named as “Nearest at 5.6 and Farthest at 6.4 Hz” (N5F6). Bold fonts are used to denote which stimulus is focused. For example, **N6F5** and **N6F5** notations indicate that the nearest and farthest stimulus were focused, respectively. In the main experiment, subjects were asked to shift their focus to select each stimulus. Due to the fact that two settings were evaluated, the experiment was divided in two parts: the first one for N6F5 setting and the second one for N5F6 setting. In the first part, subjects were asked to focus on each stimulus (**N6F5** and **N6F5**) sixty

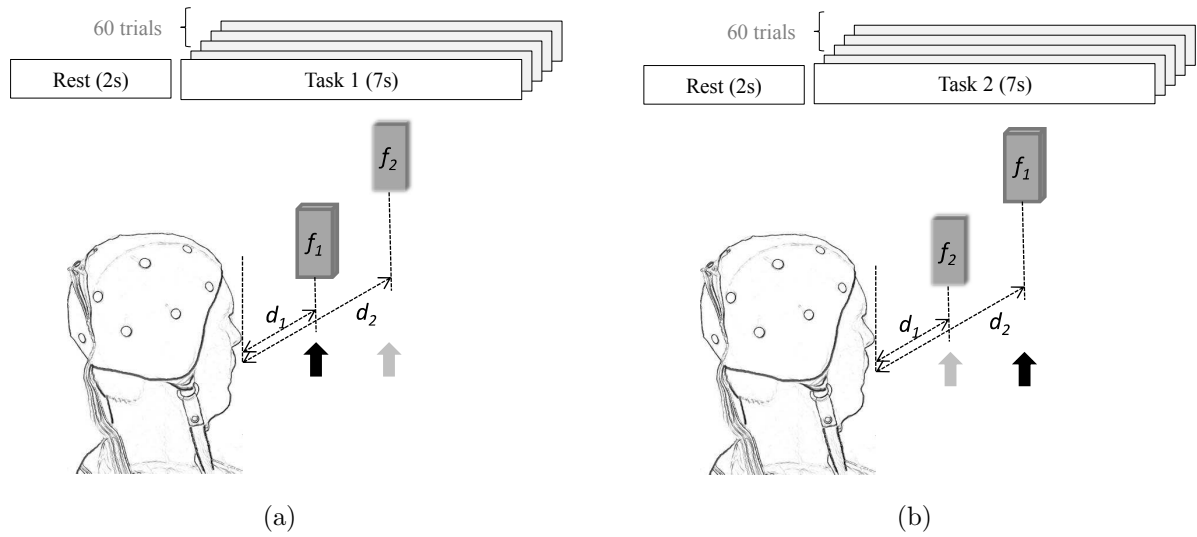


Figure 65 – Experimental procedure to evaluate the demodulation based on power spectrum peak detection. a) Protocol for “Nearest at 6.5 and Farthest at 5.6 Hz” setting (N6F5). b) Protocol, for “Nearest at 5.6 and Farthest at 6.4 Hz” setting (N5F6). Black and gray arrows indicate the focused and the non-focused stimulus, respectively; $f_1 = 6.4\text{Hz}$ and $f_2 = 5.6\text{Hz}$. In both setting, user was asked to focus one stimulus aleatory.

times randomly, which was completed in four runs of fifteen 9s trials (2s rest and 7s task) for each task. In the second part, the same procedure was followed for the case of N5F6 setting and for **N5F6** and **N5F6** tasks.

6.2 Results

Accuracies of CCA-8, CCA-12, LASSO and PSDA averaged for all subjects, for glstw of 7s and settings (N5F6 and N6F5) using Pz reference were 0.923, 0.910, 0.877 and 0.864, respectively. Average accuracies of CCA-8, CCA-12, LASSO and PSDA using CAR were 0.916, 0.906, 0.960 and 0.941, respectively. Note that CCA based methods achieve higher accuracies using Pz reference than CAR. In contrast, LASSO and PSDA has better performance with CAR than Pz. Figures 66 and 67, and Tables 2 and 3 show the results obtained by CCA-12 and CCA-8 with Pz reference, and LASSO and PSDA with CAR. The detection accuracy of each of the eight subjects and the average accuracy are depicted in Figure 66 and Figure 67, which correspond respectively to the experiments conducted with the N6F5 and N5F6 settings with different TWs from 1s to 7s. As shown in these figures, in general, accuracy increases as TW length increases; however, the accuracy curves of CCA-12 and CCA-8 methods for Subject 5 do not increase, remaining around 0.7 and 0.8 for N6F5 and N5F6 settings, respectively. Subject 7 obtained the overall worst performance during N5F6 setting with CCA-12 and CCA-8, and these particular results decreased the average accuracy of CCA, which obtained the lowest accuracy compared to

Table 2 – Detection accuracy for all subjects, average of the accuracy and its standard deviation for CCA-12, CCA-8, LASSO, and PSDA detection methods, N6F5 and N5F6 settings and $TW = 7s$.

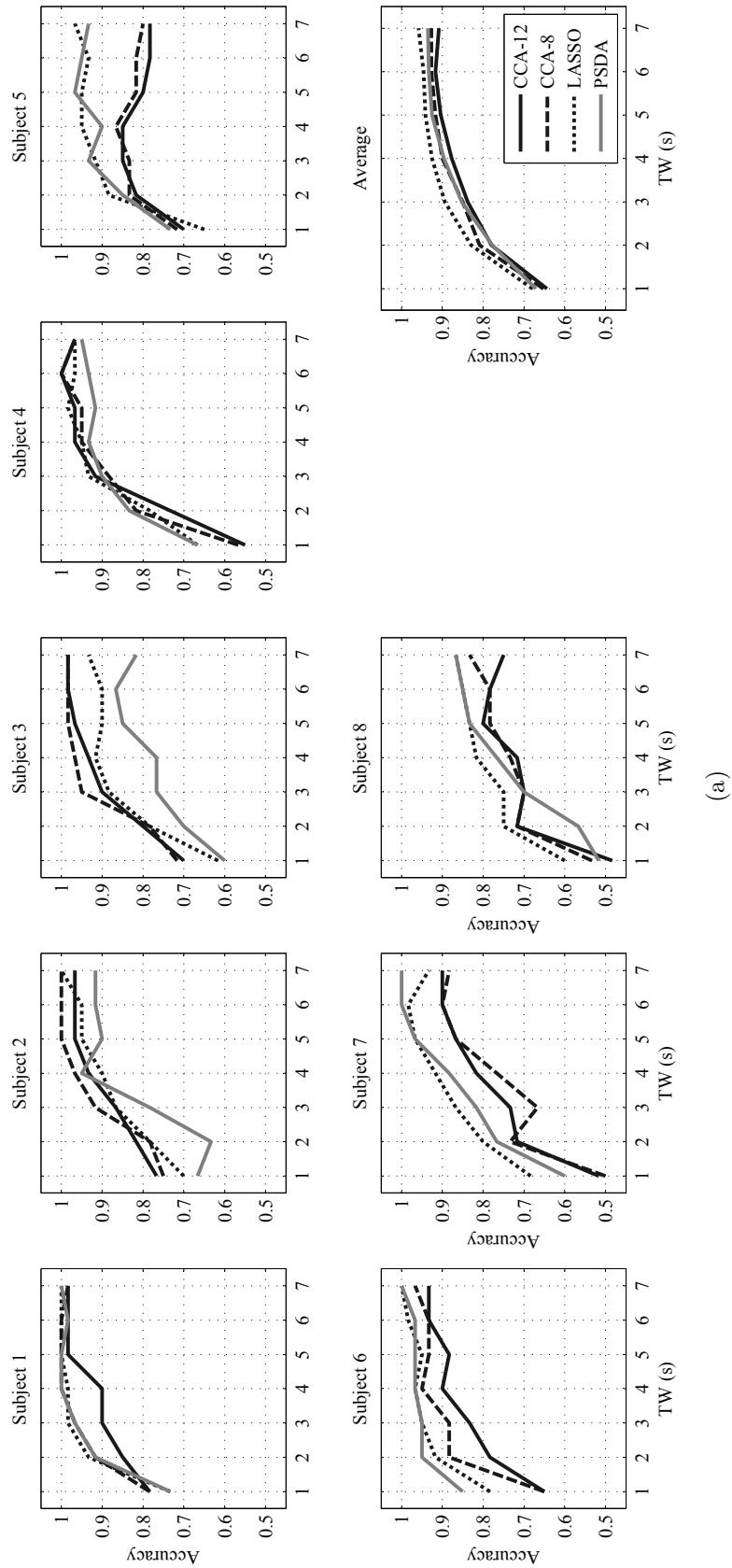
Subject	CCA-12		CCA-8		LASSO		PSDA	
	N6F5	N5F6	N6F5	N5F6	N6F5	N5F6	N6F5	N5F6
S1	0.98	0.95	0.98	0.98	1.00	1.00	1.00	0.98
S2	0.97	0.98	1.00	1.00	1.00	0.97	0.92	0.90
S3	0.98	1.00	0.98	1.00	0.93	1.00	0.82	0.97
S4	0.97	1.00	0.97	1.00	0.97	0.98	0.95	0.95
S5	0.78	0.70	0.80	0.75	0.97	0.95	0.93	1.00
S6	0.93	1.00	0.97	1.00	1.00	0.98	1.00	0.95
S7	0.90	0.73	0.88	0.77	0.93	1.00	1.00	1.00
S8	0.75	0.87	0.83	0.85	0.87	0.82	0.87	0.82
Average	0.91	0.90	0.93	0.92	0.96	0.96	0.94	0.95
SD	0.09	0.12	0.08	0.11	0.05	0.06	0.07	0.06

Table 3 – Average of the accuracy (Acc.), Cohen’s Kappa Coefficient, **AUC** and **ITR** for CCA-12, CCA-8, **LASSO**, and **PSDA** detection methods, N6F5 and N5F6 settings and for **TW** of 4 and 7 s.

Average	CCA-12		CCA-8		LASSO		PSDA	
	N6F5	N5F6	N6F5	N5F6	N6F5	N5F6	N6F5	N5F6
Acc. (TW = 7 s)	0.91	0.90	0.93	0.92	0.96	0.96	0.94	0.95
Acc. (TW = 4 s)	0.88	0.87	0.90	0.89	0.93	0.91	0.90	0.91
Kappa (TW = 7 s)	0.82	0.81	0.85	0.84	0.91	0.92	0.88	0.89
Kappa (TW = 4 s)	0.75	0.75	0.80	0.77	0.85	0.83	0.79	0.82
AUC (TW = 7 s)	0.93	0.90	0.93	0.92	0.97	0.96	0.95	0.94
AUC (TW = 4 s)	0.90	0.87	0.91	0.89	0.96	0.91	0.92	0.91
ITR (TW = 7 s)	5.30	5.69	5.83	6.08	6.76	7.04	6.10	6.36
ITR (TW = 4 s)	7.48	7.95	9.03	8.78	9.58	9.51	8.61	9.17

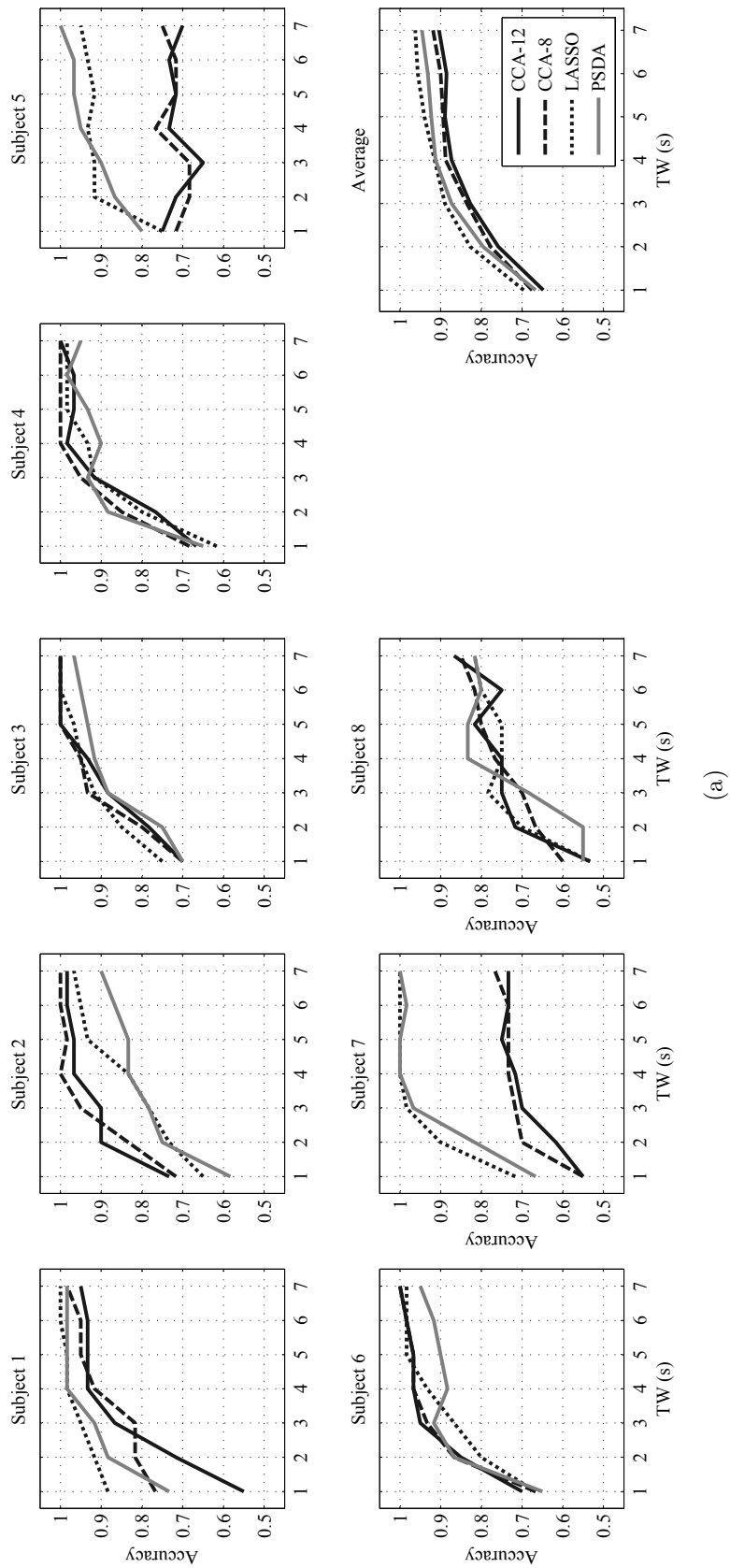
LASSO and PSDA methods. The highest average accuracy in both settings were achieved with LASSO. It is worth noting that for all methods, the average curve adopts stationary behavior after **TW** of 4s. Table 2 summarizes the accuracy attained by each subject with the largest **TW** (7s) for the experiments conducted with the two settings (N6F5 and N5F6), as well as its average and standard deviation. Subject 5 obtained the lowest accuracy of 0.7 with CCA-12. The average performance is comparable across N6F5 and N5F6 cases. LASSO obtained the maximum accuracy of 0.96 averaged among subjects, while PSDA produced a not significantly different mean accuracy of 0.94. CCA-12 and CCA-8 provided not significantly worse results than LASSO and PSDA methods with respectively 0.9 and 0.92.

For further comparisons, Table 3 shows the average accuracies, Cohen’s Kappa coefficients and AUC for **TW** of 4s and 7s. PSDA and LASSO produced lower accuracy



(a)

Figure 66 – Detection accuracy with respect to $TW = 1-7$ s length for eight subjects and with the average using CCA-12, CCA-8, LASSO and PSDA. N6F5 setting comprising 30 trials per N6F5/N6F5 tasks.



(a)

Figure 67 – Detection accuracy with respect to $TW = 1-7$ s length for eight subjects and with the average using CCA-12, CCA-8, LASSO and PSDA. N5F6 setting comprising 30 trials per N5F6/N5F6 tasks.

with 4s than 7s, with 0.91 and 0.93, respectively. CCA-12 and CCA-8 obtained 0.88 and 0.89 for **TW** of 4s, respectively, which do not represent a great difference with the results achieved with 7s. Cohen suggested the Kappa result be interpreted as follows: values higher than 0 as indicating no agreement between detected and asked frequencies; values between 0.6 and 0.8 as substantial agreement; and values between 0.8 and 1 as almost perfect agreement (JAPKOWICZ; SHAH, 2011). All detection methods obtained Cohen's Kappa coefficient higher than 0.8 for **TW** of 7s. CCA-12 and CCA-8 methods obtained values slightly lower than 0.8 for **TW** of 4s. The AUC measures discrimination, with 1 representing a perfect test, while values higher than 0.9 are considered excellent. An area of 0.5 represents a worthless test. In our study, all detection methods attained AUC values higher than 0.9 for 7s. CCA-12 and CCA-8 methods obtained values slightly lower than 0.9 for **TW** of 4s. Average ITR was calculated for all subjects. The ITR across subjects for CCA-12 detection method was 5.69 bits/min, for CC-8 method was 6.08 bits/min, for LASSO was 7.04 and for PSDA was 6.36 bits/min for **TW** of 7s. The highest ITR of 9.58 bits/min was achieved for N6F5 setting using the LASSO for **TW** of 4s.

6.3 EOG measurements

For **EOG** analysis, subjects were asked to focus on the nearest stimulus during 7s and then to shift their focus on the farthest one for 7s, and viceversa. To avoid the nose caused by blink artifacts, subjects were instructed to not blink during 2s, starting 1s before shifting stimulus and ending 1s after it (Figure 68). **EOG** signals were analyzed during

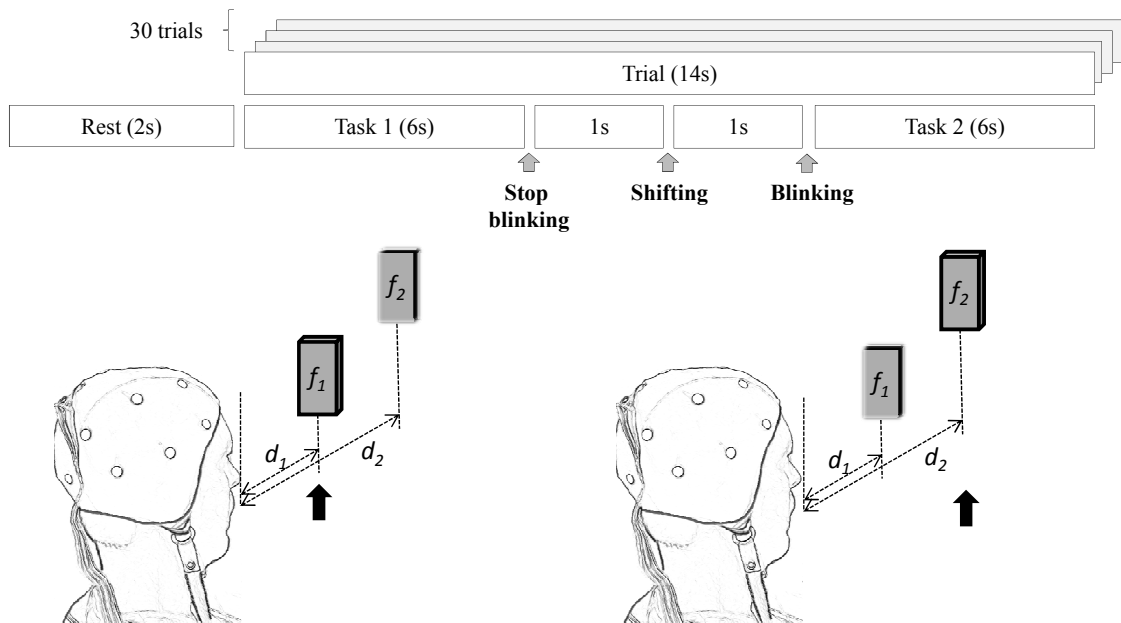


Figure 68 – Experimental procedure to evaluate the eyeball movements by using EOG device.

this period. The angle of eyeball movement was computed by interpolation. First, three angles were associated to EOG measurements; in this sense, users were asked to move their eyeballs across a plane in their front placed at 1.2m from a starting point placed at 0° to three final points that are separated 0.3m, 0.2m and 0.1m from the starting point. By employing a tangential relation between distance of the plane and the distances of separation of the final points to the starting point, the movements correspond to angles 14.0362° , 9.4623° and 4.7636° , respectively. Then, a linear interpolation between angles and EOG measurements was performed in order to determine the angle of the eyeball movement during the experiment described in Figure 68. As a result, it was measured that the average of total movement of eyeball was $1.98^\circ \pm 0.8^\circ$ for four subjects and ten trials. An analysis of eye movements by employing Kinect and eye-tracker devices, in which even if eyeball movements are not required to focus on the target stimulus, subjects perform involuntary movements can be found in a previous work of the author (COTRINA et al., 2015c).

6.4 Summary

Results from this study indicate that SSVEP pattern of a focused stimulus is elicited distinguishable regardless of the non-focused stimulus that is also presented. The highest accuracy was of 0.96 ± 0.6 achieved by LASSO detection method for TW of 7s, and the highest ITR was of 9.58 bits/min achieved by LASSO method for TW of 4 s. In general, results of Figures 66 and 67, and Tables 2 and 3 showed the accuracy of both CCA-based detection methods (with eight and twelve electrodes) were lower than LASSO and PSDA methods (both for three electrodes). This result, *prima facie*, was considered unexpected as the CCA method is widely used for detection and feature extraction (LESENFANTS et al., 2014; LIN et al., 2007; BIN et al., 2009) due to its good performance. In consequence, the slightly low performance obtained by CCA may be attributed to noise added to signals of parietal electrodes due to non-focused activity. For this reason only occipital channels were chosen in PSDA and LASSO testing. The ambiguous information present in parietal (P1, P2, P3, P4, Pz) and occipital-parietal (PO3, PO4, PO7 PO8 and POz) electrodes could be causing the slightly low performance of CCA, compared with LASSO and PSDA. These were computed by employing only occipital electrodes (O1, O2 and Oz), in which peaks at focused stimulus are higher than peaks at non-focused one ($p < 0.01$).

7 General Discussion and Conclusion

7.1 General Discussion

In this Thesis, a novel setup of stimulation in SSVEP-BCI was proposed, implemented and evaluated. In this proposal, the optical phenomenon named Depth-of-Field of human vision were explored. The most important aspect in this alternative setup is given by the dissimilar distances of the location of the stimuli, because in a scene the blurriness degree of a non-focused object depends on the Depth-of-Field of a focused object, which in turn depends on the distances between focused and non-focused objects. In SSVEP context, ophthalmology studies (SOKOL; MOSKOWITZ, 1981) found that the amplitude of VEP is reduced when the flickering stimulus is defocused. An appropriate distance of separation of two SSVEP stimuli delivers an extraordinary situation, in which if one stimulus is in focus the other one must be out of focus and vice versa. This distance of separation between stimuli can be properly estimated with aid of models, e.g., the retinal blurry model (VISHWANATH; BLASER, 2010), which helps to compute the distance that ensures the blurriness of the non-focused object. Thus, a small and portable stimulation unit was built using two light emitter diodes disposed so that if one is focused on by the user the other is non-focused, and vice versa.

Defocusing

As shown in Sections 2.1.4.1, intermittent light stimulus evokes a steady-state potential that is related with its flickering frequency. A SSVEP-BCI with binary outputs can be built by employing two stimuli flickering at different frequencies. However; as shown in Section 2.1.4.2, the amplitude or latency of evoked responses due to light stimulus are affected when there is any refractive error, such as defocusing, that modify the image projected onto the retina. In this sense, in conventional SSVEP-BCIs, researches avoid the presence of refractive errors asking users to move their head, neck or eyeballs in order to maintain the stimulus in focus. In this thesis, the refractive error given by the defocusing is explored to propose a novel SSVEP-BCI stimulation setup.

Statistical Evaluation

Regarding the novel setup, statistical evaluation provided evidence of absence of non-focused stimulus effects over the focused one. Therefore, the importance of these findings is that detection methods commonly used to recognize the target stimulus in conventional SSVEP systems could be employed successfully to recognize the focused stimulus in the novel setup. The advantage of the novel setup compared with conventional

SSVEP-BCI setup, in which user performs muscular movements to place the target stimulus into his/her field of view, is that head, neck and/or eyes movements are not required to select the target stimulus because the two stimuli are already in the field of view. In this case, shifting of stimulus is executed by performing the accommodation mechanism that is defined as the ability of the human eye to adjust itself to obtain sharp images for different object distances (GREGORY, 1997), and accommodation does not require voluntary muscular control (EBENHOLTZ, 2001).

The advantage of the SSVEP-BCI proposed in this work is that it requires minimal movement for selecting stimulus if compared with traditional SSVEP-BCIs. Also, it reaches higher accuracy rate than SSVEP systems based on covert attention. Once demonstrated the potential utility of the Depth-of-field phenomenon and the accommodation mechanism combined with SSVEP-BCI systems, this research looks toward to achieve acceptable levels of online human communication.

How the non-focused stimulus affects the response?

In Figure 62, black dotted curves are the spectral responses at parietal-occipital electrodes obtained when subjects were asked to gaze an isolated stimulus flickering at 5.6Hz (traditional response); and gray curves are the responses obtained when two stimuli were presented following the setting N6F5 (Section 5.5) when users were asked to focus the farthest stimulus that was flickering at 5.6Hz while the nearest non-focused stimulus was flickering at 6.4Hz (novel response). In both cases, the spectral responses are given by the grand average of the normalized spectral power of EEG signals of four subjects recorded in thirty trials. A trial is composed by conventional and novel tasks. In the first task, only the target stimulus was on, and subjects were asked to attend it during 7s (denoted as Nx**F5**); and in the second task, the non-target stimulus was turned on and subjects were asked to maintain their focus on the target stimulus, also during 7s (denoted as N6**F5**). Curves of Figure 63 are the spectral responses when the target stimulus was the nearest flickering at 6.4Hz, in which the conventional and novel tasks are denoted as N6**Fx** and N6**F5**, respectively.

It can be seen in Figure 62 and Figure 63 that peaks in black curves are notorious at frequencies 5.6Hz and 6.4Hz for Nx**F5** and N6**Fx** tasks, respectively, as expected in traditional SSVEP systems. Evoked responses are stronger in occipital region (O1, O2 and Oz) than in parietal region (P1, P2, P3, P4 and Pz). Regarding the response of the novel system given by gray curves, it can be seen that strong peaks are present in the frequency of focused stimulus. Besides, weak peaks also can be observed in the frequency of non-focused stimulus. As in the traditional case, peaks in the frequency of focused stimulus are stronger at occipital electrodes than the parietal electrodes. In contrast, peaks in frequencies of non-focused stimulus are slightly strong at parietal region than occipital

region. It is more evident in Figure 62, in which peak amplitudes arose in the frequency of the focused stimulus (5.6Hz) are clearly distinguishable ($p < 0.01$). Despite being smaller, peaks in the frequency of the non-focused stimulus (6.4Hz) are distinguishable at occipital region ($p < 0.05$). Peaks at 6.4Hz also are noticeable parietal-occipital electrodes (PO3, PO4, PO7 PO8 and POz). Peaks due to focused stimulus (6.4Hz) also are strong in Figure 63, while peaks due to non-focused stimulus (5.6Hz) that is placed behind the focused one, are weak. In both figures, principally in Figure 5a the peaks caused by focused stimulus are higher than the peaks caused by non-focused one at occipital electrodes ($p < 0.01$). Figure 64 shows the difference between peaks at frequencies of non-focused stimulus at electrode. The bars in the left and right and sides correspond to N6F5 and N5F6 settings, respectively. Light gray and dark gray bars are the average of the spectral power attained when non-focused stimulus was the nearest and farthest, respectively.

Why CCA obtained lower accuracy than PSDA or LASSO?

In traditional systems, potentials evoked by target stimuli are enough diffused on the parietal-occipital region (black dotted curves in Figures 62 and 63); then, multiple electrodes are used to improve the CCA performance making it more robust against noise (LIN et al., 2007). On the other hand, in the setup here proposed, in addition to the focused stimulus, the activity of the non-focused one also is diffused on the parietal-occipital region (gray curves in Figure 62 and 63). This activity present in all electrodes may be responsible for the worse performance obtained by CCA-12 and CCA-8, in comparison to the other methods evaluated. For LASSO and PSDA, higher accuracies were attained with signals of occipital electrodes O1, O2 and Oz re-referenced to CAR, which uses averaged signals of the thirteen electrodes of Figure 73. Regarding these results, two conditions may play a role for the better performance of these methods. First, peaks at the frequency of the focused stimulus are considerably higher than peaks at frequency of non-focused one in occipital electrodes only; hence, responses of the attended stimulus are very similar to responses of traditional SSVEP systems (Figures 62 and 62). Second, because of accuracies for CAR are higher than Pz reference in both methods (Section 6.2), CAR would be filtering more effectively the activity caused by non-focused stimulus that seems diffuse in the parietal-occipital region. The average value of all electrodes is subtracted; then, the common noise component caused by the non-focused stimulus is reduced. Theoretically, advantages of average reference rest on the fact that outward positive and negative currents summed across an entire sphere sum zero, this condition usually is not met completely in practice, because electrode position systems, as the international 10/20, do not cover the head entirely. However, although the entire head is not covered by electrodes, CAR provides EEG recordings that can be nearly reference-free (MCFARLAND et al., 1997) when electrodes are placed in the whole surface of the scalp. In this context, CAR was already applied successfully in conventional SSVEP systems

using electrodes at parietal-occipital region (BASTOS et al., 2014; MULLER; BASTOS; SARCINELLI, 2010).

Comparison with 2-class covert-attention SSVEP BCIs

Although the traditional SSVEP-BCIs are becoming robust systems, they are not suitable for all sort of patients because they require reliable control of eye movements. Thus, gaze independent approach based on covert attention that may have strong modulatory effects on SSVEP-BCIs are being proposed. Spatial visual selective attention-based BCI was explored in (KELLY et al., 2005b) using two bilateral flickering stimulus (with 14.2° and 4.2° of horizontal and vertical visual angles, respectively) presented on a computer screen; it obtained an average accuracy of 0.703. A BCI based on non-spatial visual selective attention with two rotational superimposed stimuli distributed in an annular area between 2° and 20° was reported in (ZHANG et al., 2010); it achieved an average accuracy of 0.726. Recently, (LESENFANTS et al., 2014) reported an average offline average accuracy of 0.85 for a healthy subject. The stimulation pattern was composed of two LEDs placed at 30cm from the user and separated 12cm ($\approx 28^\circ$ and $\approx 4^\circ$ of horizontal and vertical angles, respectively). In summary, these 2-class SSVEP-BCIs based on covert attention reached accuracy rates up to 0.85 with minimal eye movements. In our proposal based on Depth-of-field phenomenon, stimuli are delimited by horizontal and vertical angles, respectively, 2.48° and 5.49° , as shown in (3.2) and (3.1); notwithstanding lower angles, it was reached accuracies of 0.96 and 0.93 for TW of 7s and 4s, respectively. A vestigial amount of 2° minimal eye movements was measured during the shifting of the stimulus. Color, size, and luminance were the same for both LED arrangements. Also, distances of both stimuli were estimated, using the diameter blur model described in Section 3.3, in order to cause the same blurriness degree for non-focused stimulus. It is worth commenting that the proposed LED arrangement stimulation unit here developed is small, portable, easy to use and adapted for end-users applications, features which are not shared by other stimulation devices, which require a computer screen. Table 4 shows the results presented

Table 4 – Comparison of the accuracy and ITR of this Thesis with the reviewed papers. **H**: Healthy, **End**: End user, **on**: online, and **off**: offline.

Study	Class.	Acc. %	ITR bits/min	Analysis	popul.	Subj.	Eye Mov
Kelly et al. (2005a)	2	70.3	0.91	off	H	10	$<1^\circ$
Allison et al. (2008)	2	74	4.18	on	H	14	
Zhang et al. (2010)	2	72,6	2.17	on	H	18	$<1\mu V$
Walter et al. (2012)	2	70.3	0.91	off	H	14	$<25\mu V$
Lim et al. (2013)	2	80	10.8	off/on	H/End	11/1	
Lesenfants et al. (2014)	2	80		off/on	H/End	12/6	= 0
This Thesis	2	93	9.58	off	H	8	$< 2^\circ$

in Table 1 and discussed in Section 2.2 but including the results achieved in this Thesis.

Future directions in patients with paralysis

It was reported that people with paralysis are already being trained to use some kind of BCI systems based on P300, slow cortical potential or sensorimotor rhythm (BIRBAUMER et al., 2000; MARCHETTI; PRIFTIS, 2014). However, although traditional SSVEP systems are becoming robust, they are limited to patients able to perform eye movements at some degree. To overcome this limitation, SSVEP systems based on covert attention are being developed. The novel setup based in Depth-of-field phenomenon here proposed goes in that direction, as there head, neck or eye movements are not need to select a command, which is base on the accommodation mechanism. It is worth noting that although accommodation of the lens does not require eyeball movements, minimal movements were measured when subjects were asked to shift their focus, as shown in EOG results (Section 6.2). The sense of sight is not affected by neurodegenerative diseases as ALS, and patients retain minimal eye movements, including pupil and accommodation reflex mechanisms; making focus control possible even in the end stages of these pathologies. Then, as shown in this paper, our proposal achieves higher accuracy rates than SSVEP-BCI based on covert attention, and could be employed in alternative or augmentative communication systems for people with paralysis. Furthermore, a system based on shifting of focus does not demand an exhausted training stage because focusing is an optical mechanism that is used naturally by humans throughout life.

Currently, many SSVEP systems uses frequencies below 15 Hz (MIDDENDORF et al., 2000; GAO et al., 2003; PFURTSCHELLER et al., 2010; NAKANASHI et al., 2014; ZHANG et al., 2012; Hakvoort; Reuderink; Obbink, 2011; CHENG et al., 2002). However, frequencies between 5Hz and 25 Hz could cause fatigue in paralyzed patients (ZHU et al., 2010). In order to attain SSVEP systems for real applications that avoid this fatigue limitation, frequencies above 25Hz could be used (LIN et al., 2007). Furthermore, a brain switch based on motor imagery was developed to activate a SSVEP system only when needed to send a command and deactivate the stimuli during the resting periods (PFURTSCHELLER et al., 2010); then, limiting the stimulation time. In addition, the measuring of the energy of alpha rhythm of frontal cortex is proposed to correlate with stress and fatigue, in order to adjust the frequency and/or luminance of stimuli, or deactivate them (COTRINA et al., 2014b).

Limitations and Future works

The main limitation of this work is given by the minimal eye movement measured during experiments. Even if the measurement has been associated with involuntary movements of the subjects, it was greater than the other assessments. Other limitation

that is shared with the works referred in Table 4 is the quantity of commands. Beside being difficult to implement a control systems, BCI systems with two commands use to attain low ITR (MIDDENDORF et al., 2000). The stimulation unit here developed is small, portable, and does not require a computer screen. It can be consider an advantage; however, it also can be considered a limitation, due to the both stimuli cannot be implemented in computer screens. The Depth-of-field phenomenon only can be exploited when stimuli are placed at different distances of subjects. In this sense, another setup approach could use the screen to show an stimulus together with an external stimulus.

After the concept proof of the novel SSVEP-BCI setup, the future works are related to its evaluation in on-line mode with a modified stimulation unit to avoid involuntary neck, head and/or eye movements. Also, testing with end-users should contemplated.

7.2 Conclusion

In this work, a novel SSVEP-BCI setup for binary control was designed, implemented and tested. All eight subjects demonstrated reliable control achieving an accuracy average of 0.93 for LASSO detection method, corresponding to a bit rate of 9.58 bits/min. This work is a proof of concept that a SSVEP-BCI can be built relying on the fact that the SSVEP pattern of a focused stimulus is distinguishable regardless of the non-focused stimulus that is also presented. The advantage of the SSVEP-BCI proposed in this work is that it requires minimal movement for selecting stimulus if compared with traditional SSVEP-BCIs. Also, it reached higher accuracy rate than SSVEP systems based on covert attention. Once demonstrated the potential utility of the Depth-of-field phenomenon and the accommodation mechanism combined with SSVEP-BCI systems, this research looks toward to achieve acceptable levels of online human communication.

Bibliography

ALLISON, B. et al. Bci demographics: how many (and what kinds of) people can use an ssvep bci? *IEEE Transactions on Neural Systems and Rehabilitation Engineering*, v. 18, n. 2, p. 107–16, Apr 2010.

ALLISON, B. et al. Towards an independent brain-computer interface using steady state visual evoked potentials. *Clinical Neurophysiology*, v. 119, n. 2, p. 399–408, February 2008.

ATCHINSON, D.; SMITH, G. *Optics of the human eye*. Edinburgh: Elsevier Science, 2000.

BASTOS, T. et al. Towards a new modality-independent interface for a robotic wheelchair. *IEEE Transactions on Neural Systems and Rehabilitation Engineering*, v. 22, n. 3, p. 567–84, May 2014.

BASTOS, T. et al. Evaluation of feature extraction techniques in emotional state recognition. In: *4th International Conference on Intelligent Human Computer Interaction (IHCI)*. Kharagpur, India: IEEE, 2012. p. 1–6.

BENEVIDES, A. *A Brain-computer Interface Architecture Based on Motor Mental Tasks and Music Imagery*. Vitoria ES, Brazil: Federal University of Espirito Santo - Ph.D Thesis, 2013.

BENEVIDES, A. et al. An ethernet sniffer for on-line acquisition of eeg with the brainnet36 device applied to a bci. In: *Biosignals and Biorobotics Conference (2014): Biosignals and Robotics for Better and Safer Living (BRC), 5th ISSNIP-IEEE*. Salvador BA, Brazil: [s.n.], 2014. p. 1–6.

BENEVIDES, A. et al. Evaluation of motor and non-motor mental tasks to be applied to brain-computer interfaces (estudo de tarefas mentais motoras e nao-motoras para aplicacao em interfaces cerebro-computador). *Medical Journal of Minas Gerais*, v. 22, n. 6, p. 30, Set 2012.

BERGER, H. Ueber das elektrenkephalogramm des menschen. *Archiv fur Psychiatrie und Nervenkrankheiten*, n. 87, p. 527–70, 1929.

BIN, G. et al. Vep-based brain-computer interfaces: time, frequency, and code modulations. *IEEE Computational Intelligence Magazine*, v. 4, n. 4, p. 22–6, Nov 2009.

BIRBAUMER, N. Breaking the silence: Brain-computer interfaces (bci) for communication and motor control. *Psychophy*, n. 43, p. 517–32, 2005.

BIRBAUMER, N.; COHEN, L. Brain-computer interfaces: communication and restoration of movement in paralysis. *Journal of Physiology*, v. 579, n. 3, p. 621–36, 2007.

BIRBAUMER, N.; KIMMEL, H. *Biofeedback and self-regulation*. Hillsdale FL, USA: Erlbaum, 1979.

BIRBAUMER, N. et al. The thought translation device (ttd) for completely paralyzed patients. *IEEE Transactions on Rehabilitation Engineering*, v. 8, n. 2, p. 190–3, Jun 2000.

- BURGE, J.; GEISLER, W. S. Optimal defocus estimation in individual natural images. *Proceedings of the National Academy of Sciences*, v. 108, n. 40, p. 16849–54, Oct 2011.
- BUSHBY, K. et al. Diagnosis and management of duchenne muscular dystrophy, part 1: diagnosis, and pharmacological and psychosocial management. *The Lancet Neurology*, v. 9, n. 1, p. 77–93, Jan 2010.
- CASTILLO, J. et al. Adaptive bci based on software agents. In: *Proceedings of 36th Annual International Conference of Engineering in Medicine and Biology Society*. Chicago IL, USA: [s.n.], 2014. p. 5458–61.
- CASTILLO, J. et al. Proposal of a brain computer interface to command an autonomous car. In: *5th Biosignals and Biorobotics Conference*. Salvador BA, Brazil: IEEE, 2014. p. 1–6.
- CASTILLO, J. et al. Comparison among feature extraction techniques based on power spectrum for a ssvep-bci. In: *Proceedings of IEEE International Conference on Industrial Informatics*. Porto Alegre RS, Brazil: IEEE, 2014. p. 284 – 288.
- CHARTIER, G. *Introduction to Optics*. Grenoble: Springer, 2005.
- CHEN, L. et al. Image metrics for predicting subjective image quality. *Optometry and Vision Science*, v. 82, n. 5, p. 358–69, May 2005.
- CHENG, M.; GAO, S. Eeg-based cursor control system. In: *Engineering in Medicine and Biology Society (EMBC), 1999 Annual International Conference of the IEEE*. [S.l.: s.n.], 1999. p. 669.
- CHENG, M. et al. Design and implementation of a brain-computer interface with high transfer rates. *IEEE Transactions on Biomedical Engineering*, v. 49, n. 10, p. 1181–6, Oct 2002.
- COTRINA, A. et al. Evaluation of statistical features and hoc of eeg signals to be applied on emotional states recognizing (avaliacao de características estatísticas e hoc de sinais eeg no reconhecimento de estados emocionais). *Medical Journal of Minas Gerais*, v. 22, n. 6, p. 131, Set 2012.
- COTRINA, A. et al. Evaluation of erd/ers caused by unpleasant sounds to be applied in bcis. In: *Proceedings of Biosignals and Biorobotics Conference*. Rio de Janeiro: IEEE, 2013. p. 1–6.
- COTRINA, A. et al. Towards a ssvep-bci based on depth of field. In: *Proceedings of the 6th International BCI Conference*. Graz, Austria: TU Graz, 2014. p. 1–6.
- COTRINA, A. et al. Evaluation of emotional components to improve a ssvep-bci. In: *Annals of Automation Brazilian Conference*. Belo Horizonte MG, Brazil: UFMG, 2014.
- COTRINA, A. et al. Towards an architecture of a hybrid bci based on ssvep-bci and passive-bci. In: *Proceedings of 36th Annual International Conference of Engineering in Medicine and Biology Society*. Chicago IL, USA: IEEE, 2014. p. 1342–5.
- COTRINA, A. et al. A ssvep-bci based on depth-of-field. *IEEE Transactions on Neural Systems and Rehabilitation Engineering*, 2016. Submitted.

- COTRINA, A. et al. Towards a bci-speller based on binary selection. In: *1st International Workshop on Assistive Technology*. Vitoria ES, Brazil: UFES, 2015.
- COTRINA, A. et al. Statistical evaluation of a novel ssvep-bci stimulation setup based on depth-of-field. *Research on Biomedical Engineering*, v. 31, n. 4, p. 295–306, Jan 2015. In press.
- COTRINA, A. et al. Evaluation of eye movements using tracking devices in context of a novel ssvep-bci setup. In: *Proceedings of XII Brazilian Symposium of Intelligent Automation*. Natal RN, Brazil: UFRN, 2015. p. 1–8.
- COTRINA, A. et al. Computing stress-related emotional state via frontal cortex asymmetry to be applied in passive-ssbci. In: *Proceedings of Biosignals and Biorobotics Conference*. Salvador BA, Brazil: IEEE, 2014. p. 1–6.
- COTRINA, A. et al. Toward a hybrid brain-computer interface. In: ANDRADE, A. de O. et al. (Ed.). *Technology, techniques and tendencies in biomedical engineering*. Bauru: Canal6, 2014. p. 343–64.
- DAI, G.-M. *Wavefront Optics for Vision Correction*. Washington: SPIE, 2008.
- DELORME, A.; MAKEIG, S. Eeglab: an open source toolbox for analysis of single-trial eeg dynamics including independent component analysis. *Journal of Neuroscience methods*, v. 134, n. 1, p. 9–21, Mar 2004.
- EBENHOLTZ, S. M. *Oculomotor Systems and Perception*. Cambridge: Cambridge University Press, 2001.
- FARWELL, L.; DONCHIN, E. Talking off the top of your head: toward a mental prosthesis utilizing event-related brain potentials. *Electroencephalography and Clinical Neurophysiology*, v. 70, n. 6, p. 510–23, Dec 1988.
- FELIX, L. B. et al. A spatial approach of magnitude-squared coherence applied to selective attention detection. *Journal of Neuroscience Methods*, v. 229, n. 30, p. 28–32, May 2014.
- FERRARA, F. *SMDA: A System for Multimodal Assistive Domotics*. Milano: Politecnico di Milano - Master Thesis, 2014.
- FERREIRA, A. *Uma proposta de interface cérebro-computador para comando de cadeiras de rodas*. Vitoria ES, Brazil: Federal University of Espirito Santo - Ph.D Thesis, 2008.
- FERREIRA, A. et al. Human-machine interfaces based on emg and eeg applied to robotic systems. *Journal of NeuroEngineering and Rehabilitation*, v. 5, n. 1, p. 1–15, 2008.
- FERREIRA, A. et al. Human-machine interface based on muscular and brain signals applied to a robotic wheelchair. *Journal of Physics: Conference Series*, v. 90, n. 1, p. 1–8, Mar 2007.
- FISHER, R. et al. Photic- and pattern-induced seizures: A review for the epilepsy foundation of america working group. *Epilepsia*, v. 46, n. 9, p. 1426–41, 2005.
- FLORIANO, A. et al. Development of an ssvep-bci for telepresence robot control. In: *Proceedings of XII Brazilian Symposium of Intelligent Automation*. Natal: UFRN, 2015.

- GANTNER, I. et al. Our rapidly changing understanding of acute and chronic disorders of consciousness: challenges for neurologists. *Future Neurology*, v. 8, n. 1, p. 43–54, 2013.
- GAO, X. et al. A bci-based environmental controller for the motion-disabled. *IEEE Transactions on Neural Systems and Rehabilitation Engineering*, v. 11, n. 2, p. 137–40, Jun 2003.
- GRAND, Y. L.; HAGE, S. E. *Physiological optics*. [S.l.]: Springer, 1980.
- GREGORY, R. L. *Eye and brain, the psychology of seeing*. 5. ed. New Jersey: Princeton University Press, 1997.
- GRUSSER, O.-J.; GRUSSER-CORNEHLS, U. Physiology of vision. In: SCHMIDT, R. F. (Ed.). *Fundamentals of Sensory Physiology*. Berlin: Springer Berlin Heidelberg, 1986. p. 126–9.
- GUGER, C. et al. How many people are able to control a p300-based brain-computer interface (bci)? *Neuroscience letters*, v. 462, n. 1, p. 94–98, 2009.
- GUGER, C. et al. How many people are able to operate an eeg-based brain-computer interface (bci)? *IEEE Transactions on Neural Systems and Rehabilitation Engineering*, v. 11, n. 2, p. 145–7, 2003.
- GUYTON, A. C.; HALL, J. E. *Guyton and Hall Textbook of Medical Physiology*. 11. ed. Philadelphia: Elsevier Inc., 2006.
- Hakvoort, G.; Reuderink, B.; Obbink, M. *Comparison of PSDA and CCA detection methods in a SSVEP-based BCI-system*. Enschede: Centre for Telematics and Information Technology, University of Twente, 2011. (CTIT technical reports series, TR-CTI).
- HARTER, M. R.; WHITE, C. T. Evoked cortical responses to checkerboard patterns: Effect of checksize as a function of visual acuity. *Electroencephalography and Clinical Neurophysiology*, 1970.
- HE, B. et al. Brain computer interfaces. In: HE, B. (Ed.). *Neural Engineering*. 2. ed. Mineapolis: Springer US, 2013. p. 87–151.
- HERMAN, I. P. *Physics of the Human Body*. Berlin: Springer, 2007.
- HERRMANN, C. S. Human eeg responses to 1-100hz flicker: resonance phenomena in visual cortex and their potential correlation to cognitive phenomena. *Experimental Brain Research*, v. 137, n. 3-4, p. 346–53, Apr 2001.
- HOWARD, I. *Perceiving in Depth: Volume 1 Basic Mechanisms*. New York: Oxford University Press, 2012.
- HUGGINS, J. E. Bcis based on signals from between the brain and skull. In: GRAIMANN, B.; ALLISON, B.; PFURTSCHELLER, G. (Ed.). *Brain-computer interfaces. revolutionizing human-computer interaction*. Mineapolis: Springer, 2010. p. 221–39.
- INFANTOSI, A.; LAZAREV, V.; CAMPOS, D. D. Detecting responses to intermittent photic stimulation in the electroencephalogram using the spectral f test. *Brazilian Journal of Biomedical Engineering*, v. 21, n. 1, p. 25–36, Jun 2005.

- JAPKOWICZ, N.; SHAH, M. *Evaluating Learning Algorithms*. New York: Cambridge University Press, 2011.
- JURCAK, V.; TSUZUKI, D.; DAN, I. 10/20, 10/10, and 10/5 systems revisited: Their validity as relative head-surface-based positioning systems. *Neuroimage*, v. 34, n. 4, p. 1600 – 1611, 2007.
- KANDEL, E.; SCHWARTZ, J.; JESSELL, T. *Principles of Neural Science*. 4. ed. USA: Mc Graw Hill, 1991.
- KEATING, M. P. *Geometric, Physical, and Visual Optics*. Woburn: Butterworth-Heinemann, 2002.
- KELLY, S. et al. A comparison of covert and overt attention as a control option in a steady-state visual evoked potential-based brain computer interface. In: *Proceedings of Engineering in Medicine and Biology Society Conference*. San Francisco CA, USA: IEEE, 2004. v. 2, p. 4725–8.
- KELLY, S. et al. Visual spatial attention control in an independent brain-computer interface. *IEEE transactions on biomedical engineering*, v. 52, n. 9, p. 1588–96, Sep 2005.
- KELLY, S. et al. Visual spatial attention tracking using high-density ssvep data for independent brain-computer communication. *IEEE Transactions on Neural Systems and Rehabilitation Engineering*, v. 13, n. 2, p. 172–8, 2005.
- KOTHARI, R. et al. Refractive errors and their effects on visual evoked potentials. *Journal of Clinical Ophthalmology and Research*, v. 2, n. 1, p. 3–6, Dec 2014.
- LALOR, E. C. et al. Steady-state vep-based brain-computer interface control in an immersive 3d gaming environment. *EURASIP Journal on Applied Signal Processing*, v. 19, p. 3156–64, Jan 2005.
- LAUREYS, S. Death, unconsciousness and the brain. *Nature Reviews Neuroscience*, v. 6, p. 899–909, 2005.
- LESENFANTS, D. et al. An independent ssvep-based brain-computer interface in locked-in syndrome. *Journal of Neural Engineering*, v. 11, n. 3, p. 1–8, Jun 2014.
- LIM, J.-H. et al. Classification of binary intentions for individuals with impaired oculomotor function: eyes-closed ssvep-based brain-computer interface (bci). *Journal of Neural Engineering*, v. 10, n. 2, p. 1–9, Apr 2013.
- LIN, Z. et al. Frequency recognition based on canonical correlation analysis for ssvep-based bcis. *IEEE transactions on biomedical engineering*, v. 54, n. 6, p. 1172–6, Jun 2007.
- LIVINGSTONE, M.; HUBEL, D. Segregation of form, color, movement, and depth: Anatomy, physiology, and perception. *Science, New Series*, v. 240, n. 4853, p. 740–9, May 1988.
- MAHAJAN, V. N. *Aberration Theory Made Simple*. Washington: Spie Optical Engineering Press, 1991.
- MALLOT, H. A. *Computational Neuroscience. A First Course*. Switzerland: Springer, 2013.

- MARCHETTI, M.; PRIFTIS, K. Brain–computer interfaces in amyotrophic lateral sclerosis: A metanalysis. *Clinical Neurophysiology*, v. 126, n. 6, p. 1255–63, 2014.
- MCFARLAND, D. J. et al. Spatial filter selection for eeg-based communication. *Electroencephalography and Clinical Neurophysiology*, v. 103, n. 3, p. 386 – 394, 1997.
- MELGES, D.; SA, A. de; INFANTOSI, A. Frequency-domain objective response detection techniques applied to evoked potentials: A review. In: NAIK, G. R. (Ed.). *Applied Biological Engineering - Principles and Practice*. [S.l.]: InTech, 2012.
- MELLINGER, J. et al. An meg-based brain-computer interface (bci). *NeuroImage*, v. 36, n. 3, p. 581 – 593, 2007.
- MIDDENDORF, M. et al. Brain-computer interfaces based on the steady-state visual-evoked response. *IEEE transactions on neural systems and rehabilitation engineering*, v. 8, n. 2, p. 211–4, Jun 2000.
- MILLODOT, M.; RIGGS, L. A. Refraction determined electrophysiologically: Responses to alternation of visual contours. *Archives of ophthalmology*, 1970.
- MULLER-PUTZ, G. R. et al. Steady-state visual evoked potential (ssvep)-based communication: impact of harmonic frequency components. *Journal of Neural Engineering*, v. 2, n. 4, p. 123, 2005.
- MULLER, S. *Interface Cerebro-Computador Baseada em Potenciais Evocados Visuais em Regime Permanente para Comando de uma Cadeira de Rodas Robotica*. Vitoria ES, Brazil: Federal University of Espirito Santo - Ph.D Thesis, 2010.
- MULLER, S.; BASTOS, T.; SARCINELLI, M. Incremental ssvep analysis for bci implementation. In: *Engineering in Medicine and Biology Society (EMBC), 2010 Annual International Conference of the IEEE*. [S.l.: s.n.], 2010. p. 3333–6.
- MULLER, S. M. T.; BASTOS, T.; SARCINELLI-FILHO, M. Proposal of a ssvep-bci to command a robotic wheelchair. *Journal of Control, Automation and Electrical Systems*, v. 24, n. 1, p. 97–105, Apr 2013.
- NAKANASHI, M. et al. A high-speed brain speller using steady-state visual evoked potential. *International Journal of Neural Systems*, v. 24, n. 6, p. 1–17, Sep 2014.
- NIJBOER, F.; BROERMANN, U. Brain–computer interfaces for communication and control in locked-in patients. In: GRAIMANN, B.; ALLISON, B.; PFURTSCHELLER, G. (Ed.). *Brain-computer interfaces, revolutionizing human–computer interaction*. Mineapolis: Springer, 2010. p. 186–201.
- NUNEZ, P. L.; SRINIVASAN, R. *Electric Fields of the Brain. The Neurophysics of EEG*. New York: Oxford University Press, 2006.
- ODOM, J. et al. Iscev standard for clinical visual evoked potentials (2009 update). *Documenta Ophthalmologica*, v. 120, n. 1, p. 111–9, Feb 2010.
- PACKER, O.; R.WILLIAMS, D. Light, the retinal image, and photoreceptors. In: *The Science of Color*. 2. ed. Amsterdam: Elsevier Science Ltd, 2003. p. 41–102.

- PASTOR, M. A. et al. Human cerebral activation during steady-state visual-evoked responses. *The Journal of Neuroscience*, v. 23, n. 37, p. 11621–7, Dec 2003.
- PENTLAND, A. P. A new sense for depth of field. *IEEE Transactions on Pattern Analysis and Machine Intelligence*, v. 9, n. 4, p. 523–31, Jul 1987.
- PFURTSCHELLER, G.; SILVA, F. H. L. da. Event-related eeg/meg synchronization and desynchronization: basic principles. *Clinical Neurophysiology*, v. 110, p. 1842–1857, 1999.
- PFURTSCHELLER, G. et al. Self-paced operation of an ssvep-based orthosis with and without an imagery-based brain switch: A feasibility study towards a hybrid bci. *IEEE Transactions on Neural Systems and Rehabilitation Engineering*, v. 18, n. 4, p. 409–14, 2010.
- POSNER, M. I.; PETERSEN, S. E. The attention system of the human brain. *Annual Review of Neuroscience*, v. 13, n. 1, p. 25–42, Mar 1990.
- POTES, C. et al. Dynamics of electrocorticographic (ecog) activity in human temporal and frontal cortical areas during music listening. *Neuroimage*, v. 61, n. 4, p. 841–8, 2012.
- REGAN, D. *Human Brain Electrophysiology: Evoked Potentials and Evoked Magnetic Fields in Science and Medicine*. New York: Elsevier, 1989.
- RICCIO, A. et al. Eye-gaze independent eeg-based brain-computer interfaces for communication. *Journal of Neural Engineering*, v. 9, n. 4, p. 1–15, Aug 2012.
- RUSSO, F. D.; TEDER-SALEJARVI, W. A.; HILLYARD, S. A. Steady-state vep and attentional visual processing. In: ZANI, A.; PROVERBIO, A. M.; POSNER, M. I. (Ed.). *The Cognitive Electrophysiology of Mind and Brain*. San Diego: Academic Press, 2003. p. 257–72.
- SA, A. M. F. L. M. D. et al. Spectral f-test power evaluation in the eeg during intermittent photic stimulaton. *Arquivos de Neuro-Psiquiatria*, v. 64, n. 2a, p. 228–32, Jun 2006.
- SCHALK, G.; LEUTHARDT, E. Brain-computer interfaces using electrocorticographic signals. *IEEE Reviews in Biomedical Engineering*, n. 4, p. 140–54, 2011.
- SHEVELL, S. K. *The Science of Color*. [S.l.]: Elsevier Science Ltd, Amsterdam, 2003.
- SIMPSON, D. et al. Objective response detection in an electroencephalogram during somatosensory stimulation. *Annals of Biomedical Engineering*, v. 28, n. 6, p. 691–8, Jun 2000.
- SOKOL, S. Visually evoked potentials: Theory, techniques and clinical applications. *Survey of Ophthalmology*, v. 21, n. 1, p. 18–44, Jul 1976.
- SOKOL, S.; MOSKOWITZ, A. Effect of retinal blur on the peak latency of the pattern evoked potential. *Vision Research*, v. 21, n. 8, p. 1279–86, 1981.
- SONGNIAN, Z. et al. The representation of visual depth perception based on the plenoptic function in the retina and its neural computation in visual cortex v1. *BMC Neuroscience*, v. 15, n. 1, p. 1–17, Apr 2014.
- STANGOR, C. *Beginning Psychology*. [S.l.]: Creative Commons, 2012.

- SUMMA, A. di et al. Mechanism of binocular interaction in refraction errors: study using pattern-reversal visual evoked potentials. *Documenta Ophthalmologica*, v. 98, n. 2, p. 139–51, Jul 1999.
- TANAKA, T.; ZHANG, C.; HIGASHI, H. Ssvep frequency detection methods considering background eeg. In: *Joint 6th International Conference on Soft Computing and Intelligent Systems (SCIS) and 13th International Symposium on Advanced Intelligent Systems (ISIS), 2012*. Kobe: IEEE, 2012. p. 1138–1143.
- TELLO, R. et al. A high performance human-computer interface to control a robotic wheelchair and an intelligent environment. In: *Proceedings of VI International Conference of Design, Research Networks and Technology for All*. [S.l.: s.n.], 2015.
- THIBOS, L. N.; BRADLEY, A. Modeling off-axis vision ii: The effect of spatial filtering and sampling by retinal neurons. In: PELI, E. (Ed.). *Vision models for target detection and recognition : in memory of Arthur Menendez*. Singapore: World Scientific Publishing Co., 1995.
- TIERRA-CRIOLLO, C. J.; INFANTOSI, A. F. C. Low-frequency oscillations in human tibial somatosensory evoked potentials. *Archivos de Neuro-Psiquiatria*, v. 64, n. 2b, p. 402–6, Jun 2006.
- TRAUERNITZCH, M. et al. Toward eeg-based emotion recognition using brain computer interfaces. In: ANDRADE, A. de O. et al. (Ed.). *Technology, techniques and tendencies in biomedical engineering*. Bauru: Canal6, 2014. p. 319–42.
- VIALATTE, F.-B. et al. Steady-state visually evoked potentials: Focus on essential paradigms and future perspectives. *Progress in Neurobiology*, v. 90, n. 4, p. 418–38, Apr 2010.
- VIDAL, J. Toward direct brain-computer communication. *Annual review of biophysics and bioengineering*, v. 2, p. 157–180, 1973.
- VISHWANATH, D.; BLASER, E. Retinal blur and the perception of egocentric distance. *Journal of Vision*, v. 10, n. 10, p. 1–16, Aug 2010.
- VOLOSYAK, I. et al. Evaluation of the bremen ssvep based bci in real world conditions. In: *IEEE International Conference on Rehabilitation Robotics*. Kyoto: IEEE, 2009. p. 322–331.
- VOLOSYAK, I. et al. Bci demographics ii: How many (and what kinds of) people can use a high-frequency ssvep bci? *IEEE Transactions on Neural Systems and Rehabilitation Engineering*, v. 19, n. 3, p. 232–9, Jun 2011.
- WALTER, S. et al. Effects of overt and covert attention on the steady-state visual evoked potential. *Neuroscience Letters*, v. 519, n. 1, p. 37–41, Jun 2012.
- WANG, B.; CIUFFREDA, K. J. Depth-of-focus of the human eye: Theory and clinical implications. *Survey of Ophthalmology*, v. 51, n. 1, p. 75–85, Jan 2006.
- WANG, Y. et al. Practical designs of brain-computer interfaces based on the modulation of eeg rhythms. In: GRAIMANN, B.; PFURTSCHELLER, G.; ALLISON, B. (Ed.). *Brain-Computer Interfaces: Revolutionizing human-computer interaction*. Berlin: Springer Berlin Heidelberg, 2010. p. 137–154.

- WANG, Y. et al. A practical vep-based brain-computer interface. *IEEE Transactions on Neural Systems and Rehabilitation Engineering*, v. 14, n. 2, p. 234–40, Jun 2006.
- WILSON, B.; DECKER, K.; ROORDA, A. Monochromatic aberrations provide an odd-error cue to focus direction. *Journal of the Optical Society of America A*, v. 19, n. 5, p. 833–9, 2002.
- WOLPAW, J. et al. Eeg-based communication: improved accuracy by response verification. *IEEE Transactions on Rehabilitation Engineering*, v. 6, n. 3, p. 326–33, Sep 1998.
- WOLPAW, J. R. et al. Brain-computer interfaces for communication and control. *Clinical Neurophysiology*, v. 113, n. 6, p. 767–91, Jun 2002.
- WU, Z. et al. Stimulator selection in ssvep-based bci. *Medical Engineering and Physics*, v. 30, n. 8, p. 1079–88, Oct 2008.
- YIN, E. et al. A dynamically optimized ssvep brain-computer interface (bci) speller. *IEEE Transactions on Biomedical Engineering*, v. 62, n. 6, p. 1447–56, Jun 2014.
- ZANLUCA, C. et al. First report of autochthonous transmission of zika virus in brazil. *Mem. Inst. Instituto Oswaldo Cruz*, v. 110, p. 569–72, 2015.
- ZHANG, D. et al. An independent brain-computer interface using covert non-spatial visual selective attention. *Journal of Neural Engineering*, v. 7, n. 1, p. 1–11, Feb 2010.
- ZHANG, Y. et al. Lasso based stimulus frequency recognition model for ssvep bcis. *Biomedical Signal Processing and Control*, v. 7, n. 2, p. 104 – 111, 2012.
- ZHU, D. et al. A survey of stimulation methods used in ssvep-based bcis. *Computational Intelligence and Neuroscience*, v. 2010, p. 1–12, 2010.

Appendix

APPENDIX A – SSVEP-BCI in the Last Ten Years

To conduct the literature survey on stimulation strategies for SSVEP-based BCIs, in this work the Scopus¹ database was consulted by employing the same criteria used in (ZHU *et al.*, 2010) that is shown in Figure 69; in which papers were selected for review if the BCI and SSVEP of terms are present in their title, abstract or keyword list. The term BCI includes “Brain-Computer Interfac?”, “BMI” or “Brain Machine Interfac?”. Question mark “?” represents arbitrary letters (e.g., “e”, “es” or “ing”). The term SSVEP includes “Steady State Visual Evoked Potential?”, “SSVER”, or “Steady State Visual Evoked Respons?”. The search criteria is illustrated in Figure 69. The search range was between years 2005 and 2014 wrote in English language. Journal paper, Conference papers and Reviews were included in the searching

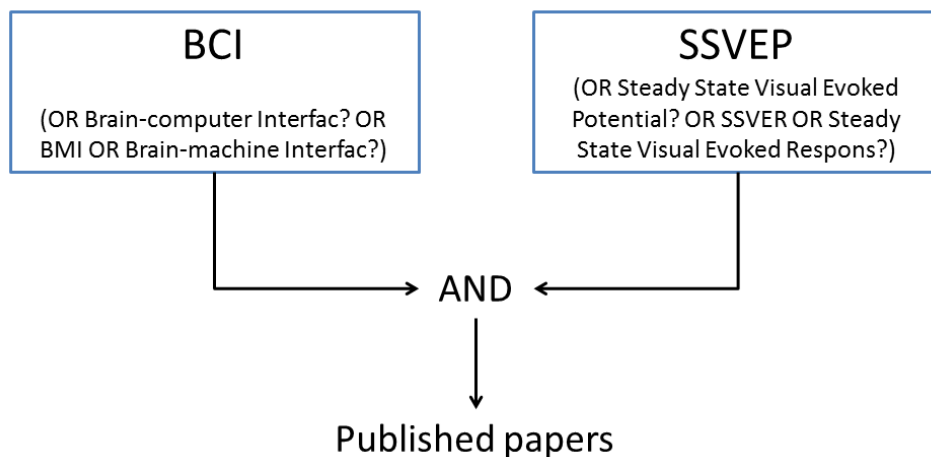


Figure 69 – Search criteria of scientific production in SSVEP-BCI. Searching was limited to papers wrote in English language between 2005 and 2014. OR and AND represent logic operators.

As a result, 635 indexed papers were found in this search². Top inset of Figure 70 shows a plot with the number of paper published by year since the year 2005. The quantity of publications related to SSVEP-BCI is growing with the time. Although the first paper was published in the year 2000 (MIDDENDORF *et al.*, 2000), the scientific production was increased substantially in 2008, 2010 and 2013.

The more relevant means of publication are shown in th bottom inset of Figure

¹ <http://www.scopus.com>

² Accessed on November 3rd, 2015

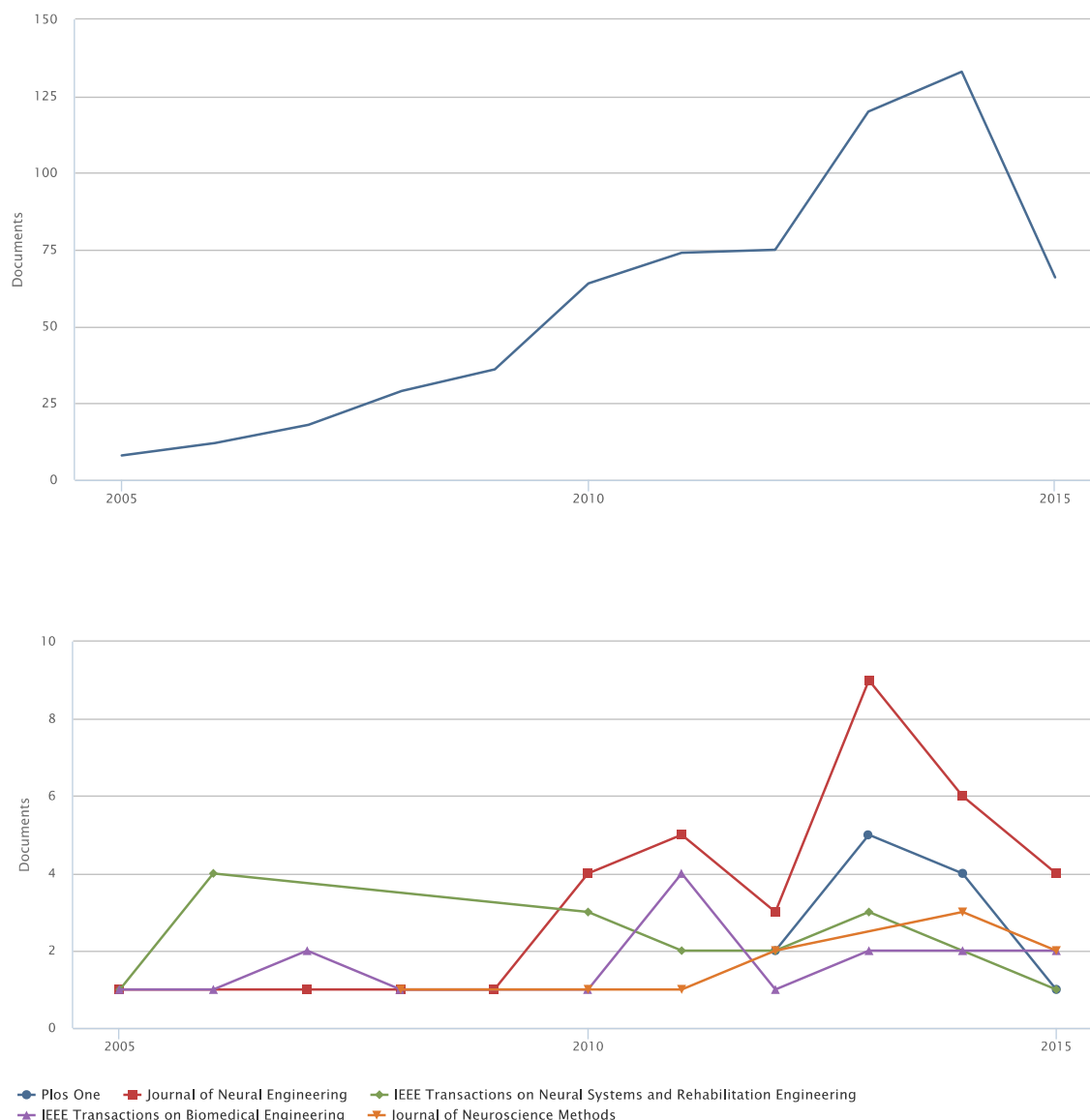


Figure 70 – (Top inset) Number of documents by year published in SSVEP-based BCI between 2005 and 2015. (Bottom inset) Number of documents published by some important peer-review journals (Journal on Neural Engineering, TNSRE, TBME and Plos One) and the EMBS conference proceedings.

70 together with the number of documents published in each one per year. The Journal of Neuroengineering³ is the journal that published thirty papers in the evaluated period, becoming the principal source of information searching. It is followed by the the Annual Conference of the IEEE Engineering in Medicine and Biology Society (EMBS) that has published twenty seven papers between 2011 and 2013. Two journals related to this society published jointly thirty papers. These are the IEEE Transactions of Biomedical Engineering⁴ (TBME) and the IEEE Transactions of Neural System and Rehabilitation

³ <http://iopscience.iop.org/1741-2552> (Impact Factor: 3.415)

⁴ <http://tbme.embs.org/> (Impact Factor: 2.233)

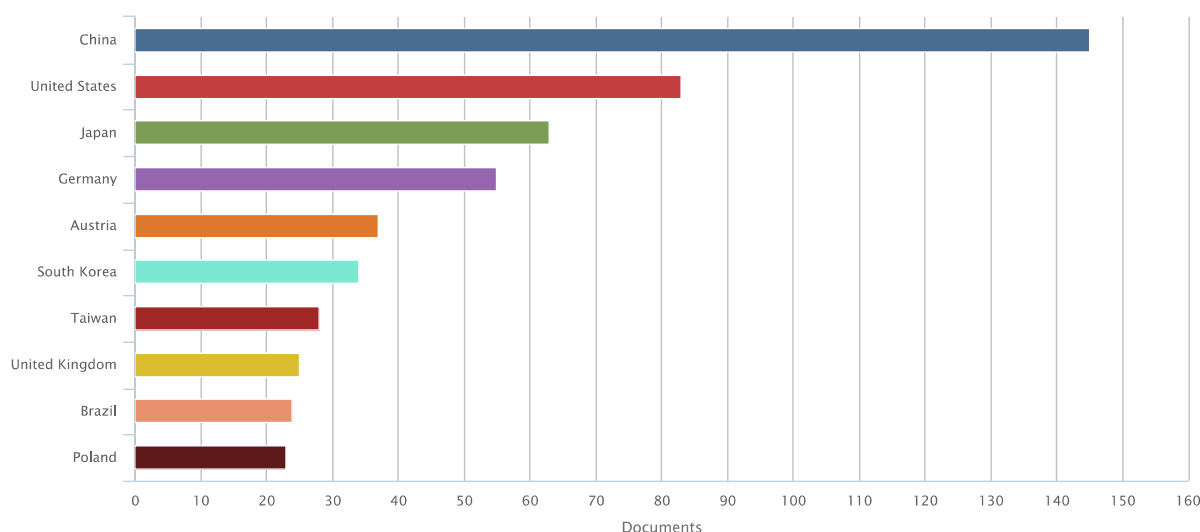


Figure 71 – The top ten countries that got the highest number of documents published.

Engineering⁵ (TNSRE). Another important searching source is the open-access online publication named Plos One that has published more papers than IEEE journals in the last three years.

Figure 71 shows the countries sorted according to the number of documents published, where Brazil ranks ninth. The scientific production in some countries are related to specific research groups. In China, United States, Germany and Austria the main group are given by Tsinghua University (Beijing), University of California San Diego, *Universitat Bremen*, and *Technische Universitat Graz*, respectively. The ranking of the top ten of research groups is shown in Figure 72. The groups mentioned above are in the first positions. The group of *Universidade Federal do Espirito Santo* (UFES), that is a representative group in Brazil, ranks fourth. Following, the most relevant groups are described.

- Tsinghua University (China)

This group is led by Xiarong Gao and Shangkai Gao and has published the results of their work since 1999. In 2002, the group developed a SSVEP-BCI with 13 stimuli that matched the ITR average of 27.15 bits/min (CHENG et al., 2002). In 2003 they conducted a practical application that consisted of the use of an infrared remote control (GAO et al., 2003). Studies on frequency and channel selection were presented. In 2006, the group developed a practical SSVEP-BCI, which aimed to reduce the differences in performance for different users. It was found that more than 90% of people could use an SSVEP-BCI with high ITR in real environments (WANG et al., 2006). The method of canonical correlation analysis for detection of frequencies of stimulation was proposed in (LIN et al., 2007). Until 2013, the group continued

⁵ <http://tnsre.embs.org/> (Impact Factor: 2.821)

working on finding a better selection of frequencies, channels and modulation, and the study of the method of canonical correlation analysis.

- University of Bremen (Germany)

This group, led by Ivan Volosyak and Axel Grasel, has been developing works with SSVEP since 2007. A method of detection of SSVEPs using multiple channels to achieve a high ITR was proposed. At the same time, an interface with the function of speller using SSVEPs (Friman et al., 2007) was developed. In a later work, the interface developed by the University of Bremen has been evaluated in real conditions (VOLOSAYAK et al., 2009) with 37 volunteers without any handling with BCIs. Results showed that 32 participants were able to complete the task of writing predetermined words, with an average accuracy of 92% and an ITR of 22.6 bits/min. In recent works, two demographical analysis were performed. In first, 106 volunteers were evaluated (ALLISON et al., 2010) and in the second (VOLOSAYAK et al., 2011) 84 volunteers were considered. The group did not reported results in the last years. In 2012 they reported a work related to age-specific mechanisms in an SSVEP-based BCI scenario.

- University of California at San Diego (USA)

There are two important groups in this university: (1) The Swartz Center for Computational Neuroscience is led by Scott Makeig. This group develops the EEGLAB, an open source environment for electrophysiological signal processing (DELORME; MAKEIG, 2004). Currently, Yuan-Pin Lin that is working in a portable BCI, developed an online SSVEP decoding in human walking using a consumer EEG headset, and a stimulus presentation on mobile devices for a truly portable SSVEP-BCI. Another researcher, Masaki Nakanishi implemented a high-speed brain speller using an SSVEP that achieved 192.26 bits/min (NAKANASHI et al., 2014). (2) Brendan Allison, who is a researcher involved with the Cognitive Neuroscience Laboratory from the Department of Cognitive Science, currently is working with a new hybrid BCI paradigm based on P300 and SSVEP in addition to collaborative BCIs.

- Federal University of Espirito Santo (Brazil)

The group is led by Teodiano Freire Bastos-Filho, who is a supervisor of the present work, and is working at Intelligent Automation Lab (LAI). This group was the first to develop a robotic wheelchair using brain signals in Brazil (FERREIRA et al., 2007). In 2013, an SSVEP-BCI to command a robotic wheelchair was proposed (MULLER; BASTOS; SARCINELLI-FILHO, 2013). From 2014, the group is developing SSVEP-BCI for control applications, such as command of an autonomous car (CASTILLO et al., 2014b), control of an updated robotic wheelchair (FERRARA, 2014; TELLO et al., 2015), and control of a telepresence robot (FLORIANO et al., 2015). The

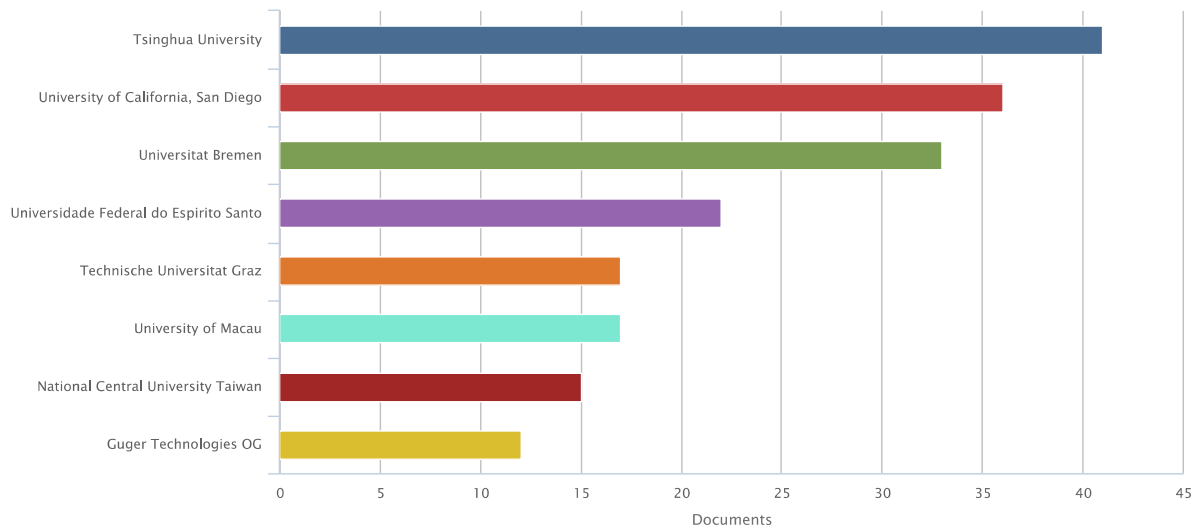


Figure 72 – Important research groups in SSVEP-BCI that got the highest number of documents published.

present work is part of communication proposal based on SSVEP-BCI, in which Depth-of-Field optics phenomenon is being applied to propose an alternative channel of communication (COTRINA et al., 2014a). The group has regular participation in the more relevant BCI scientific events around the world. It was present in the last BCI Meeting (2013), in the last Graz BCI Conference (2014) and in the last EMBS (Engineering Medical Biology Society) conferences. In 2014 the group awards the first place of Brazilian Brain-computer Interfaces Competition organized by the Brazilian Society of Biomedical Engineering.

- University of Graz (Austria)

The group is coordinated by Gernot R. Muller-Putz and Gert Pfurtscheller. In a well know work, they studied the influence of harmonic components in the detection of SSVEP (MULLER-PUTZ et al., 2005). In another work, the group used a response of the heart induced by rapid inspiration to initiate the use of ICC-SSVEP. Also, the employment of a SSVEP-BCI was proposed to control an electric prosthesis. The group is currently working on independent interfaces that can be used by people with motor diseases. A recent work published in this year reported results obtained with an independent SSVEP-based BCI for LIS (LESENFANTS et al., 2014).

APPENDIX B – Publications, Awards and Schools

Publications in Journals

1. **Cotrina, A.**; Benevides, A.; Castillo-Garcia, J.; Ferreira, A.; Bastos, T. Statistical Evaluation of a Novel SSVEP-BCI Stimulation Setup Based on Depth-of-Field. In Research on Biomedical Engineering Journal (accepted and in press production). ([COTRINA et al., 2015b](#))
2. **Cotrina, A.**; Benevides, Alessandro; Castillo-Garcia, J.; Ferreira, A.; Benevides, Alessander; Rojas, D.; Bastos, T.. A SSVEP-BCI based on Depth-of-Field. In IEEE Transactions on Neural Systems and Rehabilitation Engineering (under review). ([COTRINA et al., 2016](#))
3. Benevides, A.; **Cotrina, A.**, ; Bastos, T.; Sarcinelli, M. . Estudo de Tarefas Mentais Motoras e nao-motoras para Aplicacao em Interfaces Cerebro-Computador. Revista Medica de Minas Gerais (Belo Horizonte), v. 22, p. 30-30, 2012. ([BENEVIDES et al., 2012](#))
4. **Cotrina, A.**; Benevides, A., Bastos, T.; Ferreira, A.; Menezes, M.; Pereira, C. . Avaliacao de Caracteristicas Estatisticas e HOC de Sinais EEG no Reconhecimento de Estados Emocionais. Revista Medica de Minas Gerais (Belo Horizonte), v. 22, p. 131-31, 2012. ([COTRINA et al., 2012](#))

Grants and Awards

1. First Place at Brazilian Brain Computer Interface Competition organized by the Brazilian Society of Biomedical Engineering. October 2014. Title of the work: **A Novel Setup of BCI Stimulation Based on Depth of Field.**
2. Grant from International Centre of Theoretical Physics For School on Complex Networks and Applications to Neuroscience, Sao Paulo - Brazil 2015.

Book Chapters

1. **Cotrina A.**; Castillo-Garcia, J.; Trauernicht, M.; Souza, M. D. P.; Ferreira, A.; Bastos, T.. Toward a Hybrid Brain-Computer Interface. In: Adriano de Oliveira Andrade, Alcimar Barbosa Soares, Alexandre Cardoso, Edgard Afonso Lamounier. (Org.). *Tecnologias, Tecnicas e Tendencias em Engenharia Biomedica*. 1ed.Bauru: Canal6 Editora, 2014, v. 1, p. 343-364. ([COTRINA et al., 2014b](#))
2. Trauernicht, M.; Castillo-Garcia, J.; **Cotrina, A.**; Goulart, C.; Pomer-Escher, A.; Bastos, T.. Toward EEG-Based Emotion Recognition Using Brain Computer Interfaces. In: Adriano de Oliveira Andrade, Alcimar Barbosa Soares, Alexandre Cardoso, Edgard Afonso Lamounier. (Org.). *Tecnologias, Tecnicas e Tendencias em Engenharia Biomedica*. 1ed.Bauru: Canal6 Editora, 2014, v. 1, p. 319-342. ([TRAUERNITCH et al., 2014](#))

Conference Papers

1. **Cotrina, A.**; Glasgio G.; Rivera H.; Ferreira A.; Bastos, T.. Evaluation of Eye Movements Using Tacking Devices in Context of a Novel SSVEP-BCI Setup. In XII Intelligent Automation Brazilian Symposium, Natal, Brazil, Oct 2015. ([COTRINA et al., 2015c](#))
2. Floriano, A.; Longo B.; Baldo G.; **Cotrina A.**; Bastos, T.. Developing of a BCI based on SSVEP to command a Telepresence Robot, in XII Intelligent Automation Brazilian Symposium, Natal, Brazil, Oct 2015.
3. **Cotrina, A.**; Benevides, A.; Alves S.; Castillo-Garcia, J.; Ferreira A.; Bastos, T.. Towards a BCI-Speller Based on Binary Selection. In 1st International Workshop on Assistive Technology, Vitoria, Brazil, Feb, 2015. ([COTRINA et al., 2015a](#))
4. **Cotrina, A.**; Castillo-Garcia, J.; Ferreira, A.; Bastos, T.. Towards a SSVEP-BCI Based on Depth of Field. In: 6th International Brain-Computer Interface Conference 2014, 2014, Graz. Proc. of the 6th International Brain-Computer Interface Conference 2014, 2014. v. 1. p. 1-6.
5. Castillo-Garcia, J.; Muller, S.; **Cotrina, A.**; Caicedo , E.; Bastos, T.. Comparison Among Feature Extraction Techniques Based on Power Spectrum for a SSVEP-BCI. In: International Conference on Industrial Informatics (INDIN2014), 2014, Porto Alegre. Proc. of the International Conference on Industrial Informatics (INDIN2014), 2014. p. 1-6. ([CASTILLO et al., 2014c](#))

6. Castillo-Garcia, J.; **Cotrina, A.**; Benevides, Alessandro Botti ; Delisle, D. ; Longo , B.; Caicedo, E. ; Bastos, T.. Adaptive BCI Based on Software Agents. In: 36th Annual International Conference of the IEEE Engineering in Medicine and Biology Society (EMBC'14), 2014, Chicago. Proc. of the 36th Annual International Conference of the IEEE Engineering in Medicine and Biology Society, 2014. p. 1-4. ([CASTILLO et al., 2014a](#))
7. **Cotrina, A.**; Castillo-Garcia, J.; Benevides, A.; Longo, B.; Ferreira, A.; Pomer-Escher, A.; Souza, M. D. P.; Bastos, T.. Computing Stress-Related Emotional State via Frontal Cortex Asymmetry to be Applied in Passive-ssBCI. In: 5th IEEE Biosignals and Biorobotics Conference (BRC 2014), 2014, Salvador. Proc. of the 5th IEEE Biosignals and Biorobotics Conference, 2014. p. 6 pg.. ([COTRINA et al., 2014a](#))
8. **Cotrina, A.**; Benevides, A.; Ferreira, A.; Bastos, T.; Castillo-Garcia, J.; Menezes, M. L.; Pereira, C. Towards an Architecture of a Hybrid BCI Based on SSVEP-BCI and Passive-BCI. In: 36th Annual International Conference of the IEEE Engineering in Medicine and Biology Society (EMBC 14), 2014, Chicago. Proc. of the 36th Annual International Conference of the IEEE Engineering in Medicine and Biology Society, 2014. v. 1. p. 1-4. ([COTRINA et al., 2014c](#))
9. **Cotrina, A.**; Benevides, A.; Ferreira, A.; Bastos, T.; Castillo-Garcia, J.; Menezes, M. L.; Pereira, C. . Evaluation of Emotional Components to Improve a SSVEP-BCI. In: Congresso Brasileiro de Automatica, 2014, Belo Horizonte. Anais do Congresso Brasileiro de Automatica, 2014. p. 1-6. ([COTRINA et al., 2014b](#))
10. Benevides, A. **Cotrina, A.**; Bastos, T.; Castillo-Garcia, J.; Benevides, A. Evaluation of Emotional Components to Improve a SSVEP-BCI. In: Biosignals and Biorobotics Conference (2014): Biosignals and Robotics for Better and Safer Living (BRC), 5th ISSNIP-IEEE. p. 1-6. ([BENEVIDES et al., 2014](#))
11. **Cotrina, A.**; Bastos, T.; Ferreira, A.; Benevides, A. . Evaluation of ERD/ERS caused by unpleasant sounds to be applied in BCIs. In: 2013 ISSNIP Biosignals and Biorobotics Conference: Biosignals and Robotics for Better and Safer Living (BRC), 2013, Rio de Janeiro. 2013 ISSNIP Biosignals and Biorobotics Conference: Biosignals and Robotics for Better and Safer Living (BRC), 2013. p. 1. ([COTRINA et al., 2013](#))
12. Bastos, T.; Ferreira, A.; **Cotrina, A.**; Arjunan, S.; Kumar, D. . Evaluation of feature extraction techniques in emotional state recognition. In: 2012 4th International Conference on Intelligent Human Computer Interaction (IHCI), 2012, Kharagpur. 2012 4th International Conference on Intelligent Human Computer Interaction (IHCI), 2012. p. 1. ([BASTOS et al., 2012](#))

International Schools and Workshops

1. School on Complex Networks and Applications to Neuroscience, Sao Paulo - Brazil 2015.
2. 18th EEGLAB Workshop. Rio de Janeiro - Brazil 2014.
3. 10th BCI2000 Workshop. Asilomar - USA 2013.
4. Passive BCI - Using Neurophysiological Signals that Reflect Cognitive or Affective State. Asilomar - USA 2013.
5. BCI and Detection of Consciousness. Asilomar - USA 2013.
6. What does electrophysiology tell about neuronal and cognitive functioning? - Belo Horizonte - Brazil 2012.

APPENDIX C – EEG positions

EEG signals were recorded with a device for clinical purposes BrainNet36 together with a cap of integrated electrodes positioned according the international 10/10 system. Passive electrodes at locations P1, P2, P3, P4, Pz, PO3, PO4, PO7, PO8, POz, O1, O2, and Oz. Biauricular reference, re-referenced to Cz was employed. The ground electrode was placed on the AFz position.

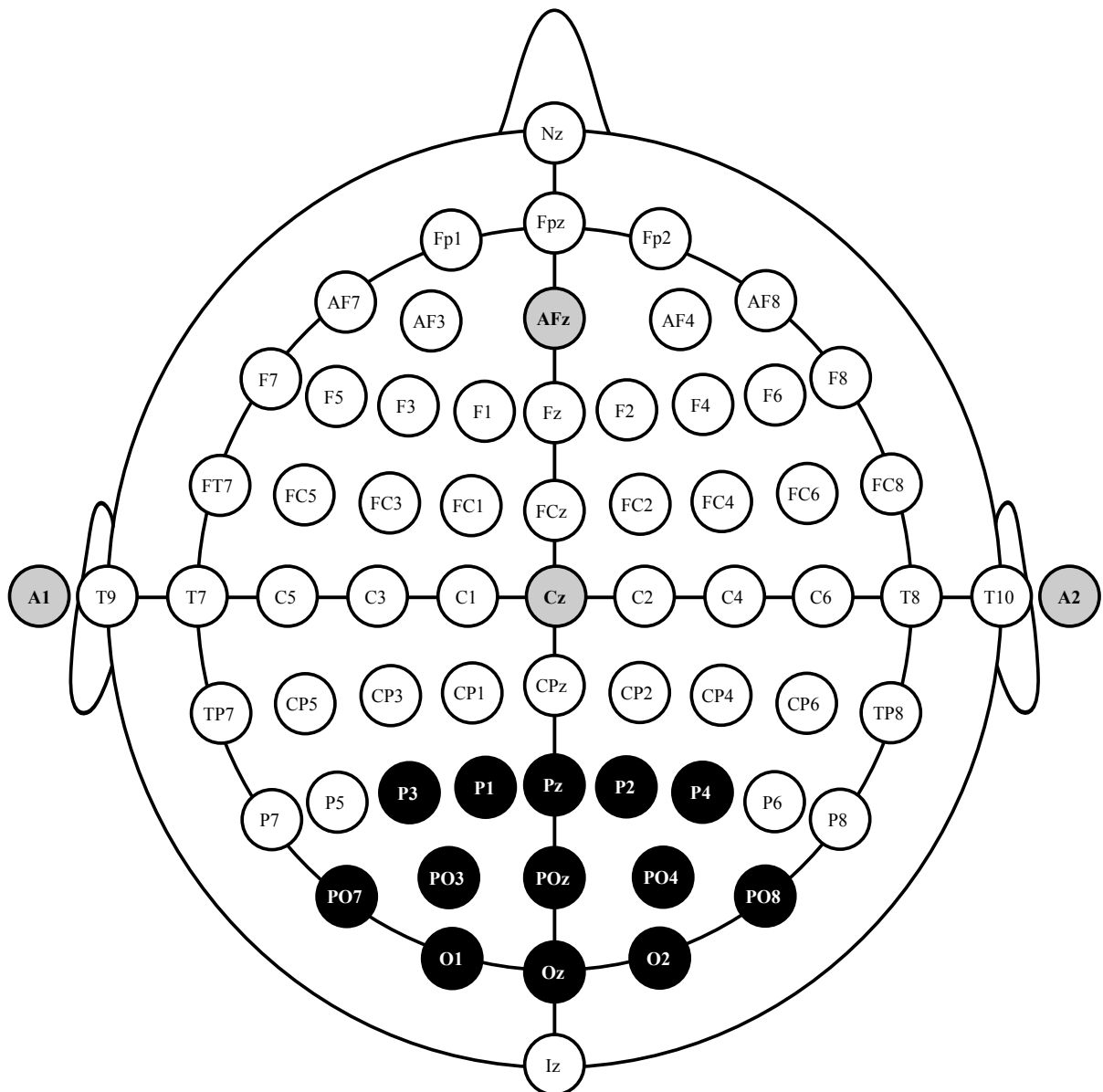


Figure 73 – Electrode placement (black circles) at the back of the head over occipital and parietal regions. Biauricular reference, Cz and ground electrode (green circles). Nz and Iz represents the scalp reference points nasion and innion, respectively.

APPENDIX D – Simulation of Retinal Blurry Model

The blurring is characterized by the PSF and most blurring processes can be approximated by convolution integrals in which low frequencies are removed. As shown previously, the PSF is the output of the imaging system for an input point source. Computationally, the image of a defocused object can be simulated by convolving the image with a PSF that can be represented by a circular average spatial filter as follows,

$$I'(\mathbf{x}) = I(\mathbf{x}) * psf(\mathbf{x}, \Delta D), \quad (\text{D.1})$$

where the blurry image $I'(\mathbf{x})$ is obtained from the original image $I(\mathbf{x})$, psf is the PDF function and ΔD represents the defocusing degree that is related to the distance between focused and non-focused objects. Gaussian filters can be used to describe a PSF, in which the standard deviation determines the amount of blurring.

$$H(\mathbf{x}) = \frac{e^{-D^2(\mathbf{x})}}{2D_0^2}, \quad (\text{D.2})$$

where $\mathbf{x} = (x, y)$, $D^2 = x^2 + y^2$, and $D_0 = \sigma$ is the cutoff frequency that measures the spread about the center. Figure 74 shows the simulation of retinal blurry model and the projected images for three values of diameter of blur circles.

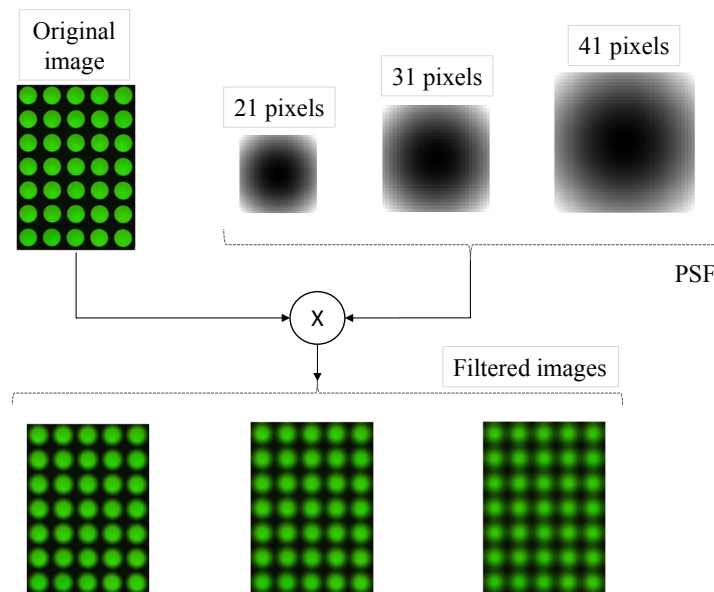


Figure 74 – Simulation of retinal blurry model for three values of diameter of blur circles.

APPENDIX E – PSF and NPSF

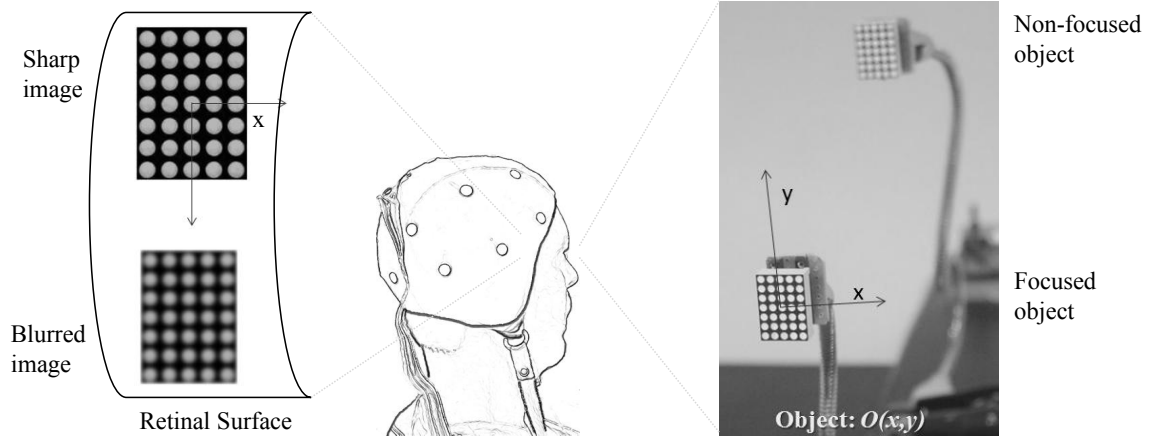


Figure 75 – Object $O(x, y)$ and its image projection $I(x, y)$.

Eye response

The idealized image can be expressed as $I(\mathbf{x}, \lambda) = T(\lambda, p)O(\mathbf{x}, M)$; where p is the area of the pupil, M is the ratio between the distance from the object (d_1) and the distance to the projected image (d_2), and can be computed from a simplified eye model, $M = d_2/d_1$ (HERMAN, 2007).

PSF extension

The expression can be expanded as follows,

$$psf(\mathbf{x}, \lambda, a(\mathbf{z}, \lambda), W(\mathbf{z}, \lambda, \Delta D)). \quad (\text{E.1})$$

The terms $a(\mathbf{z}, \lambda)$ and $W(\mathbf{z}, \lambda, \Delta D)$ specify the effect of the aperture system and the wave aberration function, correspondingly. The term \mathbf{z} is the position in the plane of aperture. In the human eye, the aperture is characterized by the shape, size and transmittance of the pupil (BURGE; GEISLER, 2011). The wave aberration function describes the other aberrations (degradation in image quality) introduced by the lens system not attributable to diffraction, such as defocusing (DAI, 2008).

Neural-PSF extension

Light reaching a given point on the retina through the center of the pupil is more visually effective than the same light reaching the same point through the edge of the

pupil. Thus, the retina is directionally sensitive and is known as Stiles Crawford effect. It can be described by a parabolic function as follows.

$$\log \eta = \log \eta_{max} - \rho(\mathbf{d} - \mathbf{d}_{max})^2 \quad (\text{E.2})$$

where η is the sensitivity at d distance from the center of the pupil, and ρ represents the magnitude of the Stiles Crawford effect. The effect decreases of the brightness of a light stimulus with increasing eccentricity of the position of entry of the light pencil through the pupil.

Index

- Aberrations, 51
- Accommodation, 26, 56
- Airy disk pattern, 51
- Amyotrophic lateral sclerosis, 17
- Area under curve, 105

- Brain-computer interface, 17, 37
- Canonical correlation analysis, 104
- Central nervous system, 28
- Circle of confusion, 50
- Cohen's Kappa coefficient, 105
- Common average reference, 104
- Cones, 26
- Cornea, 24
- Cortex V1, 28

- Demodulation, 86
- Depth-of-field, 50
- Depth-of-focus, 50
- Duchenne muscular dystrophy, 17

- EEG, 32
- EMG, 17
- EOG, 17, 104
- Eye, 24

- Fast Fourier transform, 105
- Field of vision, 30
- Fovea, 25, 27

- Guillain-Barre syndrome, 17

- Human-machine interaction, 17

- Information transfer rate, 104, 106
- International system 10/20, 32
- Iris, 24

- Least absolute shrinkage and selection operator, 104, 105

- LED, 36
- Lens, 24
- LGN, 28
- Light, 23
- Locked-in state, 17

- M-pathway, 29
- Modulation, 85

- Neural PSF, 90

- Objective response detection, 58
- Optic disk, 25
- Optic nerve, 25
- Optical power, 52
- Optical PSF, 51

- P-pathway, 29
- Perimeter of the eye, 30
- Power spectral density analysis, 104, 105
- Pupil, 24

- Retina, 25
- Rods, 27

- Spatial response, 90
- Spatial-temporal response, 91
- SSVEP, 35
- SSVEP-BCI, 39
- Statistical F-Test, 58

- Transient VEP, 34

- VEP, 33
- Vision, 24
- Visual Pathway, 28

- Wavelength, 24